# INFORMATION TO USERS

This manuscript has been reproduced from the microfilm master. UMI films the text directly from the original or copy submitted. Thus, some thesis and dissertation copies are in typewriter face, while others may be from any type of computer printer.

**The quality of this reproduction is dependent upon the quality of the copy submitted.** Broken or indistinct print, colored or poor quality illustrations and photographs, print bleedthrough, substandard margins, and improper alignment can adversely affect reproduction.

In the unlikely event that the author did not send UMI a complete manuscript and there are missing pages, these will be noted. Also, if unauthorized copyright material had to be removed, a note will indicate the deletion.

Oversize materials (e.g., maps, drawings, charts) are reproduced by sectioning the original, beginning at the upper left-hand corner and continuing from left to right in equal sections with small overlaps. Each original is also photographed in one exposure and is included in reduced form at the back of the book.

Photographs included in the original manuscript have been reproduced xerographically in this copy. Higher quality 6" x 9" black and white photographic prints are available for any photographs or illustrations appearing in this copy for an additional charge. Contact UMI directly to order.

**UMI**

A Bell & Howell Information Company
300 North Zeeb Road, Ann Arbor MI 48106-1346 USA
313/761-4700 800/521-0600

# MECHANISTIC AND KINETIC ASPECTS OF NITROGEN OXIDES FORMATION IN COAL CHAR AND MODEL CHAR OXIDATION PROCESSES

by

Masoud Abbasi

A dissertation submitted to the faculty of
The University of Utah
in partial fulfillment of the requirement for the degree of

Doctor of Philosophy

Department of Mechanical Engineering

The University of Utah

May 1999

THE UNIVERSITY OF UTAH GRADUATE SCHOOL

# SUPERVISORY COMMITTEE APPROVAL

of a dissertation submitted by

Masoud Abbasi

This dissertation has been read by each member of the following supervisory committee and by majority vote has been found to be satisfactory.

Feb 16, 1999 — Chair: Henk L. C. Meuzelaar

2/16/99 — Kenneth L. DeVries

16 Feb 99 — Gary M. Sandquist

Feb 16, 1999 — JoAnn Lighty

Feb 16, 1999 — Adel Sarofim

THE UNIVERSITY OF UTAH GRADUATE SCHOOL

# FINAL READING APPROVAL

To the Graduate Council of the University of Utah:

I have read the dissertation of Masoud Abbasi in the final form and have found that (1) its format, citations, and bibliographic style are consistent and acceptable; (2) its illustrative materials including figures, tables, and charts are in place; and (3) the final manuscript is satisfactory to the supervisory committee and is ready for submission to The Graduate School.

2/26/99
Date

Henk L. C. Meuzelaar
Chair, Supervisory Committee

Approved for the Major Department

Robert B. Roemer
Chair

Approved for the Graduate Council

David S. Chapman
Dean of The Graduate School

## ABSTRACT

Emission of nitrogen oxides ($NO_x$) is one of the major environmental problems associated with pulverized coal combustion. A significant fraction of $NO_x$ is proposed to originate from the oxidation of char nitrogen. In view of the well-known variability and heterogeneity of coals and the lack of understanding of the precise structure and origin of some nitrogen forms in coal samples, let alone in coal-derived chars, availability of well-defined nitrogen-rich model chars served as an important prerequisite for the systematic studies of the mechanisms and kinetics of $NO_x$ formation during oxidation of chars.

These studies were performed by oxidizing various chars (Carbosieve, model chars and coal chars) in a well controlled environment by examining various time- and temperature-resolved evolution profiles of carbon (CO, $CO_2$), hydrogen ($H_2O$) and nitrogen (HCN, $N_2O$, NO) products. The overall effect of oxygen level on the mechanisms of NO, $N_2O$ and HCN formation was also investigated. Furthermore, the catalytic effect of molecular carbon sieve in the heterogeneous and homogeneous secondary reaction mechanisms of NO, $N_2O$ and HCN, and their involvement in the formation and reduction of $NO_x$, were examined.

Two different reactor configurations were utilized to help detect and evaluate the possible effects of mass transport limitations. The original reactor (Perkin Elmer TGA7 furnace tube) data indicated that the early stages of char oxidation processes are under chemical control. During the middle portion of the oxidation reaction, falling oxygen levels

within the reactor bed strongly affect measured reaction rates. The observed effects are in good agreement with the first order relationship between oxygen levels and char oxidation rates most commonly proposed in the literature. Towards the end of the process, oxygen levels within the char bed as well as the corresponding reaction rates tend to recover to the initial levels.

The modified version of the TG system (tubular reactor) configuration was mainly used for mechanistic studies of NO, HCN and $N_2O$ studies. The formation of a major part of NO was found to result from the homogeneous oxidation of HCN. An investigation of HCN and $H_2O$ profiles suggests that $H_2O$ is a hydrogen provider for the CN functionality in char to form HCN. The bimodal behavior of NO was discovered to be a result of desorption of the chemisorbed exited NO onto the active carbon sites. The same reactive NO molecules also appear to be responsible for the formation of $N_2O$ molecules. In the presence of carbon, NO and $N_2O$ can undergo reactions at temperatures in the excess of 900 °C to form HCN.

To my parents and brother for their patience,

sacrifice, support and love.

CONTENTS

## LIST OF TABLES

LIST OF FIGURES

ACKNOWLEDGMENTS

I wish to submit my sincere thanks and appreciation to Dr. Henk L. C. Meuzelaar for his tireless and enlightening guidance and encouragement throughout this study. His perseverance and forbearance with me during the past 5 years have been amongst the few important factors inspiring me in finishing this work.

Many thanks to Dr. Adel Sarofim for his many valuable inputs and helpful discussions. Thanks also go to other members of my advisory committee: Dr. JoAnn Lighty, Dr. Larry DeVries and Dr. Gary Sandquist for their constructive comments, and Advanced Combustion Engineering Research Center (ACERC) for providing financial support for this work.

Dr. Ashish Tripathi is thanked for his many heated discussions, his simple and yet productive ideas, and mostly his encouragement and friendship. Mr. Paul Cole is thanked for assisting me with the experimental set up, Dr. William McClennen and Dr. Jacek Dworzanski and Mr. Genshen Deng for many valuable inputs and Ms. Lori Sather for her help and assistance.

Heart felt appreciation goes to my parents Mr. Mansoor Abbasi and Mrs. Ferdouse Aminian and my brother Mr. Kamran Abbasi for their support, sacrifice, patience, encouragement and love, and to my wife Mrs. Firoozeh Khodaverdian for bringing joy and happiness into my life specially during the last six months of this work.

**ERRATUM**

Page numbers 1-15 were not assigned in this manuscript.

# CHAPTER 1

# BACKGROUND

## 1.1 Introduction

The possibility of characterizing coal char nitrogen forms, elucidating the combustion mechanisms of char nitrogen and determining its role in the formation of $NO_x$ by means of combined thermogravimetry (TG), gas chromatography (GC), infrared spectrometry (IR) and mass spectrometry (MS) techniques is investigated. Until the 1980s, when environmental issues gained more consideration and attention, nitrogen was probably among the least studied major elements in coal. The majority of nitrogen atoms in coal are known to be bound to aromatic organic moieties. Investigations on solid coals and coal-derived materials have illuminated the fact that the organic nitrogen is mainly bound to five-membered "pyrrolic" and six-membered "pyridinic" ring structures. [1 & 2]

Since aromatic nitrogen forms tend to become incorporated into the char residue during the initial devolatilization step of coal, char nitrogen may, in fact, play a more important role than nitrogen released with volatiles products in production of $NO_x$ during coal combustion. However, notwithstanding a significant body of experimental work, the mechanisms and kinetics of $NO_x$ formation are far from completely understood. The complexity of the coal and resulting char as well as their heterogeneity have been the main

factors impeding the development of comprehensive mechanistic and kinetic $NO_x$ formation models in coal combustion processes.

This study focuses on mechanistic aspects of $NO_x$ formation from char in a small-scale fluidized bed combustor (described in details in the following chapter). Major advantages of fluidized bed combustors revolve around their fuel flexibility as well as low emissions of $SO_2$ and $NO_x$.[3] One reason behind the low $NO_x$ emission is the low operating temperature (1050-1150 K). However, the relatively low combustion temperatures tend to increase the emission of $N_2O$ relative to other combustion systems.[4 & 5] Operating conditions and their relative effect upon the many different homogeneous and heterogeneous reaction pathways play a major role in the formation and destruction of $NO_x$.

## 1.2 Literature Review

Lázaro et al.[6] investigated the effect of pyrolysis conditions on the release of nitrogen during char combustion by using a fluidized bed pyrolysis unit to produce several chars at different temperatures and pressures from a Spanish coal. They observed two zones for the NO evolution profiles, leading them to believe that two different nitrogen sources, with different reactivities and activation energies, are present in the chars. The first, as they suggested, could arise from the nitrogen in the volatile matter, and the second from the fixed nitrogen. They proposed that the fraction of the total nitrogen char released as NO depended on the volatile matter and the specific surface area of the chars. In addition, they noted that the nitrogen released as $NO+N_2$ accounts for nearly all the nitrogen in chars of low surface area and high volatile matter content. In the case of the chars of high specific surface and low

volatile matter content, they suggested that other nitrogen species, probably $N_2O$, are formed during oxidation of such chars.

Additionally, based on their observations they noted that with the oxidative reactions yielding NO, three reductive reactions affecting NO, CO and char carbon can occur. In the first reductive reaction, NO is reduced to $N_2$ by CO in the gas phase. Since the highest conversion yield to $N_2$ was detected for high volatile matter chars, they concluded that the presence of volatile matter enhances the reduction of nitric oxide to molecular nitrogen. The second reductive reaction, as they proposed, is a gas-solid reaction between carbon in char and NO, yielding $N_2O$ and CO. They noted that, irrespective of whether the NO conversion to $N_2O$ is a catalyzed or noncatalyzed reaction, it seems that adsorption of NO on the char surface, and hence the char surface area, appeared to play an important role in the reaction. The third reductive reaction pointed out by Lázaro and coworkers is also a reductive reactions with $N_2$ and $CO_2$ as products instead.

Harding et al. [7] studied the release of nitric oxide during the combustion of coal chars prepared from a wide range of coals in an entrained flow reactor over a range of combustion temperatures (823-1323 K) using a thermogravimetric analyzer coupled with a mass spectrometer. The conversion of char nitrogen to NO (NO/char-N) was investigated in relation to coal and char structural characterization parameters. The results of these studies showed that higher levels of conversion of char-N to NO were observed for the high rank coal chars at lower combustion temperatures, where the reaction is under chemical control. They noted a decrease in the NO/char-N conversion ratio as the combustion temperature increased and further suggested that chars with low surface areas and low reactivities tend to have

higher levels of conversion of char-N to NO during combustion.

Their data imply that the NO/(CO+$CO_2$) ratio increases with increasing burn-off for the combustion of low- and high-rank coal chars under chemical as well as diffusion controlled conditions. This was attributed to two reasons: (1) the retention of nitrogen in the char, and (2) the lower extent of reduction of the primary char nitrogen oxidation product NO, in the pores or on the surface of the char as the structure changes during burnoff.

Yue et al. [8] performed continuous measurements on the CO, $CO_2$, and NO emissions of oxidizing char particles at temperatures between 750 and 1000 K. The fractional conversion of fuel nitrogen to NO, derived from the experimental data as a function of char burnout, showed that the fraction of char-nitrogen converted to NO increases with increasing char burnout and with increasing temperature. They derived a closed form approximate expression for NO emission that took into account the influence of the parallel diffusion and chemical reaction of $O_2$ into the pores on NO formation, and the partial NO destruction by the reaction with CO (carbon as catalyst) or with carbon as it diffused out of the particles. They also observed that NO release profiles always show a maximum following those of CO and $CO_2$. In addition, the ratio of peak NO production to the sum of the peak of CO and $CO_2$ production increased with decreasing particle size, suggesting that NO might have been reduced as it diffused out of a particle, and that the extent of reduction decreased with decreasing particle size.

Crelling et al. [9] investigated the variation in nitrogen and sulphur content of macerals and their release during combustion. They conducted their experiments in 20% oxygen/argon in a combined thermogravimetry/mass spectrometry system. They observed that the nitrogen

oxide released during combustion of the EFR chars reached a maximum at a higher temperature than the corresponding CO and $CO_2$ peaks for all maceral concentrates studied.

They noted that nitrogen evolved as NO during the gasification of these chars, accounting for approximately half of the nitrogen evolved, peaked after the $CO_2$ evolution maximum in all cases. In most of their samples the NO gas evolution profile is asymmetric with a definite shoulder on the low-temperature side. Furthermore, they observed the NO peak reaching a maximum at a higher temperature than the corresponding $CO_2$ peak. They suggested that this bimodal nature is due to at least two mechanisms or types of functionality for NO release.

Brown et al. [10] presented the results of temperature-programmed oxidative gasification of six coals and their chars. These chars were obtained from their corresponding coals at 1000 °C in a nitrogen environment. Next, they were oxidatively gasified with 20% oxygen in argon at a heating rate of 15 °C/min. The ratio of both $NO/CO_2$ and NO/CO decreased with increasing temperature, whereas in higher temperature ranges these ratios showed inverse trends with the same temperature histories. They concluded that this suggested higher conversion of volatile nitrogen to NO. For the low rank coals, they also detected a peak due to HCN in this region as well as at the initial char formation step. They also pointed out that the NO gas evolution profiles reach a maximum after the corresponding CO and $CO_2$ profiles for both the coals and entrained flow reactor prepared chars. Based on their observations the ratio of NO released during gasification to the total nitrogen varies from 0.14 to 0.44 for the entrained flow reactor prepared chars.

Illán-Gómez et al. [11] have investigated the effect of chars on NO reduction at low

temperatures. They suggested that the activity for NO reduction is governed by active catalyst sites on the char. At high temperatures, however, the reactivity of the char (i.e., the number of carbon active sites) appears to control the NO reduction behavior. They pointed out that chars that exhibit the highest increase in NO reduction also have the highest reactivity in oxygen.

Teng et al. [12] studied the heterogeneous reduction of NO by carbon (a relatively pure carbon derived from phenolic resin) in a thermogravimetric analysis system, employing both pseudo steady and transient reaction methods. They performed the studies in a range of temperature (near ambient up to 1073 K) and pressures (1.01-10.1 kPa). They suggested that the gasification of carbon by NO involves two parallel processes: (1) somewhat slow desorption of relatively stable surface complexes; (2) processes involving NO attack on active unoccupied sites that results in essentially immediate desorption of gaseous products. They recommended that the first process controls the overall gasification rate at lower temperatures and is governed by a distribution of desorption activation energies, involving mainly surface oxides that yield CO upon desorption. The second process, as they noted, dominates at high temperatures (somewhat arbitrarily defined by T>923 K) and is suggested to be controlled by the dissociative chemisorption of NO on the carbon surface.

Visona et al. [13] performed computational modeling to study the formation of nitric oxide during the combustion of a single spherical char particle. Combustion conditions were representative of pulverized coal in the temperature range 1250 to 1750 K. The model introduced by these investigators was a generalized mechanistic model with nitric oxide or HCN being released directly from the char-N. Homogeneous gas phase reactions of NO

occur within the particle, as well as heterogenous NO reduction on the char's surface. Their modeling suggested that two mechanisms are possible for the conversion of char-N to NO at high temperatures: char-N converting completely to NO and being subsequently reduced on the char's surface; or char-N converting completely to HCN and being oxidized and reduced in the atmosphere external to the particle.

Shimizu et al. [14] studied the conversion of char bound nitrogen to nitric oxide during combustion of nine coals in a fixed bed reactor. In their studies they established a relation between carbon combustion rate and conversion of char-N to NO. In their model initial porosity of char was given as a parameter but its sensitivity on the conversion versus carbon combustion rate curve was not so large. They correlated the conversion of char-N to NO by noting that an increase in conversion is directly resulted from a decrease in combustion rate.

Formation of $N_2O$ has been another subject of investigation in char combustion processes. A finding regarding the formation of $N_2O$ by Goel et al. [15] suggests that the reaction of NO with organically bound nitrogen forms this species. In this scenario oxygen breaks open the nitrogen containing aromatic rings. Oxygen then reacts with the nitrogen atoms to form an intermediate, still bound to the char surface. The intermediate splits to form NO and reacts with NO to form $N_2O$ as given below:

$$\text{char-N} \xrightarrow{O_2} \text{- I} \begin{matrix} \xrightarrow{NO} & NO \\ & N_2O \end{matrix} \qquad (1\text{-}1)$$

An alternative pathway to $N_2O$ formation during char combustion, as is suggested by Goel et al. is by the oxidation of HCN. During devolatilization organic nitrogen present as a heteroatom in aromatic ring species is released as HCN. Its evolution may continue during

char combustion via a process termed as slow or secondary devolatilization of char, and then may undergo homogeneous reactions with oxygen to form NO and $N_2O$. Note that this HCN would be additional to that released during the initial devolatilization phase of coal. Therefore, these investigators find it logical to postulate that HCN is a source of $N_2O$ production even during char combustion. They also suggest that HCN may be released in absence or in presence of oxygen with the following reaction being the most important one for formation of $N_2O$ from HCN:

$$HCN \xrightarrow{O} NCO \xrightarrow{NO} N_2O \qquad (1\text{-}2)$$

Thomas et al. [16] used nitrogen doped carbon-13 for coal char gasification to distinguish the $N_2O$ and $N_2$ from $CO_2$ and CO in a combined thermogravimetry/mass spectrometry instrument, respectively. During a temperature-programmed gasification process in 20% oxygen (in argon) environment nitric and nitrous oxides were formed from the nitrogen in the carbon matrix. It was apparent from these studies that under the conditions used, the $NO/CO_2$ ratio increased with the extent of gasification. Thomas also observed bimodality in the NO time-evolution profile, with the higher temperature peak being delayed relative to the carbon dioxide peak and having significantly higher intensity than the lower temperature peak when gasification was conducted in 20% oxygen in argon. They proposed that the bimodal NO profiles are due to two main types of nitrogen functionality in chars. The same effect was also observed in gasification of some of their model carbons in 5% oxygen but the lower temperature peak had a similar intensity to the higher temperature peak.

Miettinen et al. [17] investigated the formation of $N_2O$ from burning char particles under different combustion conditions (particle size, inlet gas mixture, oxygen concentration, NO concentration, inlet gas flow rate and bed temperature) in a fixed bed reactor containing quartz sand ($SiO_2$) to support the coal particles. They observed that addition of NO to the flue gas ($O_2$ and Ar) increased the $N_2O$ yield. From their studies it was evident that a low combustion temperature also favors high yields of $N_2O$. In addition, a prominent influence of the oxygen concentration on $N_2O$ yield was discovered.

Under an oxidizing environment with NO as the only oxidizing agent, Miettinen et al.[18] have reported the effect of different NO concentrations in the inlet gas, as well as, the effect of changing gas residence time within, and after, the fixed bed on the emission of $N_2O$ from the char particles burning under single particle conditions. They observed that the $N_2O$ formation increased with increasing NO concentration in the inlet gas for low NO concentrations (5-20%) and reached a plateau for higher levels of NO. This led them to conclude that primary formation of a cyano compound is the result of the reaction of NO with char. The cyano compound then reacts further in the gas phase with NO to form $N_2O$. They proposed that this means not only that char nitrogen can form a cyano species but also that NO from the gas phase can be reduced to a cyano species on the char surface. The $N_2O$ formation increased with increasing gas residence time within and after the fixed bed.

Tullin et al. [19] in a small-scale fluidized bed showed that the conversion of $N_2O$ decreases with increasing temperature, whereas that to NO exhibits a maximum between 1023 and 1095 K. They also observed opposite trends in the instantaneous conversion of $N_2O$ (decreasing) and NO. They proposed a model explaining the NO and $N_2O$ emissions by the

nitrogen bound in the char conversion to NO and $N_2O$ on oxidation within pores. The NO and $N_2O$ formed are subsequently reduced as they diffuse out of the pores. In addition, they suggested that the split between the NO and $N_2O$ depends on the local NO concentration and the temperature. Their model also explains the increase in fractional conversion to NO and decrease in fractional conversion to $N_2O$ with increasing carbon conversion.

Tullin and coworkers proposed that NO is formed during char oxidation and is partially destroyed as it diffuses out of the pores. As the particle shrinks, less NO will be destroyed in the pores and as a result the conversion to NO increases with burnout. The instantaneous conversion to NO approaches a value of unity at complete carbon conversion because in the final stage of combustion the NO produced has little opportunity to react with char.

Pels et al. [20] investigated the NO and $N_2O$ formation and destruction in a laboratory-scale fluidized-bed combustor for a set of coals ranging from lignite to anthracite. They observed that the sum of fuel-N conversions to $N_2O$ and NO was found to be constant over a range of temperatures, although emission levels of individual species were strongly temperature-dependent. They proposed that this trade-off between $N_2O$ and NO emissions can be regarded as a constant conversion of fuel-bound nitrogen to $N_2$. When adding NO at a concentration level typical for fluidized-bed combustion, they found that NO reduction on the char surface was strongly enhanced in the presence of oxygen. The majority of the added NO was converted to $N_2$, but some $N_2O$ was also formed. They qualitatively explained the temperature-governed trade-off between emissions of NO and $N_2O$, and the formation of $N_2O$ and $N_2$ from NO reduction, on the basis of known heterogeneous and homogeneous

$NO/N_2O$ chemistry.

Pels and coworkers suggest that HCN and $NH_3$ are the responsible precursors to formation of NO and $N_2O$. In this scenario the char is gasified in the presence of oxygen, but still under relatively oxygen-lean conditions. Char-N is converted to HCN and $NH_3$, and subsequently $NO/N_2O$ formation proceeds in the gas phase. They noted that the gasification according to this mechanism takes place in the pores of the char with NO and $N_2O$ formed close to the char surface. Therefore, they expected that the overall emission of NO and $N_2O$ is strongly influenced by intra particle NO and $N_2O$ reduction.

Feng et al. [21] studied the emission of $N_2O$ and $NO_x$ from char combustion in a fixed bed reactor in the temperature range of 973-1323 K. Their findings mainly revolved around the strong effects of oxygen concentration, temperature and char type on both $N_2O$ and $NO_x$ emissions. They observed that, as the temperature is increased, $N_2O$ reaches a maximum at 1073 K and then decreases with temperature. Increase in oxygen concentration causes an increase in the $N_2O$ concentration and an increase followed by a decrease in the $NO_x$. In addition, the char with higher nitrogen content emits more $N_2O$, indicating that nitrogen oxides are formed from char-N. They noted that when NO is included in the inlet gas, much higher levels of $N_2O$ production from char combustion were observed suggesting that $N_2O$ can be generated by reduction of NO on the surface of chars even in the absence of $O_2$. They also pointed out the importance of the homogeneous oxidation of HCN from the gasification of chars.

Lu [22] studied the fuel and char nitrogen conversion to nitrogen oxides in pressurized fluidized bed combustion in a laboratory-scale batch reactor, which was controlled at well-

defined operating conditions. He observed both homogeneous and heterogeneous reactions contributing to the formation of $NO_x$ and $N_2O$. His observations also indicated that in the batch reactor the reduction mechanism also played a significant role in the emissions of nitrogen oxides under the examined conditions. He also observed that the ending time for $N_2O$ conversion was earlier than the times from the $NO_x$ and $CO_2$ conversion, which suggested that $N_2O$ formation from char-N is related to carbon conversion and NO concentration; i.e., the reaction of NO with char-N is the principal path for $N_2O$ formation in the presence of oxygen.

Illán-Gómez et al. [23] studied the mechanism of NO reduction by activated carbons. Their results illustrate the fact that relatively disordered, nongraphitic carbons (e.g., activated carbons and chars) free from significant quantities of inorganic impurities (e.g., potassium or iron) are effective in reducing NO at temperatures in excess of 500 °C.

Miettinen et al. [24] investigated the effect of different NO and CO concentrations in the inlet gas, as well as the effect of changing gas residence time within, and after the fixed bed on the emission of $N_2O$ from char particles burning at single particle conditions. To distinguish between char nitrogen and NO from the inlet gas a $^{15}N$-isotope-marked NO was used in the inlet gas. The addition of $^{15}NO$ to the inlet gas led to the formation of $^{15}N^{14}NO$ and $^{15}N_2O$, and the formation of these species increases with increasing concentration of $^{15}NO$ in the inlet gas, especially the formation of $^{15}N_2O$. They observed that the formation of $^{15}N^{14}NO$ was greater than the formation of $^{15}N_2O$ under all circumstances examined, but with increasing $^{15}NO$ concentration in the inlet gas the $^{15}N_2O$ formation increased, and was almost as great as the formation of $^{15}N^{14}NO$. In addition the influence of gas residence time

within the fixed bed and after the fixed bed was confirmed, and the $N_2O$ formation and formation of $^{15}N^{14}NO$ and $^{15}N_2O$ increased substantially with increasing gas residence time.

They suggested that the enhancement of the $^{15}N^{14}NO$ yield as the residence time increases can be explained by the two-step mechanism, where the first step is the release of a CN containing compound. This first step is independent of the residence time. Miettinen and coworkers suggested that the second step, where the CN- containing compound is oxidized and with the help of $^{15}NO$ forms $^{15}N^{14}NO$, ought to be residence time dependent.

For the increase in the formation of $^{15}N_2O$ with increasing $^{15}NO$ concentration in the inlet gas these investigators propose another two-step mechanism. The first step is $^{15}NO$ reduction on the char surface with simultaneous formation of cyano species. The $^{15}NO$ acts as an oxidizing agent and together with $O_2$ they oxidize the char particle. During this oxidation the char particle undergoes intensive bond breaking and as a result from this massive chemical and physical rupture the char particle releases not fully oxidized compounds (for example cyano compounds formed during NO reduction) which react further in the gas phase. The second step in this two-step mechanism as proposed by Miettinen and coworkers is the reaction between $^{15}NO$ and the released and partly oxidized char compounds forming $^{15}N_2O$.

Wójtowicz et al. [25] in a review paper examined coal combustion as a source of nitrous oxide. They suggested that in fluidized bed combustors, cyano species are solely responsible for the formation of $N_2O$, whereas $NH_3$-based compounds tend to react towards production of NO. In addition, formation of $N_2O$ appears to be competitive with respect to NO formation, and more $N_2O$ appears to be produced at the expense of NO as temperature

decreases. They pointed out that NO release follows the same trend as temperature, whereas $N_2O$ follows an opposite trend. They also noted that only up to 10% of char nitrogen has been found to produce $N_2O$, and NO reduction on char surface is not a significant source of $N_2O$.

It has been shown by Tullin et al. [26] that char nitrogen contributes more significantly to the formation of NO and $N_2O$ than the volatiles. In addition they discovered a decreasing trend for $N_2O$ and an increasing trend for NO with increasing temperature. In a fluidized bed, they measured the concentrations of NO, $N_2O$, $CO_2$, CO, and $CH_4$, for temperatures between 975 and 1148°K to obtain the fractional conversion of nitrogen to NO and $N_2O$. They concluded that the cumulative fuel nitrogen conversion to NO ranged from 18 to 46%, and to $N_2O$ ranged from 4 to 18%. They suggested that at lower temperatures NO is produced and destroyed as it diffuses out of the pores of the char. As temperature increases the material shrinks resulting in less destruction of NO in pores and, therefore, an increase in NO production. The formation of $N_2O$, however, is thought to be dependent upon the availability of NO at the point where char nitrogen is oxidized.

Gavin et al. [27] studied the nitrogen conversion to NO and $N_2O$ for 15 chars prepared at temperatures between 300 to 800°C. They discovered that the conversion of nitrogen to NO and $N_2O$ followed an opposite trend to temperature in their fluidized bed combustor. Another interesting observation was that the sum of the conversions of fuel nitrogen to NO and $N_2O$, expressed as a percentage of fuel nitrogen was constant. They made a comparison between the trends obtained from one coal experiment and from pyridine and pyrrole absorbed onto a low nitrogen concentration active carbon. It was discovered that they both

followed similar patterns in terms of conversion of nitrogen to NO.

Kramlich et al. [28] used a kinetic modeling approach along with experimental results to show that if HCN appears in the temperature range of 1150 to 1500 °K a partial conversion to $N_2O$ is possible. They believed that based on their experiments the main source of HCN may be either direct devolatilization or a char gasification reaction and suggested that the appearance of $N_2O$ in coal flames may originate from the homogeneous reaction of devolatilized char nitrogen in the fuel-lean postflame region.

De Soete et al. [29] investigated NO and $N_2O$ formation from char-nitrogen on highly devolatilized coal chars in the temperature range of 500 to 1300°K, for a fixed bed batch combustion method. They suggested that both NO and $N_2O$ are desorption products of oxidized (-CN) sites, and only a very small percentage of nitrous oxide is produced by reactions involving hydrocyanic acid as a reactant. Their experiments also revealed that there is only a rough proportionality between the fraction of char-nitrogen converted to NO and $N_2O$ and the degree of char burnout. In addition, based on their results, they suggested that the final fraction of char-nitrogen converted to NO and $N_2O$ is smaller than one (0.3 to 0.7, depending on char type, oxygen concentration and particle size) due to simultaneously occurring heterogenous reduction of NO and $N_2O$ on bound carbon atoms.

Åmand et al. [30] measured the emissions of NO and $N_2O$ from an 8-MW circulating fluidized bed boiler. They used three different coals to investigate the influence of the volatile content of the coals, as well as boiler type, at various bed temperatures, primary air stoichiometries, and excess air ratios. Based on these investigations, the emissions of NO are extremely low and dependent upon the char loading of the boiler as well as on the existence

of unburned combustible matter such as CO and $H_2$ in the gas phase. They reported high levels of $N_2O$ emission evident at the low temperatures used in fluidized bed. They also noted that the $N_2O$ emission is influenced by bed temperature and oxygen concentrations as well, but the influence of bed temperature is opposite compared to the dependence of bed temperature on the NO emission.

Åmand and coworkers suggested that the char nitrogen is released during combustion as NO or $NH_3$, depending on the rank of the coal. They emphasized on the importance of char itself as well as the CO produced in the reduction stage which more or less takes place in the pores of the char, when the coal is not oxidized completely. They also noted the production of $N_2O$ from NO reaction on char surfaces. They suggested that the NO and $N_2O$ chemistry within the walls of a fluidized bed reactor is extremely complex. Based on their observations, not only heterogenous reactions, in which mass transfer is included, but also the combustion process itself, interact with the NO-$N_2O$ chemistry.

Wang et al. [31] investigated the influence of pyrolysis heat treatment temperature and heating rate on the reactivity and the release of char-N during temperature-programmed combustion of a set of wire mesh reactor chars in a thermogravimetric-mass spectrometer system. They noted the observation of bimodal gas evolution profiles and suggested that this indicates the presence of species of different reactivity. Based on this study heat treatment of the chars at lower heating rates and longer soak times to temperatures in the range 1100-1400 °C lead to reduced char reactivity and higher NO/char-N ratios under temperature-programmed combustion conditions. They also observed a consistency in their results with the reduction of the primary oxidation product NO on the surface and in the pores of the char.

In addition, these investigators observed that HCN is mainly detected in the initial stage of char combustion in accordance with the first $CO_2$ peak. Based on their observation the char-N conversion to HCN is low with the conversion decreasing slightly with increasing extent of pyrolysis. They also noted the presence of $N_2O$ amongst the evolved gases. They suggested that $N_2O$ was formed by the reaction of char nitrogen with NO in the presence of oxygen. A higher concentration of oxygen, as they noted, gave rise to both higher NO and $N_2O$ concentrations.

Chambrion et al. [32] studied the reduction of NO with carbon in the presence and the absence of oxygen with mass spectrometry and gas chromatography for gaseous products analysis. They used phenol formaldehyde resin (PF) char as carbon source throughout their studies. In a typical experiment, about 200 mg of PF char was placed in a fixed bed reactor under They flow and then heat treated at 950 °C for 30 minutes immediately before use. In the absence of oxygen at 600 °C NO reduction on PF char was almost negligible. They showed that before introduction of NO into the reactor, only residual evolution of CO was noticed, indicating the desorption of oxygen complexes from the pretreated char. They observed a dramatic increase of CO production as well as $CO_2$ and $N_2$ after introduction of NO. They suggested that this indicates the effective reduction of NO even in the absence of $O_2$. In addition, they noted that the presence of oxygen containing sites in char play a key role in this reaction. In the presence of oxygen the main products were CO and $CO_2$. Their concentrations increased together with $O_2$ conversion relating to the activation of PF char. Thereafter, as they noted, concentrations stabilized and later CO and $CO_2$ production slowly decreased, perhaps because of the loss of carbon. They further noted that the conversion of

NO to $N_2$ increased, accompanied with the activation of PF char.

Naruse et al. [33] investigated the effect of catalytic reactions by char particles on the $N_2O$ formation. In this study they proposed that HCN contributes more to the formation of $N_2O$ than $NH_3$ in the low temperature range. Based on their observations, as soon as HCN is destroyed, $N_2O$ and NO are formed. Both the maximum and the final concentrations of $N_2O$ increase with decreasing temperature.

In high temperature coal combustion, as Naruse and coworkers pointed out, the $N_2O$ formed in the initial stage is quickly reduced, because the $N_2O$ reduction reaction is fast at high temperature. Therefore, based on their observations, only a very low $N_2O$ concentration remains at the exit of the furnace. In low temperature combustion, however, slow destruction of $N_2O$ results in high emission levels.

Gulyurtlu et al. [34] carried out experimental studies with an 80 mm i.d. fluidized bed combustor over the temperature range 700-950 °C to determine the amounts of $N_2O$ formed during the combustion of different chars as well as the heterogeneous reactions involving char and $N_2O$ leading to the reduction of the latter. The results suggested that the combustion of volatiles contributes more to the formation of $N_2O$, as the $N_2O$ levels measured were approximately 40% of that observed during the combustion of the parent coal. The study also demonstrated the significant reactivity of char with respect to $N_2O$ as $\geq$90% of the inlet $N_2O$ concentration was adsorbed.

Wójtowicz et al. [35] used the X-ray photoelectron spectroscopy (XPS) to investigate the nitrogen functional forms present in several coals and their chars. In their experiments the chars were prepared under different severity conditions to capture transformations in nitrogen

functionality occurring during pyrolysis. Based on their studies they concluded that nitrogen functionality was related to the conversion of fuel-bound nitrogen to $NO_x$ and $N_2O$ in fluidized-bed combustion and in low-temperature char oxidation. They also pointed out the lack of evidence for a strong dependence on nitrogen functionality for char-N partition between NO and $N_2O$. Under the experimental conditions used in their work, pyrrolic and pyridinic functionalities were found to release NO and $N_2O$ in the same proportion of about 5:1.

Moritomi et al. [36] studied the effect of char surface in reducing NO. Based on their findings the char surface very effectively reduces NO to $N_2$. Reduction of NO to $N_2O$, however, as Moritomi and coworkers showed, is not very effective. Tullin et al. [37] studied the formation of $N_2O$ from NO and char-N. Based on their investigation the reaction of char nitrogen with NO in the presence of oxygen is the major reaction pathway leading to formation of $N_2O$.

Tullin et al. [38] further investigated the effects of NO concentrations on the emissions of $N_2O$ and NO from a single particle of coal burning in a fluidized bed combustor. The experiments were carried out in a laboratory scale quartz glass fluidized bed reactor in the temperature range 1023-1123 K. They observed that during the char combustion stage, addition of NO (250 ppm) resulted in an increased formation of $N_2O$, whereas the net NO formation decreased. They proposed that as the char is oxidized, the char nitrogen may either react with oxygen to form NO or it may react with NO formed at another site to form $N_2O$. Since the $N_2O$ formation rate depends on the local pore concentration of NO it will increase with increasing NO concentration.

Winter et al. [39] studied the formation rates of NO, $N_2O$ and HCN in an exclusively electrically heated, laboratory-scale, fluidized bed combustor made of quartz glass by using a high performance FTIR spectrometer in combination with a long-path, low-volume gas cell. Based on their observations, the formation characteristics during devolatilization could be explained mainly by the homogeneous HCN oxidation and NO and $N_2O$ formation. They proposed that NO and $N_2O$ formation during char combustion consists of two different paths. NO is mainly heterogeneously formed by char-nitrogen oxidation. But a volatile species, which was identified as HCN, was simultaneously released in low concentrations. This species was homogeneously oxidized to NCO, which further reacted with the heterogeneously produced NO to form $N_2O$.

Kilpinen et al. [40] investigated the importance of homogeneous gas-phase reactions of fuel-nitrogen species to the formation of $N_2O$ in fluidized bed combustion based on detailed chemical kinetic modeling. They used a kinetic scheme consisting of over 250 elementary reactions for an ideal plug flow reactor, and the most important reaction paths leading to $N_2O$ were identified and quantified for a number of conditions relevant for fluidized bed combustion. In addition, they studied the effect of different operating parameters on $N_2O$ formation, and compared the results to the existing data from laboratory and full-scale experiments. Based on their calculations if fuel-nitrogen species in form of simple cyano (HCN) species entered a fuel-lean gas phase between 1000 and 1200 K, a significant conversion to $N_2O$ would be found. They proposed that the $N_2O$ formation occurs principally through the following reaction:

$$NCO + NO \longrightarrow N_2O + CO \qquad (1\text{-}3)$$

where NCO originates from HCN mostly via the following reaction:

$$HCN + O \longrightarrow NCO + H \qquad (1\text{-}4)$$

Their calculations also indicated that $N_2O$ formation increased steeply as the temperature decreased. At high temperatures less $N_2O$ was produced because the key intermediate NCO was rapidly removed by the radicals, mostly via the following reactions:

$$NCO + H \longrightarrow NH + CO \qquad (1\text{-}5)$$

$$NCO + O \longrightarrow NO + CO \qquad (1\text{-}6)$$

Their work indicates that the homogeneous gas-phase reactions are an important contributor to the $N_2O$ formation in the fluidized bed combustion.

Krammer et al. [41] showed the conditions that favor the formation of $N_2O$ from char under fluidized bed combustion conditions to be the oxidation of the char to make the nitrogen bound in the heterocyclic rings accessible so that it can react heterogeneously either with oxygen to form NO or with nitric oxide to form $N_2O$. This was demonstrated by measurements of the gas composition when a batch of coal particles was introduced into a fluidized sand bed electrically heated to 1023 K and oxygen and nitric oxide were added to the fluidizing helium gas in varying concentrations. They reported $N_2O$ formation in amounts that increased with increasing NO concentration showing the importance of NO for $N_2O$ formation. The $N_2O$ concentration, however, fell to zero when the $O_2$ supply was interrupted underlying the essential role of oxygen in freeing the organically bound nitrogen so that it can react with NO to form $N_2O$.

Glarborg et al. [42] performed an experimental and theoretical study of HNCO oxidation. The experiments were carried out in an isothermal quartz flow reactor, and the

effects of temperature, CO concentration, and NO concentration were investigated at atmospheric pressure in the temperature range 1025-1425 K. They suggested that the oxidation of HNCO proceeds mainly through NCO, which subsequently is oxidized to NO or reacts with NO to form $N_2$ and $N_2O$. Their experimental results showed that the mutual presence of HNCO and NO strongly inhibits CO oxidation at lower temperatures. Based on their experiments HNCO consumption proceeds very slowly at temperatures below 1250 K. Above 1250 K however, HNCO decay is faster, but even at 1400 K only around 50% of the inlet HNCO is consumed. Oxidation of HNCO as they proposed, led to concentrations of $CO_2$ that are consistently larger than CO. NO and $N_2O$ constituted a comparatively small fraction of the products.

In addition, they proposed that OH is the main chain carrier in their experiments, and HNCO is primarily consumed by the HNCO + OH reaction, presumably forming NCO and $H_2O$. In the presence of NO, NCO would be consumed mainly by the NCO + NO reaction. They observed that in the absence of NO, consumption of NCO was considerably slower, occurring mainly through reaction with O and, at higher temperatures, possibly with $O_2$.

Glarborg et al. [43] further investigated the oxidation of hydrogen cyanide under flow reactor conditions (atmospheric pressure and 900-1400 K). Under the conditions investigated, they noted that the main oxidation route for HCN proceeds through NCO, formed by the following reaction sequence:

$$HCN + OH \longrightarrow CN + H_2O \qquad (1\text{-}7)$$

$$CN + O_2 \longrightarrow NCO + O \qquad (1\text{-}8)$$

The subsequent reactions of NCO as proposed by them, determine the fate of the nitrogen

atom. Depending on the gas composition and temperature, NCO is converted to HNCO (by reaction with $H_2O$ or HCN), $N_2O/N_2$ (by reaction with NO) or NO (by reaction with O). They further noted that both HNCO and $N_2O$ are important intermediates in HCN oxidation under these conditions.

Hayhurst et al. [44] studied the $NO_x$ and $N_2O$ formations from three quite different coals burned batchwise in electrically heated beds of sand fluidized with $O_2$ and $N_2$ at either 800 or 900 °C. Under the conditions of their experiments they observed that for a low rank coal, 70%-90% of all the $N_2O$ produced appeared while the coal was undergoing devolatilization. The fraction dropped to 40% for a coal with a low volatile content. The figures reported by Hayhurst for $NO_x$ emissions ranged from 55% of the $NO_x$ arising from the volatiles in a low rank coal to 25% for a coal of high rank. They also noted that changing the bed temperature altered the ratio $[N_2O]/[NO_x]$ in the off-gases and not the total quantity of oxides of nitrogen emitted. They reported that lower concentrations of $O_2$ resulted in slightly less $N_2O$ and $NO_x$ being produced. The observations they made during devolatilization conformed to effectively all the fuel-nitrogen in the volatile matter being converted to HCN. Nitric oxide was then produced, most probably heterogeneously, on the sand from CN radicals, which alternatively produced NCO radicals. They proposed the probable generation of $N_2O$ during devolatilization by reaction (1-3) occurring in the gas phase. As for burning of char in a fluidized bed, they noted the large size of the particle (> 1 mm) controlling the mass transfer of oxygen to the particle. Oxidation was thus confined only to the exterior of the char. In addition, they observed that CO, together with reaction between NO and solid carbon, are important in converting NO to $N_2$. They noted that this is the reason behind the lower yield

of NO from char-N than from volatile-N.

Pels et al. [45] measured and studied the emissions of $N_2O$ and NO during fluidized bed combustion of six coals and their chars. Fractional conversion of coal-bound nitrogen to $N_2O$ was found to increase with coal rank. A similar, although much weaker, trend was observed for NO. They also observed that, for a given coal, the sum of coal-N conversions to $N_2O$ and NO is practically constant over the whole temperature range (1000-1300 K). They evaluated the contributions to $N_2O$ and NO emissions from gas phase reactions and from heterogeneous reactions by comparing emissions from coal and char combustion. Results showed that, although only a relatively small proportion of coal-N was released with the volatiles, gas phase reactions account for the majority of $N_2O$ emitted from a fluidized bed combustor. They explained this by the efficient heterogeneous reduction of $N_2O$ to $N_2$, which occurs on the char surface immediately after $N_2O$ is formed from char-N. In contrast to $N_2O$, they discovered that char-N was the main source of NO.

Oude Lohuis et al. [46] used a set of coals, ranging in rank from lignite to anthracite, as well as chars of some of these coals in a laboratory scale fluidized bed reactor to assess the influence of fuel properties and the major process related parameters on $N_2O$ and NO formation during low temperature coal combustion. They observed that the main parameters that affect $N_2O$ formation from fuel nitrogen were the nitrogen content of the coal, the temperature and the coal rank. In addition, decreasing temperatures resulted in increasing $N_2O$ formation and simultaneously decreasing NO formation. Based upon their work, bituminous and anthracite coals showed substantially higher $N_2O$ yield. Formation of $N_2O$ resulted from the combustion of the volatiles as well as from the char.

Oude Lohuis and coworkers also observed that for all coals, the sum of the NO and $N_2O$ yield remained more or less constant over the whole temperature range. Based on this observation they suggested an inverse relationship of NO and $N_2O$ formation as a function of temperature. From their work they concluded that NO and $N_2O$ are formed from a common gas phase precursor, probably HCN. They proposed that this mechanism is based on the gas phase oxidation of HCN to HCNO and NCO, which subsequently react with NO to generate $N_2O$ following reactions 1-4, 1-6 and 1-3 sequentially. They also observed the formation of $N_2O$ from char combustion. They proposed that probably the char nitrogen is partially entering the gas phase reaction scheme (reaction 1-4, 1-6 and 1-3 sequentially) by gasification reactions to CN species.

Aho et al. [47] investigated the formation and destruction of $N_2O$ under dilute pulverized coal combustion conditions in an entrained-flow reactor. They studied the effects of temperature, atmosphere (oxidizing and reducing) and reaction environment (homogeneous and heterogenous). They measured the $N_2O$ by on-line FTIR spectroscopy. They reported no $N_2O$ formation above 950 °C. At oxygen concentrations below 1.5% and in the presence of CO, they reported rapid destruction of the formed $N_2O$ at 830 °C and above. At higher oxygen concentrations, destruction was reported to occur more slowly but none below 900 °C. Aho and coworkers did not report any heterogeneous reactions to be prominently responsible for any noticeable increase in destruction of $N_2O$ in the dilute fuel-air suspension.

Hulgaard et al. [48] studied the effect of NO on formation on $N_2O$ in a bench-scale entrained flow reactor. They discovered that the presence of additional NO in the flow enhances the production of $N_2O$ further suggesting that NO and NCO are the primary

precursors to formation of $N_2O$. Khan et al. [49] confirmed Hulgaard's findings for NO concentrations less than 400 ppm. They found that presence of NO had an increasing effect on formation of $N_2O$ until the concentration of NO was increased beyond about 400 ppm. At this point the concentration of $N_2O$ experienced a drastic decrease.

Suuberg et al. [50] in a study suggested two regimes for the reaction of NO with carbon which involve rate control by site creation in the low temperature regime and dissociative chemisorption in the high temperature regime. They proposed that examination of the rates and dynamics of the NO-carbon reaction must always establish in which temperature regime the processes of interest are occurring. Therefore, there is no possibility of deriving "general" conclusions concerning mechanism without careful consideration of this point. In addition, based on their observations, the rates in the low temperature regime appear to be generally more sensitive to any factors that affect active site populations than are rates in the high temperature regime. In their opinion, it is clear that the process of NO destruction (or gasification) is somehow different at the higher temperatures. Additionally, they do not discount the possibility of a different set of active sites beginning to dominate the rate due to a different reaction pathway becoming favorable, or perhaps as a result of an increase in available active sites a second step in a reaction pathway becomes limiting.

Wang et al. [51] studied the $NO_x$ release from a wide range of chars prepared in an entrained-flow reactor from coals and vitrinite concentrates of different rank and geographic origin. They observed that the fractional conversion of char-N to $N_2$ was roughly constant throughout the suite of chars. In addition, the HCN level was significantly lower for the chars than for the parent coals. They correlated the conversion of char-N to NO with char

reactivity and proposed that the intrinsic reactivity of the char was important in determining the reduction of NO on the carbon during combustion.

It has been demonstrated that the char active surface area is a relevant parameter for evaluating the reactivity of low and high temperature coal chars. Rashid Khan et al. [52] worked on modeling of oxygen chemisorption kinetics on coal char. They pointed out the importance of this study being due to the mechanisms involved in oxygen chemisorption, as heterogenous combustion is influenced by the chemisorption of oxygen on char surface. For the purpose of this study they monitored the rates of oxygen uptake by char at a range of chemisorption temperatures using a thermogravimetric balance.

Kunii et al. [53] and Beer et al. [54] confirmed the reduction of nitric oxide by carbon surfaces in the presence of oxygen. They proposed that the reduction of NO is either by a direct reaction involving CO and NO catalyzed by carbon surface

$$NO + CO \longrightarrow CO_2 + \tfrac{1}{2} N_2 \qquad (1\text{-}9)$$

or involvement of a reaction with CO and chemisorbed oxygen on the char surface resulting in formation of a carbon active site and ultimately reacting with NO (Chan et al., [55] Levy et al. [56] and Yamashita et al. [57]):

$$CO + C(O) \longrightarrow CO_2 + C_f \qquad (1\text{-}10)$$

$$NO + C_f \longrightarrow C(O) + \tfrac{1}{2} N_2 \qquad (1\text{-}11)$$

where C(O) and $C_f$ correspond to the char surface chemisorbed oxygen and the carbon active site, respectively. Chan and coworkers proposed that at high temperatures due to desorption of the chemisorbed oxygen and consequently formation of CO, the effect of CO on NO/char

reaction diminishes. This in turn, would result in formation of less carbon active sites.

Song et al. [58] studied the reactions of organically-bound nitrogen in coal char during combustion in a laboratory furnace using size-graded char particles prepared by the pyrolysis of a Montana lignite. They observed that the time-resolved variations of nitrogen-to-carbon ratio during char oxidation have revealed that there is no selectivity between nitrogen and carbon loss due to oxidation but that the char nitrogen can undergo devolatilization in parallel with the oxidation.

Wendt et al. [59] theoretically examined the physical and chemical characteristics that influence the conversion of fuel nitrogen to nitrogen oxides during coal char combustion by using a simplified model in which nitric oxide was an intermediate product between fuel nitrogen and $N_2$. Their results showed that for larger particles at low temperatures, such as are applicable to fluid by combustion, pore size is important, and that low nitric oxide emissions are favored by long narrow pores. They pointed out that at higher temperatures, pore size is not a major factor because then everything of interest occurs at the pore mouth, and diffusion within the pore is not a factor. They suggested that at low temperatures, however, both diffusion as well as homogeneous and surface reaction are important.

In addition, in their studies they examined the role of diffusion and reaction in a stagnant film surrounding the char particle. Based on this, they showed that the carbon monoxide concentration in the free stream was a more important variable than the $O_2$ concentration in determining the overall effect of excess air.

Harding et al. [60] studied the NO release from the isothermal combustion of coal chars. Chars for the purpose of their studies were prepared in an entrained flow reactor with a zone

length of 1.66 m and a particle residence time of approximately 1 second at 1273 K in a nitrogen atmosphere. They studied the isothermal combustion of low rank coal chars at two different temperatures. At 873 K the combustion took place where the reaction was under chemical control while at 1273 K, the reaction was under diffusion control. They observed that the $NO/(CO+CO_2)$ ratio increased with increasing burn-off for combustion at both temperatures. In addition, they noted that the clear correlation of NO/char-N with gasification rate observed for isothermal combustion at 873 K was less evident when the rate was normalized by the surface area of the char. They suggested that this indicated the porous structure to be a factor that influenced the gasification of the char under chemical control and also the conversion of char-N to NO during combustion.

Harding and co-investigators also observed that coal chars that have lower surface areas tend to be associated with higher levels of NO release. They proposed that this is an indication of lower reactivity and available surface area of the high rank coal chars giving rise to higher NO/char-N conversion ratios due to a lower reduction of the primary char oxidation product NO on the surface and/or in the pores of the char.

One way of understanding the role of char nitrogen in formation of $NO_x$ in an oxidation process is by examining various model chars under the same conditions. This method has proven valuable due to the fact that models can eliminate some of the variables which create unnecessary complications. In addition, since models are usually the basic constituents of char and coal macromolecules, their analysis can potentially open doors to better understanding of many processes involving these complex molecules.

Wang and Thomas [61] used thermogravimetry and mass spectrometry techniques to

analyze the evolved gases from their model chars (cocarbonized acridine and naphthol). They observed a factor of two to three increase in the $NO/CO_2$ and NO/CO ratios at temperatures corresponding to 40% burn-off and above, leading them to conclude that at lower temperatures the char nitrogen reacts slowly to produce NO. This slow reaction in turn leads to retention of nitrogen in char with increasing burn-off. They also concluded that the production of NO and HCN (detected in small quantities) is a direct function of gasification temperature. Wang and Thomas repeated the same series of studies with a different kind of model char (cocarbonized carbazole and naphthol) and obtained the same behavior and profiles except at lower temperatures where the NO profiles for both chars were found to consist of two distinct peaks, possibly corresponding to different types of nitrogen in the chars.

It has been known that the mass spectrometry technique, although known as a powerful technique in detecting and analyzing various kinds of gas mixtures, can encounter complications and ambiguities because of the (at nominal resolution) of $N_2$ and CO m/z 28, $N_2O$ and $CO_2$ m/z 44, and $NO_2$ and $C^{16}O^{18}O$ m/z 46. Thomas et al. [62] suggested that these complications and ambiguities can be eliminated by the use of carbon 13 labeled compounds. The model chars used in their processes mainly consisted of nitrogen doped $^{13}C$. In their char gasification processes in a 20% oxygen in argon environment they observed release of more $N_2O$ than NO. In addition they observed a bimodality in NO and $N_2O$ evolution profiles with two distinct peaks. They proposed that this bimodality is due to two principal nitrogen functionalities in the model chars, which do in turn give rise to different relative quantities of NO and $N_2O$. Another important observation in their series of experiments involved the

dependency of $N_2O$ release on the types of chars prepared for the purpose of these experiments. They observed that chars prepared at lower temperatures have a higher $N_2O$ release compared to those prepared at higher temperatures.

Houser et al. [2] did experiments with model compounds such as pyridine, HCN, and benzene/HCN in both plug- and stirred-flow reactors. They discovered that at low temperatures and/or concentrations the fuel nitrogen was converted to primarily $N_2$ and $N_2O$. The NO release profiles showed a maximum at lower temperatures and concentrations for these model compounds. Based on their observations along with calculations related to the previously reported rate constants they also concluded that $N_2O$ and NO are produced by a common precursor with neither $N_2O$ nor NO formed sequentially from the other. In addition, they proposed that $N_2O$ and NO follow opposite trends as a function of temperature, and below a certain temperature (which is concentration, fuel type, and flow rate dependent), NO yield from fuel-nitrogen oxidation becomes minor, whereas that of $N_2O$ becomes major.

Wang et al. [64] studied the release of nitrogen species from model carbons derived from high pressure co-carbonization of carbazole and naphthol in argon using a thermogravimetric analyzer coupled to a mass spectrometer. The $NO/CO_2$ and NO/CO ratios increased substantially with increasing burn-off over the range of gasification temperatures 873-1273 K. They reported detection of small amounts of HCN. Further, comparison with the results for carbons derived from acridine and naphthol showed that (1) the carbazole-naphthol carbon was more reactive at a given temperature in the chemical-control region, (2) the $CO/CO_2$ ratio was usually higher for the carbazole-naphthol carbon, and (3) the $NO/CO_2$ ratio increased with increasing burn-off for both carbons. In addition, their results suggested

that during gasification of the nitrogen in the char the concentrations of nitrogen-containing species relative to the carbon species vary with reaction temperature, heat treatment temperature and burn-off.

# CHAPTER 2

# INSTRUMENTAL CONFIGURATION, EXPERIMENTAL DESIGN, AND MATERIALS PREPARATION

## 2.1 Introduction

Modern instrumental techniques, principally thermogravimetry (TG) combined with gas chromatography (GC), infrared spectroscopy (IR), and mass spectrometry (MS) were used to characterize the role of char nitrogen in formation of $NO_x$ in coal char and/or model char combustion processes. The instrument configurations of TG/(GC)/IR/MS, TG/GC/IR, and TG/GC/MS have been shown to provide important information about mechanisms of major pyrolysis and chemical reactions and to enable characterization and quality control of fossil fuels, natural products, and synthetic polymers.[64 & 65] In addition, quantitative detection and analysis of nitrogen in coal and char samples by means of GC/IR/MS analysis of combustion products and TG based microsimulation of combustion processes provide powerful new tools for studying the behavior of nitrogen functionalities as well as their concentration in coal during devolatilization and subsequent char oxidation.[66]

There are definite advantages to parallel usage of IR and MS detection systems. Although efficient preseparation of mixture components by GC is an essential concept for GC/MS type detection procedures, parallel use of IR and MS type detectors reduces this

concern significantly. As an example, consider an MS peak at m/z value 44, typically corresponding to both $N_2O$ and $CO_2$ molecules in combustion gases, in addition to a whole range of other possible molecular and/or fragment ions or isotope peaks. If the concentration of one of these is significantly lower than the other, a selected ion chromatogram obscures the lower component. However, use of IR in parallel with MS provides an alternative in analyzing these signals (Figures 2.1). In addition, the presence of certain molecules such as $N_2$ and $O_2$, due to their nonpolarizable nature, are not detectable by IR absorption (Figure

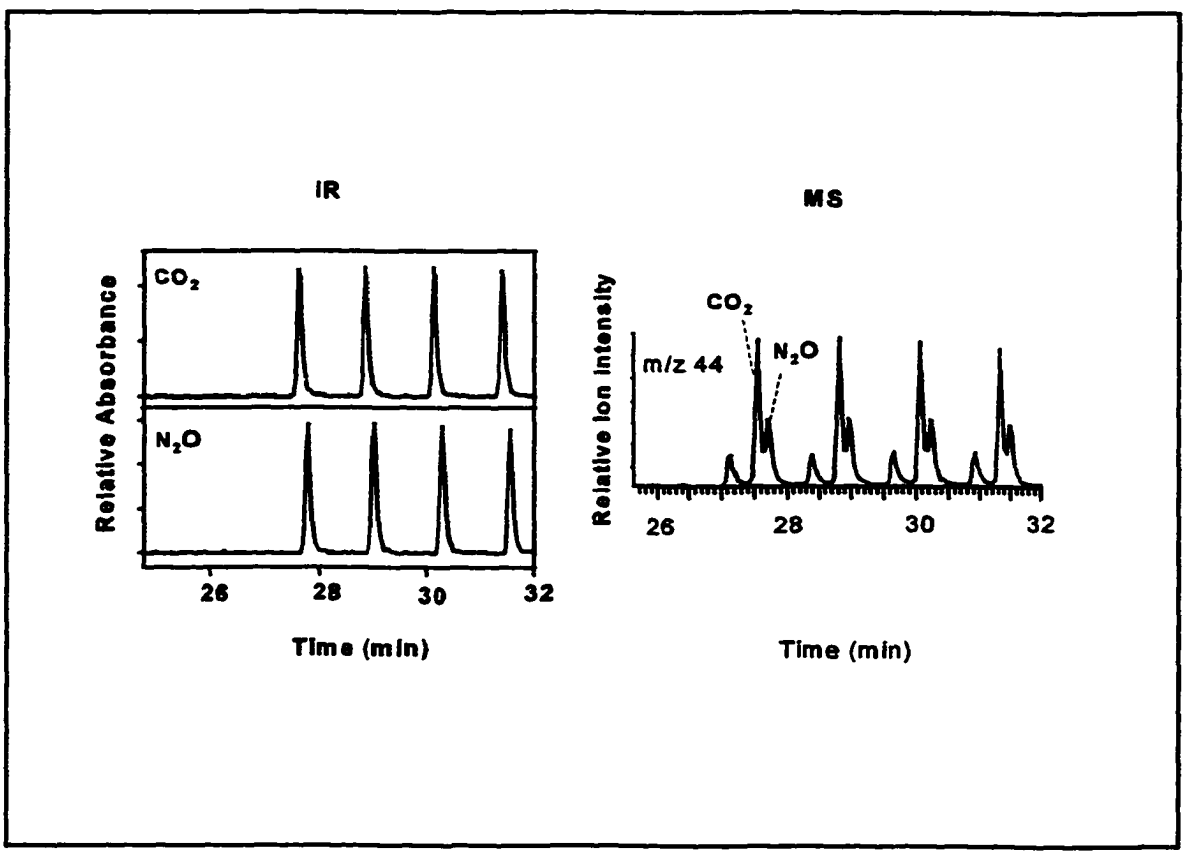


Figure 2.1 The IR and MS chromatograms for $CO_2$ and $N_2O$. At m/z 44 the MS profiles of these two compounds are only distinguishable under efficient chromatography separation. The IR chromatogram however, presents two noninterfering profiles even when no GC preseparation techniques is applied.

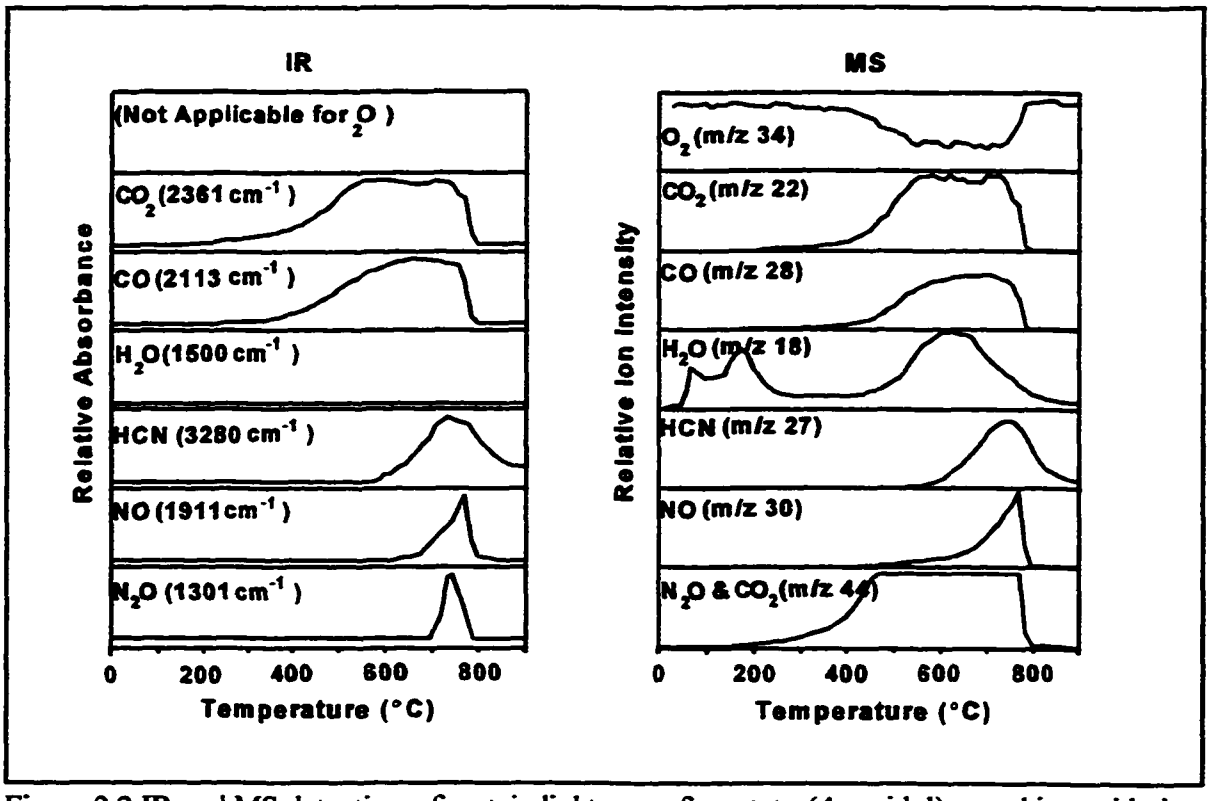


Figure 2.2 IR and MS detection of certain light gases from tetra(4-pyridyl)-porphine oxidation in 5% $O_2$ (in He) at 25 °C/min heating rate. The parallel usage of these two units provides a more efficient detection of certain compounds of interest as well as a validity check for the results obtained by only one technique.

2.2). Lastly, the validity of results obtained by one technique for a given compound can be confirmed by the other (Figure 2.2).

In spite of a sizeable body of experimental work, the inherent complexity and heterogeneity of the coal and resulting char remain an important factor impeding the complete understanding of the underlying reaction mechanisms and kinetics of $NO_x$ formation in char oxidation processes. Therefore, the need for simple model compounds are needed. The known presence of relatively high concentrations of nitrogen-containing functional groups (i.e. pyrrole, pyridine, etc.) and the absence of many potential interferants in these compounds makes the task somewhat easier.

## 2.2 Overall System Configuration

An overall schematic of the instrumental setup is presented in Figure 2.3. A Perkin Elmer high temperature thermogravimetry analyzer (TGA7), a Hewlett Packard 5890 gas chromatogram (GC), along with a Hewlett Packard 5965A infrared detector (IRD) and a 5971A mass selective detector (MSD) were used for these experiments. An electrically heated stainless steel transfer line (ultimetal tubing from Chrompack, 2m long, 0.53mm ID, 0.8mm OD, uncoated and methyl deactivated) runs from the TG system into the GC. The stainless steel line is connected to a porous layer open tubular (PLOT) column (5m long, 0.53mm ID) containing porous polymer (porapak Q from J & W Scientific). The column outlet flow is divided between two parallel transfer lines. Diameter and length of the two lines are selected to obtain a 1:1 split between IRD and MSD.

One of the essential parameters, that has to be carefully controlled during the transfer of evolved gaseous products to the detectors, is temperature. It is important to transfer these gaseous products at carefully controlled temperatures selected to prevent condensation and/or further reactions inside the transfer lines and columns. Alternatively, unavoidable condensation processes (because of the maximum operating temperatures of column and transfer lines) are designed to occur in a special section of wider bore quartz capillary tubing which can be readily replaced, if necessary. The temperature of the transfer line running from the TG to the GC system is controlled electrically. Electrical contacts welded to the ends of the line are connected to a VARIAC which controls the current output into the line. A K-type thermocouple is connected to the line halfway between the bridges to monitor the temperature of the line during a run. The line is insulated with two layers of Fiberfrax

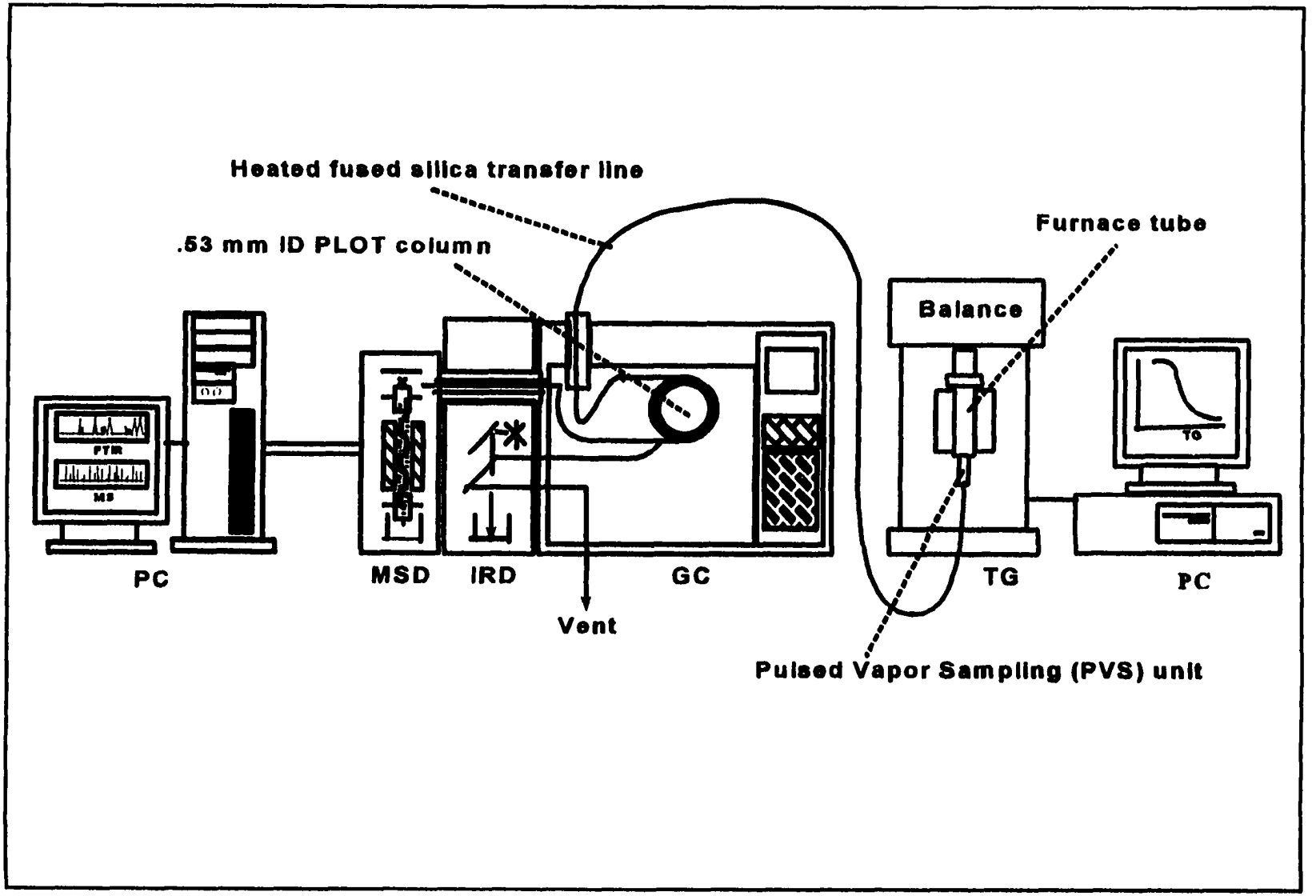


Figure 2.3 A schematic of the instrumental setup used for preparation of coal chars and model chars as well as the mechanistic and kinetic studies of their oxidation processes.

materials to prevent any significant heat loss during operation.

The line is connected to the TG system via a specially built interface. The interface not only provides a leak-free means of connection between the furnace tube and the quartz-lined stainless steel transfer line as well as a controlled condensation zone, but is also equipped with heater probes to control the temperature of the gaseous products leaving the furnace tube. A schematic of the interface is shown in Figure 2.4. The interface consists of a stainless steel Cajon union, a specially modified stainless steel fitting, aluminum heater blocks, a temperature sensor, and heater cartridges. The furnace tube end is fused to a quartz tube with the same OD as the fitting. The furnace tube and the fitting are coupled to each other by means of the Cajon union. When assembled, a 7 cm long quartz tube (3 mm OD and 1 mm ID) inside the fitting extends from the bottom of the fitting all the way up to 1 cm below the crucible inside the TG furnace tube. The transfer line is extended into the quartz tube about 2.5 cm from the bottom of the fitting and fixed in place by means of a stainless steel nut and ferrule assembly. When sampling is in progress the extended quartz tube provides a good means of carrying a sample of the effluent gases from the crucible into the stainless steel transfer line.

In order to perform suitable sampling of the gaseous products for detection a Automated Vapor Sampling (AVS) system was added to the interface. A schematic of this system connected to the interface is presented in Figure 2.5. The system is designed such that helium gas is continuously fed into the furnace tube at a certain flow rate via an inlet to the interface through the bottom, where the stainless steel transfer line is connected to the furnace tube. The flow rate adjustment is a function of the purge gas flow rate and the

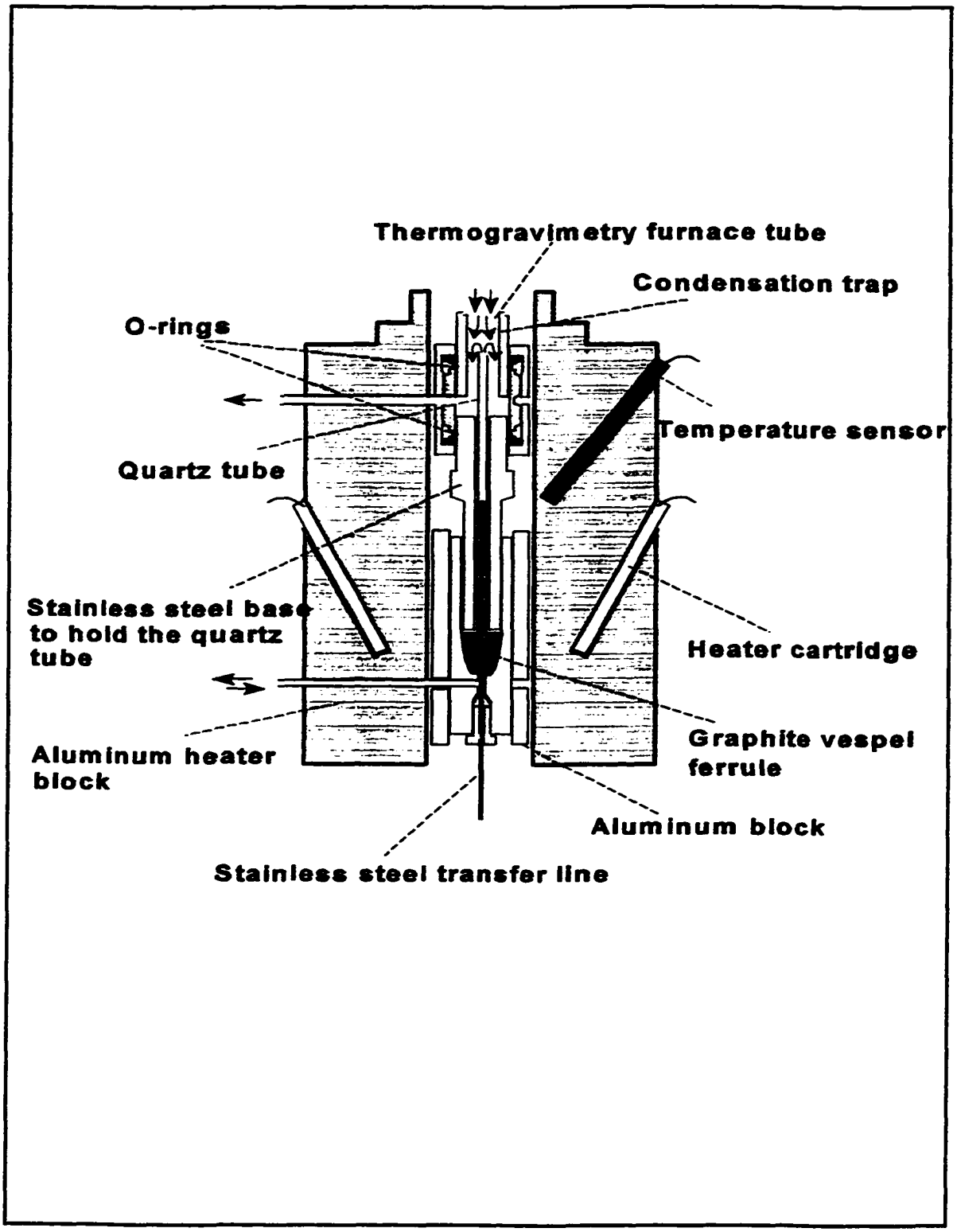


Figure 2.4 A schematic of the interface between the outlet of the TG furnace tube and the stainless steel transfer line. The interface is also capable of controlling the temperature of the gaseous products entering the transfer line by means of heater probes.

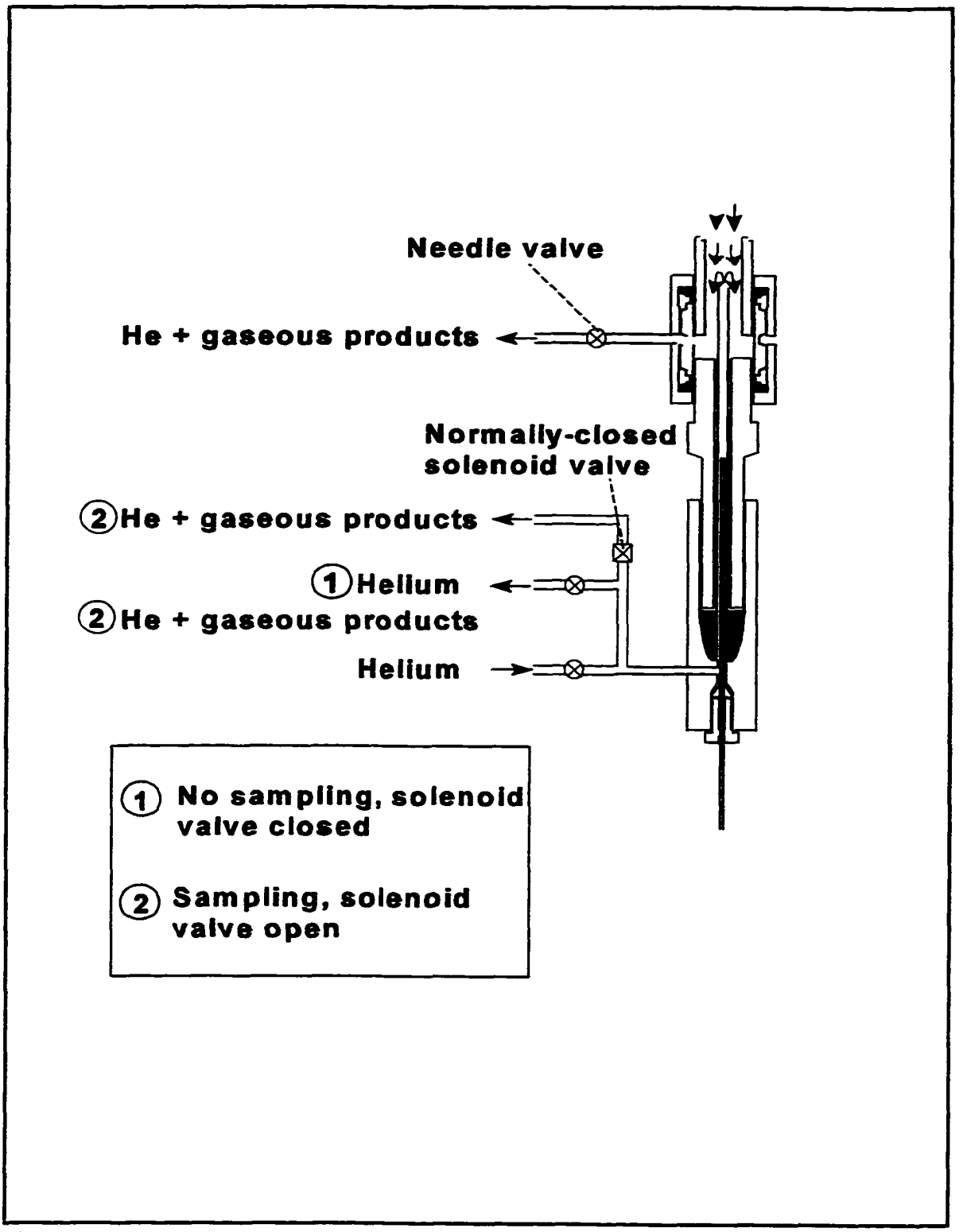


Figure 2.5 A schematic of the Automated Vapor Sampling (AVS) system. This system provides an efficient means for charomatography purposes. Note that various components of this system are described in Figure 2.4 .

pressure inside the TG furnace tube. To the same interface inlet a normally-closed solenoid valve is connected via a T-union. The solenoid valve is controlled by an electrical timer with adjustable pulse duration and period. To prevent any stagnation of gaseous products between the T-union and the solenoid valve, the volume is continuously purged by an extremely low flow of Helium (Figure 2.5). When no sample is taken (solenoid valve closed), the transfer lines and columns, and thus the IR and MS detectors, are continuously purged by He. When a sample is taken (solenoid valve open), the He flow into the furnace tube from the bottom is discontinued resulting in product gases flowing into the transfer line. When the solenoid valve is closed again at the end of the sample injection process the He gas flows back into the furnace tube and transfer line, carrying the product gases through the PLOT column into the IR and MS detectors. It should be noted that an outlet is also connected to the upper part of the interface to maintain a continuous purge inside the TG furnace tube and to maintain the required pressure in a more efficient manner.

The TG system consists of a quartz furnace tube and a highly sensitive microbalance (Figure 2.6). The furnace tube (15.5 cm long with 2.5 cm OD) passes through a cylindrical heating unit with a quartz tubing extension (7.5 cm long with 0.9 OD and 0.5 ID) fused to it at the bottom. A K-type thermocouple sits next to an alumina crucible hanging from a balance to monitor temperature and control the rate of heat transfer from the heater to the sample. A cylindrical heater block surrounds the furnace tube. While in operation, the crucible is hanging half-way from the top of the heater block and about 0.75 cm above the point where the quartz tube extension is fused onto the furnace tube. The microbalance is an electronic scale connected to the alumina crucible by means of a nichrome wire. The scale

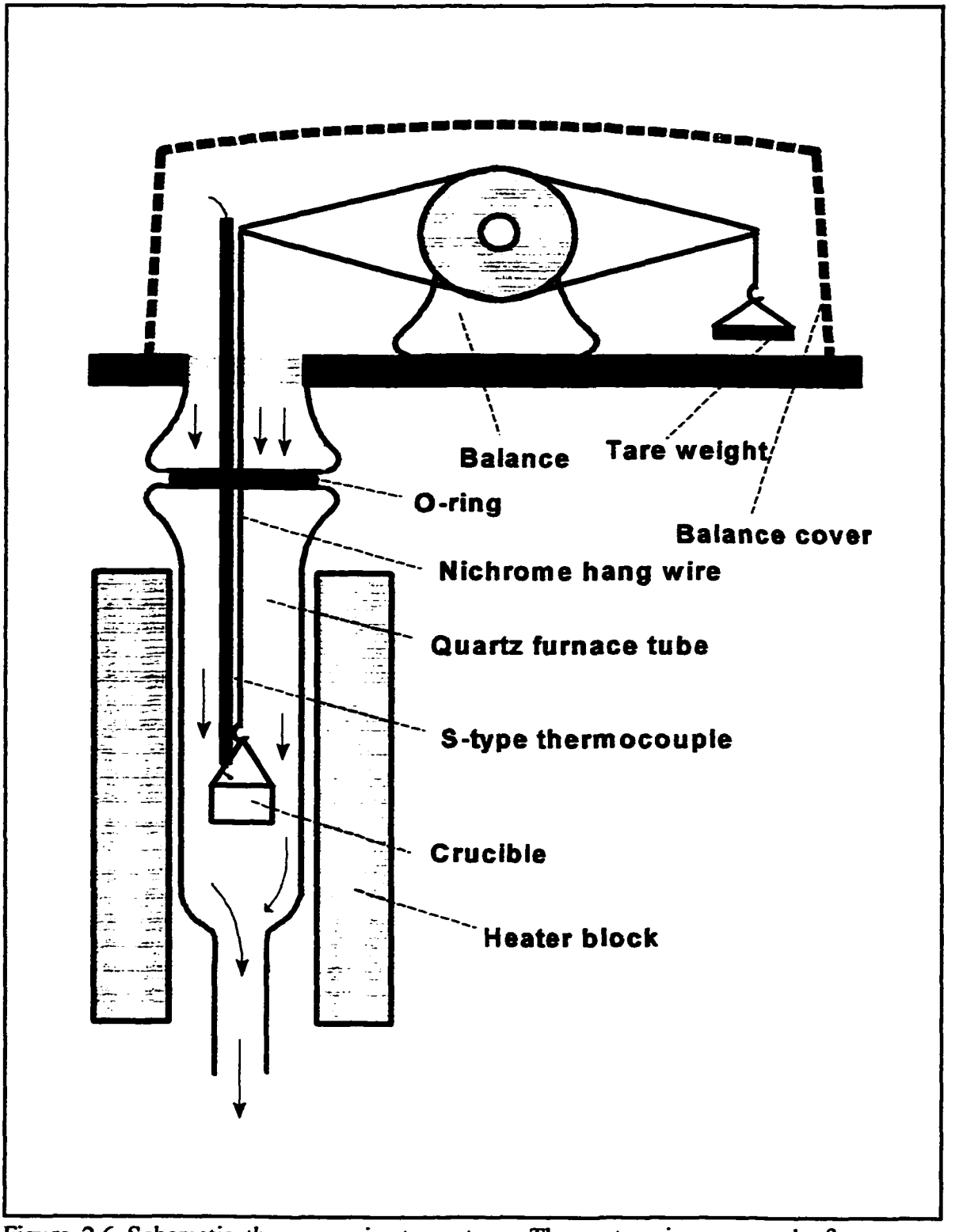


Figure 2.6 Schematic thermogravimetry setup. The system is composed of a reactor chamber (quartz furnace tube) surrounded by a cylindrical heater block and topped off with a microbalance.

is tarred by a certain weight which compensates for the weight of the crucible. The tare weight can be modified to accommodate heavier or lighter crucible weights. The furnace can operate from room temperature up to 1000 °C at heating rates of 0.1 to 40 °C/min. The TG system is controlled by means of a standard Perkin Elmer software program loaded onto an IBM-compatible 80286 computer. This program provides the user with direct control of various parameters as well as monitoring the weight loss percentage as a function of temperature during operation.

The GC system is a large oven with temperature programming features. The main purpose of this instrument is to separate various components of a gaseous mixture for detection. Separation is done solely by a GC column containing a triple layered sandwich of materials: polyamide coating surrounding the fused silica tubing, with a thin film of stationary phase material bonded to the inner tubing surface. As mentioned earlier, the column used for the purpose of these experiments is a porous layer open tubular (PLOT) column. This column contains a layer of adsorption material coated on the inner wall of the fused silica tubing. Gas-solid adsorption rather than a gas-liquid partitioning is the separation mechanism. This type of column is known to be suitable for analysis of light hydrocarbons, inert, sulfur and nitrogen gases at temperatures moderately above ambient.

The IR detector functions by passing a beam of infrared radiation through an interferometer and then the sample. The light is detected by a mercury cadmium telluride (MCT) detector that produces electrical signals. The interferometer is a device with a combination of fixed and moving mirrors that splits and then recombines the IR beam, creating an interference pattern. The IR source generates high radiation intensities over the

4000 to 550 wavenumber (2.5 to 20 micron wavelength) range. The sample flows through the flow cell assembly for detection. Inside the flow cell assembly there exists a light pipe, 12 cm long with gold plating inside to prevent light loss, with ends connected to two GC/IRD interfaces. The interfaces are transfer lines running from the GC oven into the IR system (Figure 2.3). Each interface is equipped with an electric heater and a K-type thermocouple. The temperature of each interface is controlled independently according to set points entered from the Chemstation software (a software that controls IR, MS and GC functions).

The MS detector operates by selectively accounting for the mass-to-charge ratio (m/z) of every ion. The sample first enters an ion source by means of an interface between the GC and the MS. Inside the ion source a filament produces large enough numbers of electrons to readily ionize one out of every $10^3$-$10^5$ sample molecules. A quadrupole or mass-filter then selectively transports ions from the ion-source into an electron multiplier. The electron multiplier is a funnel-shaped device with the top connected to a high negative voltage and the bottom to ground. Once a selected ion enters the funnel and impinges upon its surface, electrons are produced and released. These electrons then keep impinging upon the surface of the funnel and multiply as they progress towards exit. The burst of electrons leaving the multiplier at a preset mass-to-charge ratio defines the identity of the sample. It should be noted that in order to control the temperature of the sample flowing into the MS system, the interface between the GC and the MS is also equipped with a heater and a temperature sensor (temperature resistance thermometer) which are controlled by the Chemstation software.

The Chemstation software from Hewlett Packard (Ver. A.00.02) provides the user with the capability of controlling and monitoring the GC, the IR, and the MS systems

simultaneously. The software is operated by means of an IMB-compatible Pentium 90 Mhz computer with 16 Mb of RAM and 500 Mb of hard drive storage. The software is interfaced to both GC and IR systems via a Chemstation interface and a HPIB control card. The MS, however, is interfaced only by the Chemstation interface card.

As mentioned earlier, the interface between the TG furnace tube and the stainless steel transfer line is equipped with heater probes and a temperature sensor to control and monitor the temperature of the gaseous products carried into the transfer line. In addition, the same heater probes and temperature sensor are also used in the interface (transfer line) between the GC and the MS. Since the GC detectors were not used for the purpose of these experiments, their corresponding electrical ports for controlling and monitoring heater probes and temperature sensors, respectively, were dedicated to those of the interfaces between the TG furnace tube and the stainless steel transfer line, and the GC oven and the MS system. This provides the user with the capability of controlling and monitoring the aforementioned temperatures with the Chemstation software as well.

## 2.3 Model Char Preparation and Characterization

As mentioned earlier one way to examine the formation of $NO_x$ in coal char oxidation processes is by investigating the same process with model compounds. Preparation and characterization of these compounds is not necessarily trivial. These compounds were selected based on the presence of high concentrations of nitrogen containing functional groups (i.e., pyrrole, pyridine, etc.) and the absence of potential interfering components.

Two model compounds containing only carbon, hydrogen, and nitrogen, namely

tetraphenyl-porphine (FW=614.75) and tetra(4-pyridyl)-porphine (FW=618.71) (chemical structures shown in Figure 2.7) were selected for the purpose of these experiments. These compounds were selected since they both contain functional groups similar to the ones found in coal (pyrrolic groups in both and pyridinic group in tetra(4-pyridyl)-porphine). These compounds were devolatilized in ultra high purity He form 10 to 700 °C at 10 °C/min heating rate, in the thermogravimetry system described earlier. During this devolatilization process about 50% of both materials was found to be gasified with the rest remaining as char. The weight remaining percentage versus temperature for tetraphenyl-porphine and tetra(4-

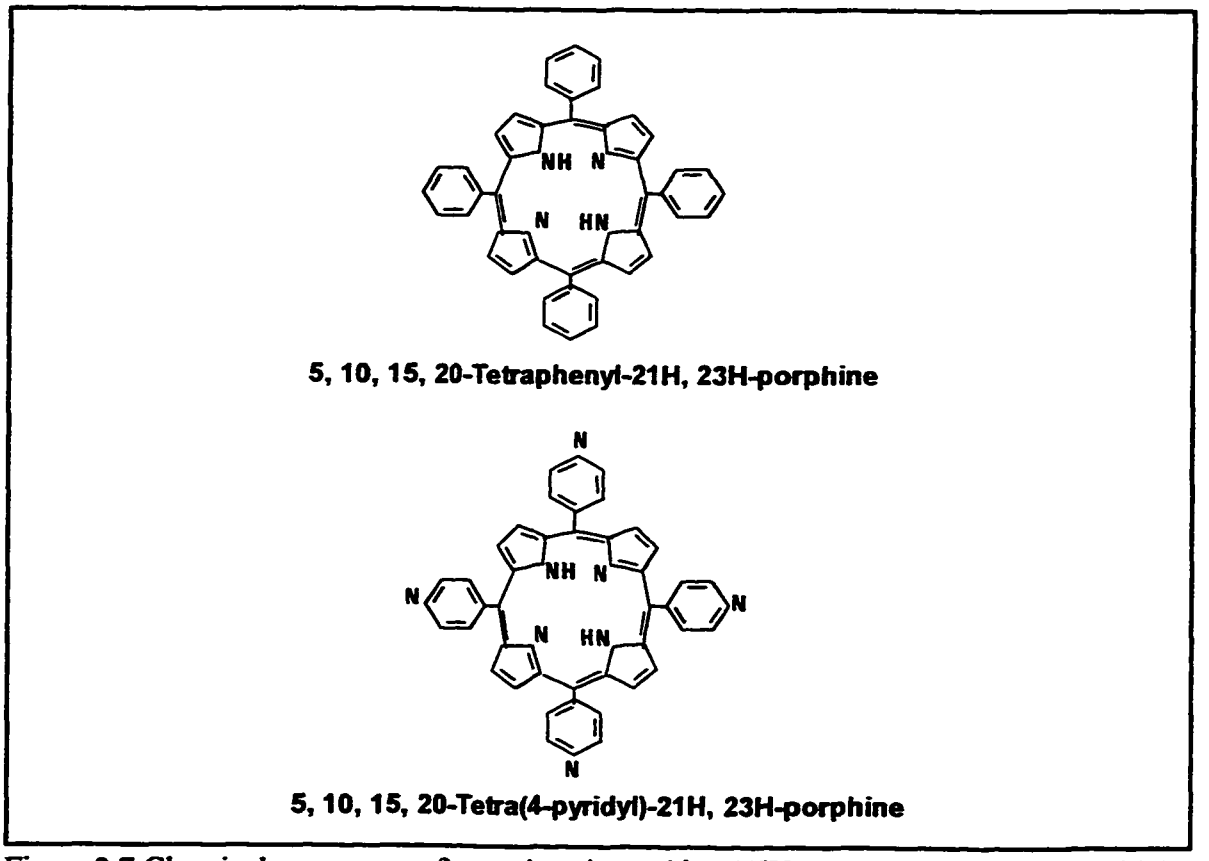


Figure 2.7 Chemical structures of tetraphenyl-porphine (FW=614.75) and tetra(4-pyridyl)-porphine (FW=618.71). The chars from these two compounds were used as model compounds.

pyridyl)-porphine during the char making processes are presented in Figure 2.8. It should be noted that the TG profiles presented in this figure are well reproducible.

The appearances of both chars are rather different. Tetraphenyl-porphine char is in the form of a hard black block, whereas for the tetra(4-pyridyl)-porphine the char is in the form of a very fine black powder. In addition, the density of the tetraphenyl-porphine char is almost twice as high as that of tetra(4-pyridyl)-porphine char.

In order to investigate the contents of these chars elemental analysis was performed on the model compounds and their corresponding chars. The results of these analyses are presented in Table 2.1. It should be noted that the analyses on model compounds were performed only to examine the accuracy of the technique used in this respect. As can be observed in Table 2.1, the carbon, hydrogen, and nitrogen weight percentages of the model compound match the corresponding calculated weight percentages from the chemical structures closely.

To develop an understanding of the chemical structures and nitrogen functionalities of these model chars, more analyses were performed on these materials. To investigate the composition and chemical state of the near surface region ESCA (electron spectroscopy for chemical analysis) was performed on these samples (Table 2.2). This technique is known to be a nondestructive, surface-sensitive analytical technique which provides qualitative and semiquantitative elemental composition of the first 5 nm thickness of a solid and continues to be one of the most widely used in the surface analysis schemes.[67 & 68] Additionally, in this technique, oxidation and/or bonding of the constituent elements can be detected by the chemical shifts of the observed signals.[69] From this investigation it was determined

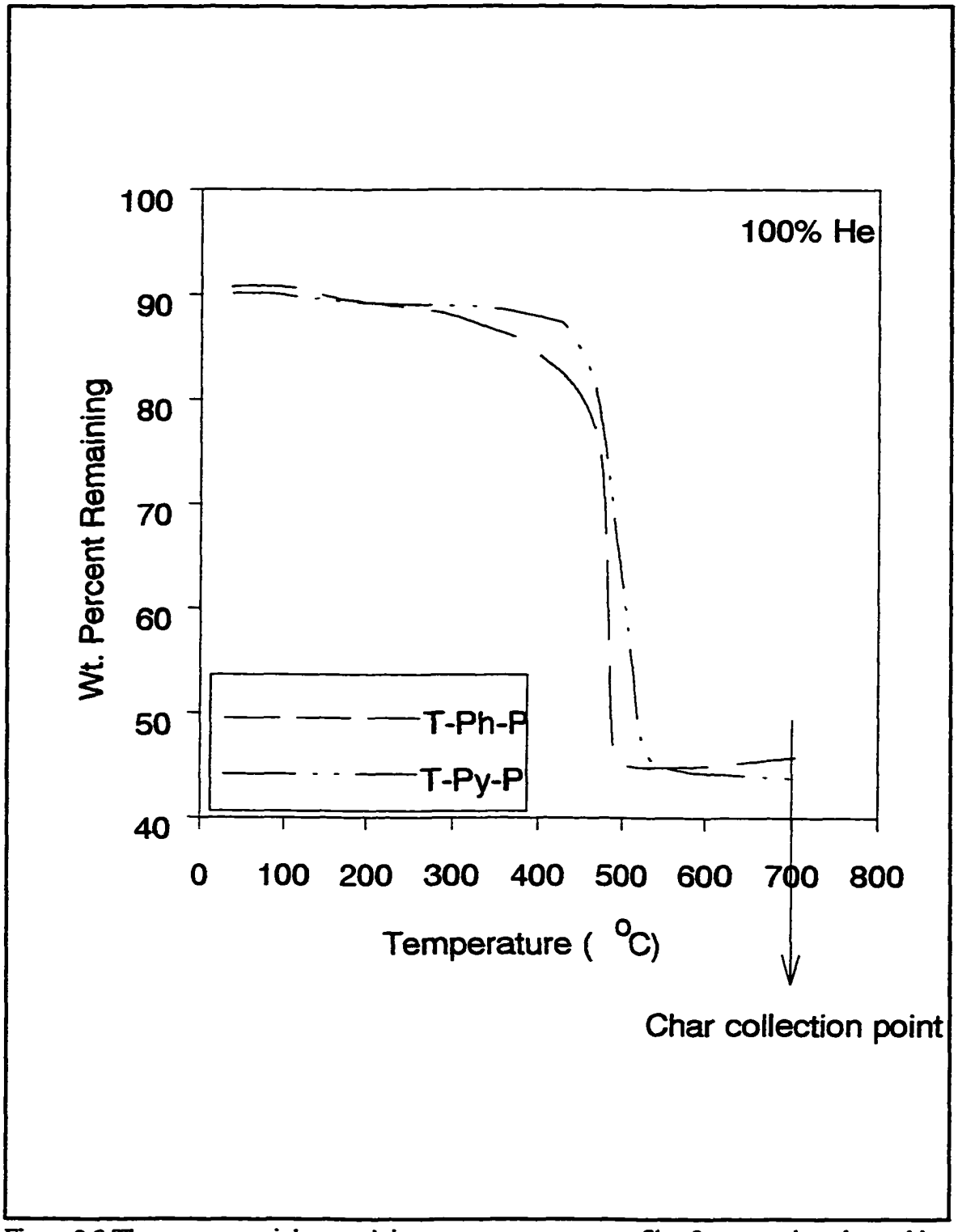


Figure 2.8 The percent weight remaining vs. temperature profiles for tetraphenyl porphine and tetra(4-pyridyl) porphine during the char preparation processes in ultrahigh purity helium from 20 °C to 700 °C at 10 °C/min heating rate in the thermogravimetry system.

Table 2.1 Elemental analysis of the model compounds and their corresponding chars. The calculated values of C, H and N percentages were obtained from the chemical structures of these compounds (Figure 2.7).

| Materials | Measured | | | Calculated | | |
|---|---|---|---|---|---|---|
| | C% | H% | N% | C% | H% | N% |
| Tetraphenyl Porphine | 86.5 | 5.09 | 8.46 | 86 | 4.89 | 9.12 |
| Tetrapyridyl Porphine | 78.3 | 4.64 | 17.1 | 77.7 | 4.21 | 18.1 |
| Tetraphenyl Porphine Char | 89.3 | 1.89 | 8.94 | - | - | - |
| Tetrapyridyl Porphine Char | 82.8 | 1.48 | 14.3 | - | - | - |

Table 2.2 XPS analysis of model char samples for pyridinic, pyrrolic and quaternary nitrogen functionalities. Note that in both model compounds pyridinic and pyrrolic moieties are the major nitrogen functionalities. In addtion, the presence of pyrrolic and pyridinic nitrogen in both model chars was also confirmed by GC/MS analysis of hydrogasification products.

| Materials | Nitrogen Functionality (Mole Percent) | | |
|---|---|---|---|
| | Pyridinic | Pyrrolic | Quaternary |
| Tetraphenyl Porphine Char | 31 | 63 | 6 |
| Tetrapyridyl Porphine Char | 44 | 54 | 3 |

that pyrrolic and pyridinic nitrogen functionalities with pyrrolic slightly having the upper hand are the major nitrogen functionalities in these chars (Table 2.2). The presence of pyrrolic and pyridinic nitrogen moieties in both chars was also confirmed by GC/MS analysis of hydrogasification products.

Another important characterization technique used for determining the chemical structure of these model chars is nuclear magnetic resonance (NMR). This technique has been applied for characterizing coals and coal-chars extensively.[70 & 71] Briefly, in this technique a number of interactions occur between the magnetic moments of spins or between the spin and the magnetic field. In these interactions spin is accompanied by a magnetic moment, so that nuclie with spin tend to become oriented in a magnetic field. This technique as well as ESCA and GC/MS hydrogasification of products, proved the fact that pyrrolic and pyridinic nitrogen moieties are the major nitrogen functionalities in these model chars.

## 2.4 Coal Char Preparation and Characterization

A suite of three coals, Pittsburgh #8 (hvAb), Wadge (PSOC-1498, hvCb) and Lower Hartshorne (PSOC-1521, lvb) were selected for the purpose of these studies. Chars from the two latter coals (PSOC-1498 and PSOC-1521) were prepared exactly in the same manner as for the model compounds. It should be noted that these coals were obtained form the Penn State Coal Sample Bank. Parent coals were placed in the thermogravimetry furnace tube under continuous ultrahigh purity helium purge. The devolatalization process was then performed from room temperature (20 °C) up to 700 °C at a heating rate of 10 °C/min in the thermogravimetry system. A schematic of the char preparation weight loss profiles for these

two coals as a function of temperature is illustrated in Figure 2.9. During this devolatalization process about 30% of both materials was found to be gasified with the rest remaining as char. It should be noted that the TG profiles presented in this figure are well reproducible. Char from Pittsburgh #8 was prepared by the combustion group in the U-shaped furnace at the University of Utah Advanced Combustion Engineering Research Center. To investigate the C, H and N quantities, elemental analysis was performed on all three chars. Results of these analyses are presented in Table 2.3.

## 2.5 Thermogravimetry Furnace Tube Configurations

The original thermogravimetry tube furnace is shown in Figure 2.6. In this configuration as explained earlier, an alumina crucible hangs from a balance by means of a nichrome wire. A fixed quantity of 20 mg sample in crucible was used for the purpose of these experiments. In this design the material containing crucible, if not fully, represents to some extent a bed, and therefore, the overall design can be referred to as a fluidized bed reactor. The furnace tube has a large enough inner diameter such that considerable spacing has been provided around the crucible for the purge gas to carry the evolved gaseous products out of the crucible. The short distance between the crucible and the sampling probe inlet (0.5 cm), however, gave rise to a very specific problem. Lack of reproducibility in results from repetition of identical experiments led us to the belief that the evolved gases traveling from the crucible to the sampling probe inlet did not experience sufficient mixing with the carrier gas. An effort was also utilized to obtain a correction factor to compromise for this scenario. Unfortunately, the experiments involved appeared to be tedious,

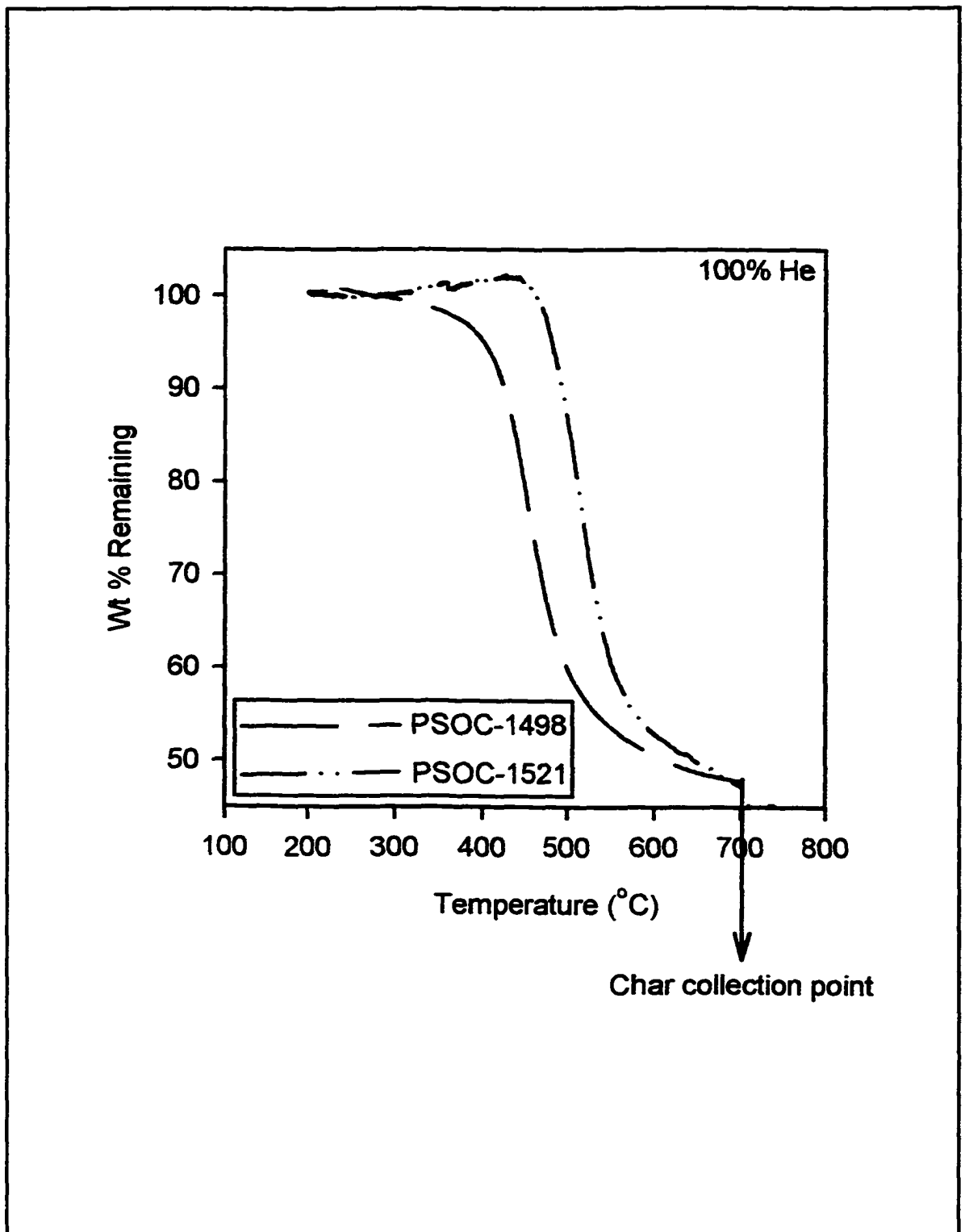


Figure 2.9 The percent weight remaining vs. temperature profiles for PSOC-1498 and PSOC-1521 coals during the char preparation processes in ultrahigh purity helium from 20 °C to 700 °C at 10 °C/min heating rate in the thermogravimetry system.

Table 2.3 Elemental analysis as well as rank information for the three char precursor coals used in these experiments.

| Coal Chars | Coal Rank | C% | H% | N% | Others |
|---|---|---|---|---|---|
| PSOC-1521 | lvb | 81.22 | 2.26 | 2.03 | 14.49 |
| PSOC-1498 | hvCb | 82.32 | 2.08 | 1.7 | 13.9 |
| Pitt #8 | hvAb | 68.08 | 0.7 | 1.14 | 30.08 |

problematic and lacked overall accuracy.

In order to solve this problem, a different design of furnace tube with a smaller inner diameter (0.5 cm ID and 0.9 cm OD) was utilized (Figure 2.10). The material of construction (quartz) and the length (15.5 cm) of the new furnace tube were selected to be the same as the original tube to meet the standards of the thermogravimetry system. Quartz wool was selected as the bed material to hold the powdered samples used and ultimately to replace the crucible. In order to eliminate the effect of sample size on the overall outcome of these experiments a similar sample quantity (20 mg) was also used. When an experiment in progress, the carrier gas and the evolved gaseous products traveled through the sample as well as the quartz wool, experiencing a more efficient mixing process. To enhance the mixing process even further, the sampling probe inlet was set at a distance of 1 cm below the bed to allow longer residence time in the tube for utmost mixing efficiency. It should be noted that the flow rate of the carrier gas in the coal char experiments (15 ml/min) was about 1/4 of that done with the model chars (60 ml/min). This was done due to the fact that the nitrogen content of the coal chars is approximately 1/10 of that of model chars. As a result, less dilution of the evolved gaseous products from coal char oxidation appeared to result in a better detection of the nitrogen products of interest. In addition, due to replacement of the

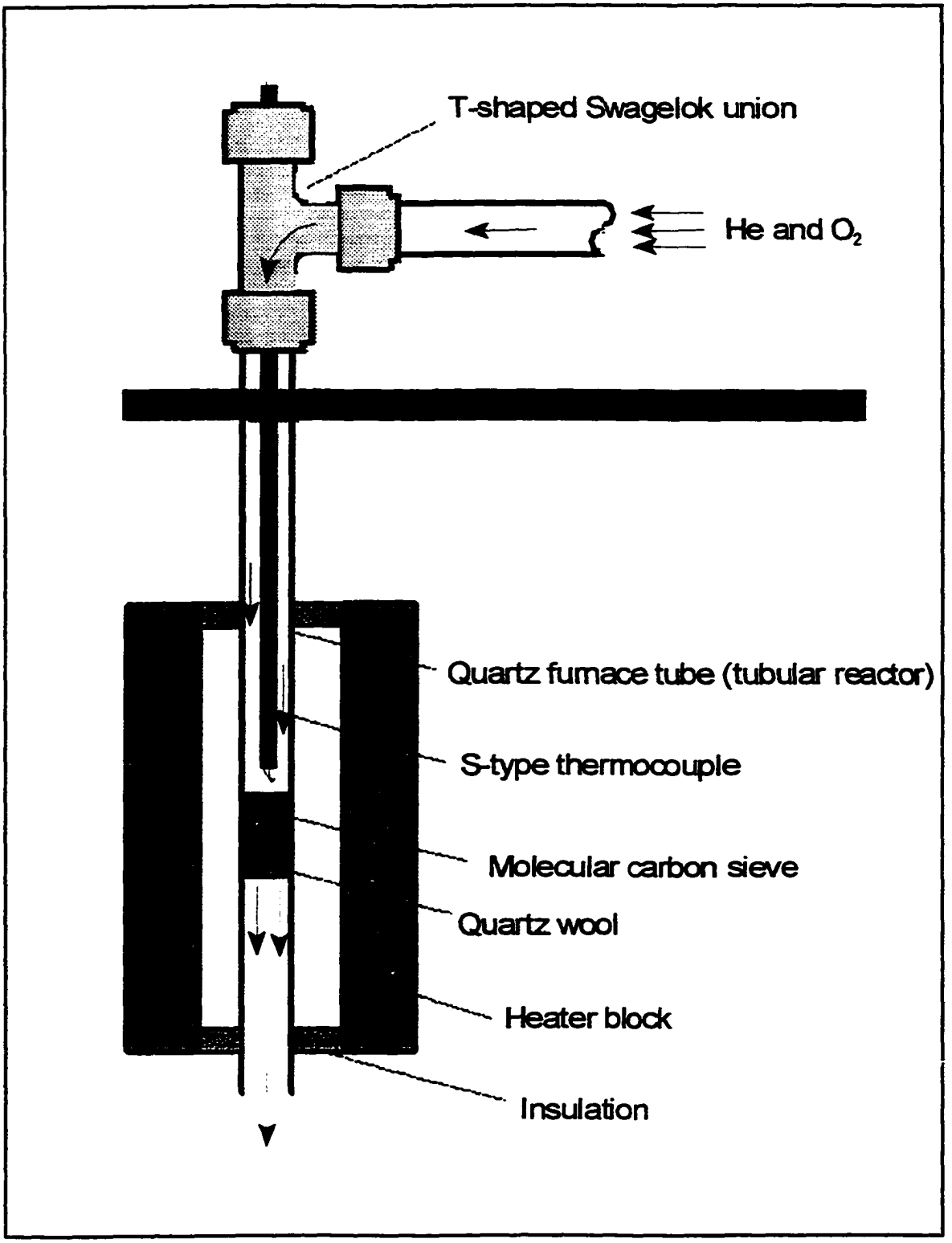


Figure 2.10 Schematic tubular reactor thermogravimetry setup. The system is composed of a reactor chamber (quartz furnace tube) surrounded by a cylindrical heater block and a sample bed supported by a bed of quartz wool.

crucible with the quartz wool (bed) the balance of the thermogravimetry system was not used any further. The heater block of the original design was the only component of the thermogravimetry system that was utilized in this configuration.

# CHAPTER 3

# REACTIONS OF NO, $N_2O$ AND HCN WITH CARBOSIEVE, IN THE PRESENFCE AND THE ABSENCE OF $O_2$

## 3.1 Introduction

Coal char oxidation involves a complex fabric of primary as well as secondary, and homogeneous (gas phase) as well as heterogeneous reactions that one can attempt to unravel by performing experiments on relatively simple model compounds under well-defined experimental conditions. Exposing carbon, in the form of carbon molecular sieve (Carbosieve) particles (Applied Science Laboratories Inc.), to various concentration levels of NO, $N_2O$ and HCN in the presence and absence of oxygen enables detection of secondary homogeneous (gas phase) as well as heterogeneous reaction pathways, including possible physicochemical and/or chemical incorporation and activation processes. In addition, the time- and temperature-resolved profiles obtained provide detailed information on the mechanistic aspects of secondary product formation.

Based on prior reports, carbon plays two different roles in the formation of nitrogenous products such as NO, $N_2O$ and HCN. The first role is the direct involvement of carbon in a series of chemical reactions to form NO, $N_2O$ and HCN. [13, 15, 19 & 21] The second role, however, is the involvement of carbon as a catalyst during the formation of any of the

aforementioned nitrogen species. [6, 11, 12 & 45]

Lázaro et al. [6] observed two zones for the NO evolution profiles leading them to believe that two different nitrogen sources with different reactivities and activation energies are present in the chars. Thomas el al. [16] also observed the same phenomenon in the NO time-evolution profiles, with the higher temperature peak being delayed relative to the carbon dioxide peak and having significantly higher intensity than the lower temperature peak when gasification was conducted in 20% oxygen in argon. They, like Lázaro et al., [6] proposed that the bimodal NO profiles are due to two main types of nitrogen functionality in chars. Wang el al. [31] reported the observation of bimodal gas evolution profiles and suggested that this indicates the presence of species of different reactivity.

The presence of HCN, and its role in the formation of NO and $N_2O$, has also been observed and studied by many investigators. Goel et al. [15] proposed that one of the possible reaction pathways leading to formation of $N_2O$ involves HCN. During devolatilization organic nitrogen present heteroatomic aromatic ring species is released as HCN. Its evolution may continue during char combustion via a process termed "slow or secondary devolatilization" of char, and then may undergo homogeneous reactions with oxygen to form NO and $N_2O$. Pels et al. [20] suggested that HCN is one of the responsible precursors to formation of NO and $N_2O$. Char-N is converted to HCN, and subsequently NO/$N_2O$ formation proceeds in the gas phase. Naruse et al. [33] reported that HCN contributes more to the formation of $N_2O$ than $NH_3$ in the low temperature range. Based on their observation, as soon as HCN is destroyed $N_2O$ and NO are formed. Winter et al. [39] suggested that a volatile species, identified as HCN, was simultaneously released in low concentrations. This

species was homogeneously oxidized to NCO which further reacted with the heterogeneously produced NO to form $N_2O$. Kilpinen et al.[40] confirmed the above hypothesis by performing chemical kinetic modeling. Based on their calculations, if fuel-nitrogen species in the form of simple cyano (HCN) species entered a fuel-lean gas phase between 1000 and 1200 K, a significant conversion to $N_2O$ would be found. Galborg et al.[43] investigated the oxidation of hydrogen cyanide under flow reactor conditions. They noted that the main oxidation route for HCN proceeds through NCO. Depending upon the gas temperature and composition NCO is converted to HCNO (by reaction with $H_2O$ or HCN), $N_2O/N_2$ (by reaction with NO) or NO (by reaction with O).

Reduction and destruction of NO by the char surface and the catalytic role of carbon in the formation of $N_2O$ from NO have been other intriguing subjects of study by many researchers. Teng et al.[12] suggested that the gasification of carbon by NO involves two different processes: (1) slow desorption of relatively stable surface complexes; and (2) processes involving NO attack on active, unoccupied sites that results in rapid desorption of gaseous products. Vesona et al.[13] used computational modeling to show that homogeneous gas phase reactions of NO occur in between the particles, as well as heterogeneous NO reduction on the char surface. Lu [22] observed that both homogeneous and heterogenous reactions contribute to the formation of $NO_x$. Based on his observations, $N_2O$ conversion ends earlier than $NO_x$ and $CO_2$ conversion. This suggested that $N_2O$ formation from char-N is related to carbon conversion and NO concentration, i.e., the reaction of NO with char-N is the principal path for $N_2O$ formation in the presence of oxygen. Illán-Gómez et al. [23] illustrated the fact that relatively disordered, nongraphitic carbon moieties (e.g., activated

carbon and chars) free from significant quantities of inorganic impurities (e.g., potassium and iron) are effective in reducing NO at temperatures in excess of 500 °C. Wójtowicz et al. [25] showed that formation of $N_2O$ appears to be competitive with respect to NO formation, and more $N_2O$ appears to be produced at the expense of NO as temperature decreases. Åmand et al. [30] also noted the production of $N_2O$ from NO reaction on char surfaces.

In order to unravel some of the underlying pathways and mechanisms 20 mg aliquots of Carbosieve were used in these experiments. Fixed or variable concentrations of NO, $N_2O$ or HCN in helium were separately fed onto the Carbosieve, in the presence and absence of $O_2$, and the evolved products were monitored simultaneously by MS and FTIR. It is noteworthy that the heating rate (25 °C/min), the total flow rate into the reactor (50 cc/min), the sample size (20 mg), and the temperature range (20-1000 °C) were the same for all experiments performed.

## 3.2 Experimental and Instrumentation Setup

An overall schematic of the instrumental setup is presented in Figure 2.3. An in-house-modified Perkin Elmer high temperature thermogravimetry analyzer (TGA7), a Hewlett Packard 5890 gas chromatogram (GC), along with a Hewlett Packard 5965A infrared detector (IRD) and a 5971A mass selective detector (MSD) were used for these experiments. An electrically heated stainless steel transfer line (Ultimetal tubing from Chrompack, 2m long, 0.53mm ID, 0.8mm OD, uncoated and methyl deactivated) runs from the TG system into the GC. The stainless steel line is connected to a porous layer open tubular (PLOT) column (5m long, 0.53mm ID) containing porous polymer (Porapak Q from J & W Scientific). The

column outlet flow is divided between two parallel transfer lines. Diameter and length of the two lines are selected to obtain a 1:1 split between IRD and MSD.

One of the essential parameters that has to be carefully controlled during the transfer of evolved gaseous products to the detectors is temperature. It is important to transfer these gaseous products at carefully controlled temperatures selected to prevent condensation and/or further reactions inside the transfer lines and columns. Alternatively, unavoidable condensation processes (because of the maximum operating temperatures of column and transfer lines) are designed to occur in a special section of wider bore quartz capillary tubing which can be readily replaced, if necessary. The temperature of the transfer line running from the TG to the GC system is controlled electrically. Electrical contacts welded to the ends of the line are connected to a VARIAC which controls the current output into the line. A K-type thermocouple is connected to the line halfway between the bridges to monitor the temperature of the line during a run. The line is insulated with two layers of Fiberfrax materials to reduce heat loss during operation.

The line is connected to the TG system via a specially built interface and an Automated Vapor Sampling (AVS) device. This system is explained in details in Chapter 2. The modified TG system consists of a 15.5 cm long quartz furnace tube (0.5 cm ID and 0.9 cm OD). The modification was done due to the fact that the original design of the TG furnace tube with the crucible did not provide a sufficient percolation of the evolved gases with the main gas stream ($O_2$ and He). Quartz wool was selected as the bed material to hold the powdered samples used and ultimately to replace the crucible. In order to eliminate the effect of sample size on the overall outcome of these experiments a similar sample quantity

(20 mg) was also used. When an experiment was in progress, the carrier gas and the evolved gaseous products traveled through the sample as well as the quartz wool, experiencing a more efficient mixing process. To enhance the mixing process even further, the sampling probe inlet was set at a distance of 1 cm below the bed to allow longer residence time in the tube for utmost mixing efficiency. It should be noted that due to replacement of the crucible with the quartz wool (bed) the balance of the thermogravimetry system was not parlayed any further. The heater block of the original design was the only component of the thermogravimetry system that was utilized in this configuration.

## 3.3 Reactions of NO

A series of experiments at two concentration levels of NO (with and without Carbosieve) was performed in the presence and the absence of $O_2$. In the first investigation Carbosieve was exposed to 2% (v/v) NO in the presence of 20% (v/v) $O_2$ in helium. Temperature-resolved IR and MS profiles of evolved gases ($CO_2$, CO, NO, $N_2O$, HCN, $O_2$ and $H_2O$) were studied (Figure 3.1). A sudden release of NO at 170 °C is evident in Figure 3.1. From this point on the NO concentration at the exit of the reactor leveled off until production of $CO_2$, CO and $N_2O$ began. When the production of the aforementioned compounds started to fade away, the NO profile showed another release and then leveled off to the same steady amount as before. Note that oxygen concentration showed a significant drop in level right where formation of $CO_2$ and CO started. This obviously represents the

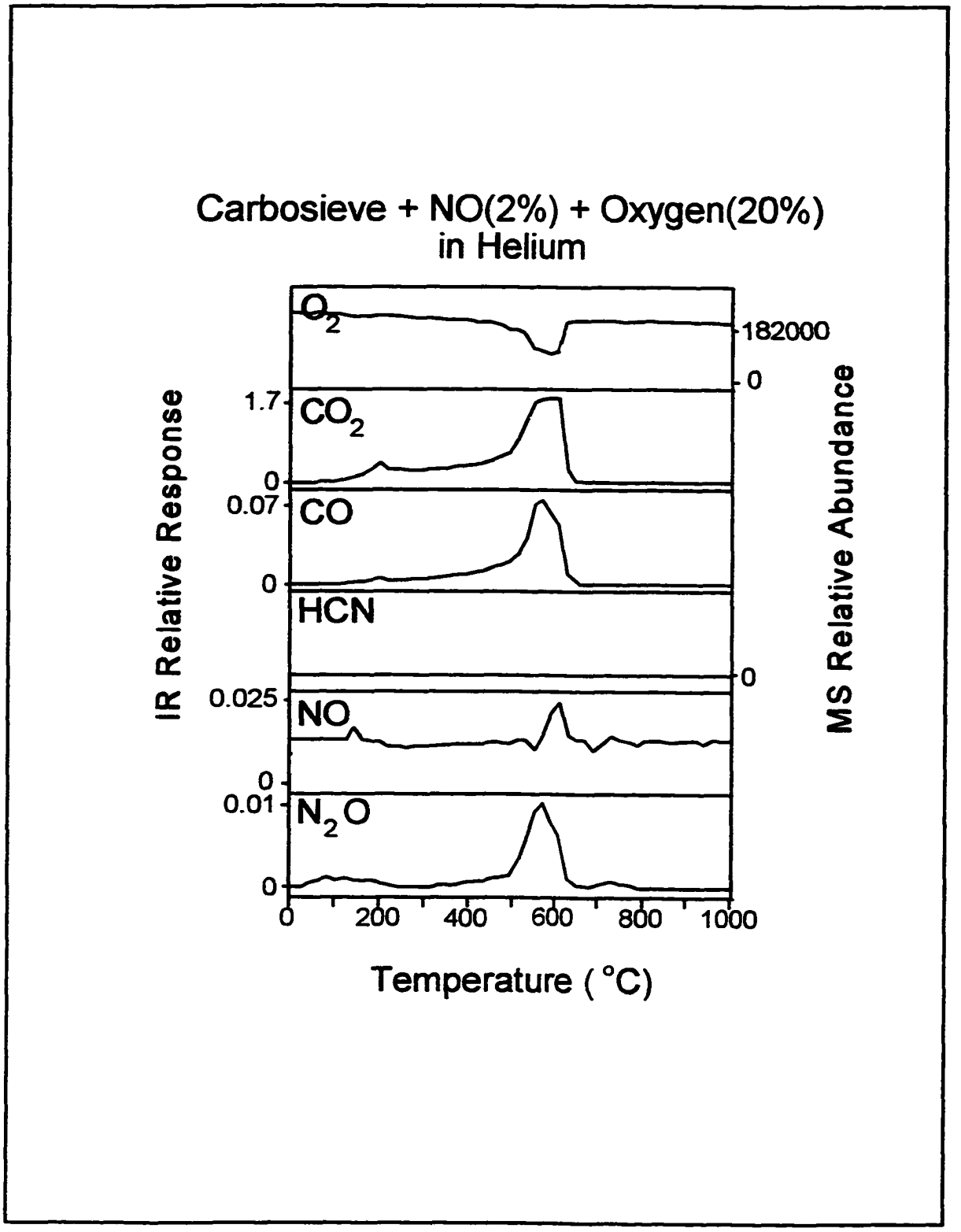


Figure 3.1 Temperature-resolved FTIR and MS profiles of $O_2$, $CO_2$, CO, HCN, NO and $N_2O$. Carbosieve was exposed to 2% (v/v) NO in the presence of 20% (v/v) $O_2$ in He.

oxygen consumption of the carbon oxidation process.

In order to examine the validity of this idea a blank run with Carbosieve exposed to only 20% (v/v) $O_2$ in helium was performed (Figure 3.2). The results showed the same $CO_2$ and CO production profiles. This led us to conclude that, even in the presence of NO, $CO_2$ and CO formation are primarily $O_2$ dependent. The similarity in production levels of CO and $CO_2$ for both experiments also confirmed the validity of this conclusion.

To investigate this further another experiment with Carbosieve, exposed to only 2% (v/v) NO in helium, was performed (Figure 3.3). In this experiment very low levels of $N_2O$, corresponding to minor impurities in the NO source were detected. A rather interesting observation was the formation of $CO_2$ and CO, starting as low as 200 °C, thus confirming the oxidizing nature of NO. The amounts of $CO_2$ and CO produced, however, were much less than those produced in the presence of $O_2$. This oxidizing effect of NO on carbon has also been observed by Miettinen et al. [24]

These observations suggest that $N_2O$ is formed by reactions involving NO, $O_2$, and carbon. Due to the oxidizing nature of oxygen, active sites would form on Carbosieve once exposed to it. Three scenarios are proposed for $N_2O$ formation from NO on carbon active sites. These active sites can play the role of catalysts in the formation of $N_2O$ from NO.

In the first scenario, at a certain temperature (170 °C) NO is adsorbed onto one of these active sites and therefore becomes excited. At a higher temperature (520 °C), a passing NO molecule attracts the nitrogen of the excited NO and therefore forms $N_2O$. Meanwhile, the oxygen left behind from the NO activation process reacts with carbon and forms CO while further reacting with $O_2$ to form $CO_2$ (Figure 3.4). In other words,

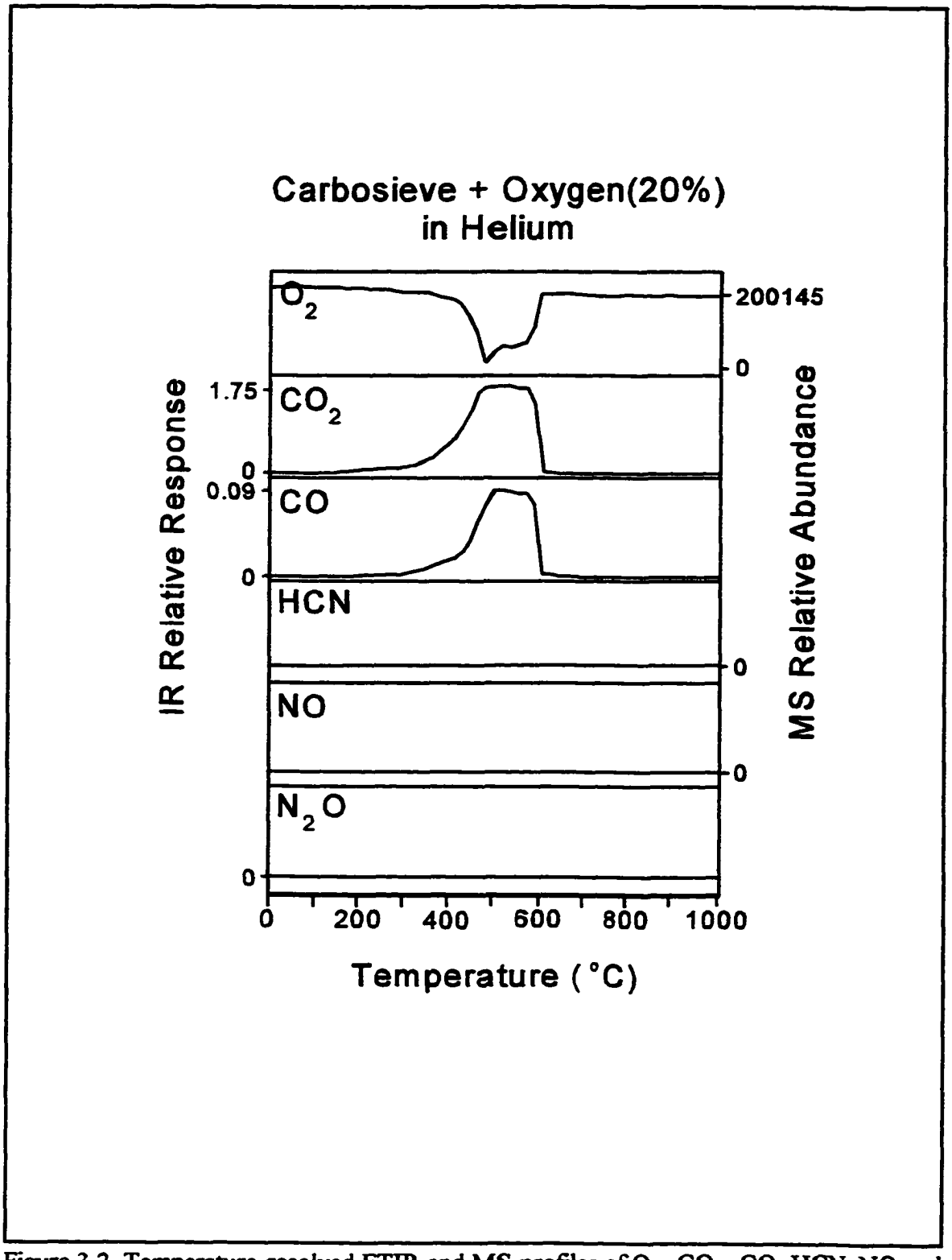


Figure 3.2 Temperature-resolved FTIR and MS profiles of $O_2$, $CO_2$, CO, HCN, NO and $N_2O$. Carbosieve oxidized in 20% (v/v) $O_2$ in He.

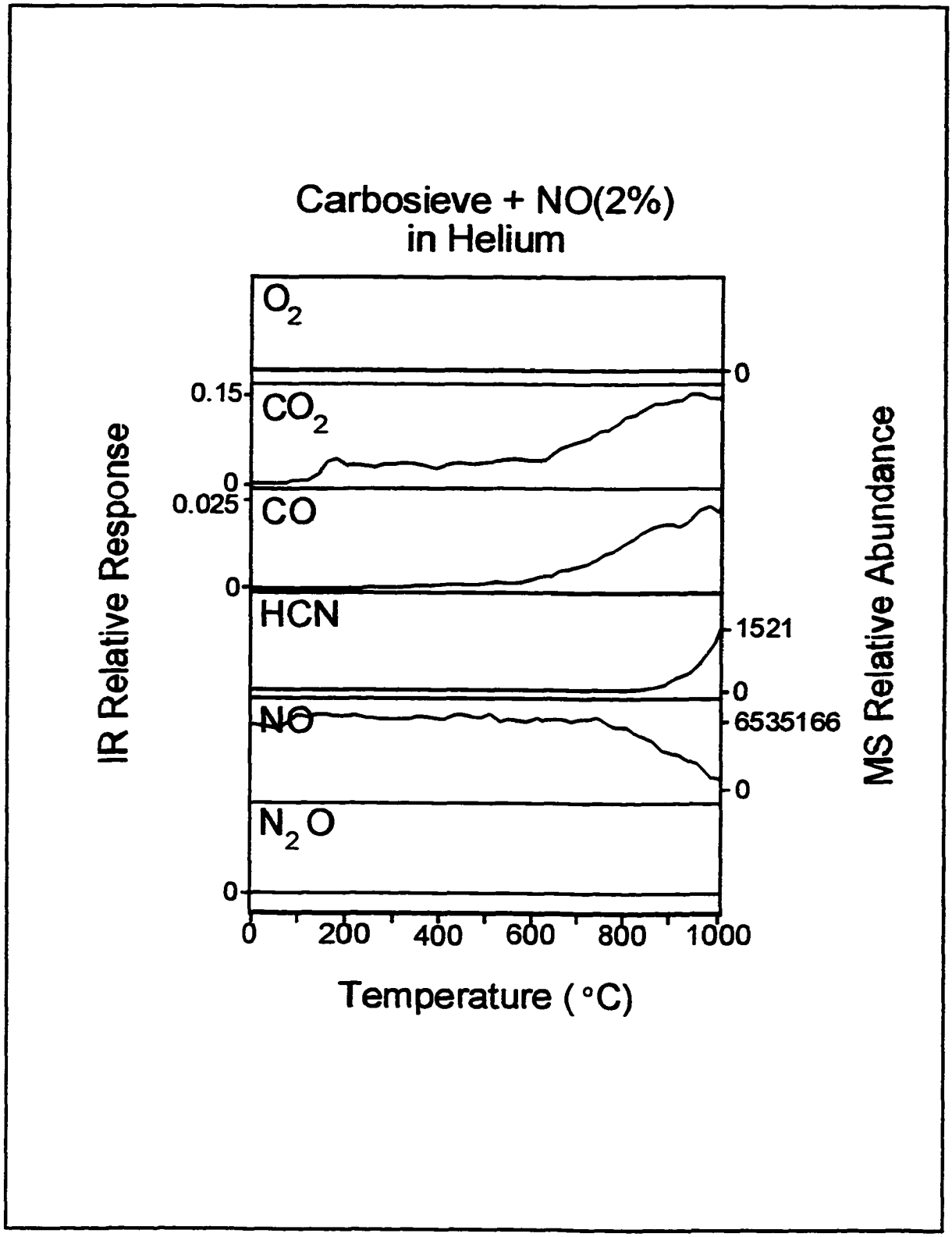


Figure 3.3 Temperature-resolved FTIR and MS profiles of $O_2$, $CO_2$, CO, HCN, NO and $N_2O$. Carbosieve was exposed to 2% (v/v) NO in He.

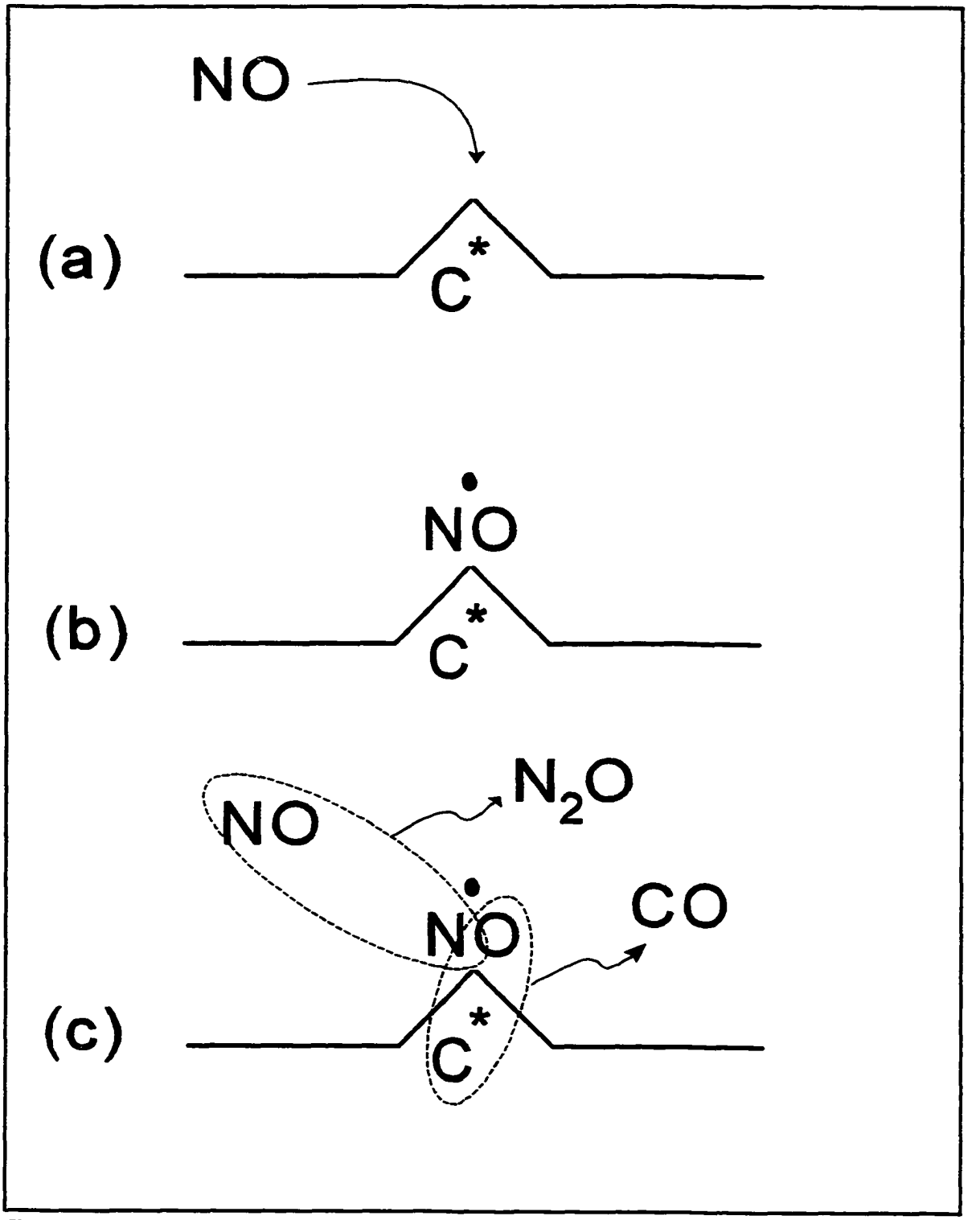


Figure 3.4 Various steps in the first hypothetical scenario of $N_2O$ formation from NO. (a) Gas phase NO attacks the active carbon site, (b) NO is adsorbed on the active carbon site and therefore is excited and, finally, (c) another bypassing NO attacks the excited NO on the active carbon site forming $N_2O$ and, simultaneously, CO.

$$N\bullet + NO = N_2O \quad (3.1)$$

$$C^* + O\bullet = CO \quad (3.2)$$

$$CO + O\bullet = CO_2 \quad (3.3)$$

In the second scenario, at 170 °C two NO molecules are adsorbed onto one active carbon site and therefore are excited (Figure 3.5). At a higher temperature (520 °C) the nitrogen from one of the excited NO molecules attacks the other excited NO, which results in formation of $N_2O$. Meanwhile, similar to the first scenario, the oxygen left behind from the activated NO activation process reacts with carbon and forms CO while further reacting with $O_2$ to form $CO_2$ (Reactions 3.1 - 3.3).

The last scenario resembles the second scenario fairly closely except for the adsorption of NO molecules onto the same active site. Here, two NO molecules are adsorbed onto two different neighboring active sites (Figure 3.6). The nitrogen from one excited NO molecule attacks the other, resulting in formation of $N_2O$. Formation of CO and $CO_2$ follows the same reaction pathways explained in the two previous scenarios.

Reduction of NO by active carbon sites to other moieties has also been proposed by other investigators.[6, 13, 18, 29, 30, 31, 50, 54 & 62] Many have suggested that a gas-solid reaction between carbon in char and NO, yields $N_2O$ and CO. Others have reported a somewhat different finding, where NO reduction on the char surface resulted in the formation of $N_2$ as the end product.

The explanation given earlier is also confirmed by the temperature-resolved profile of NO in the study done with Carbosieve exposed to 2% (v/v) NO in the presence of 20% (v/v) $O_2$ in helium (Figure 3.1). At 145 °C a hump appears suggesting the actual NO level

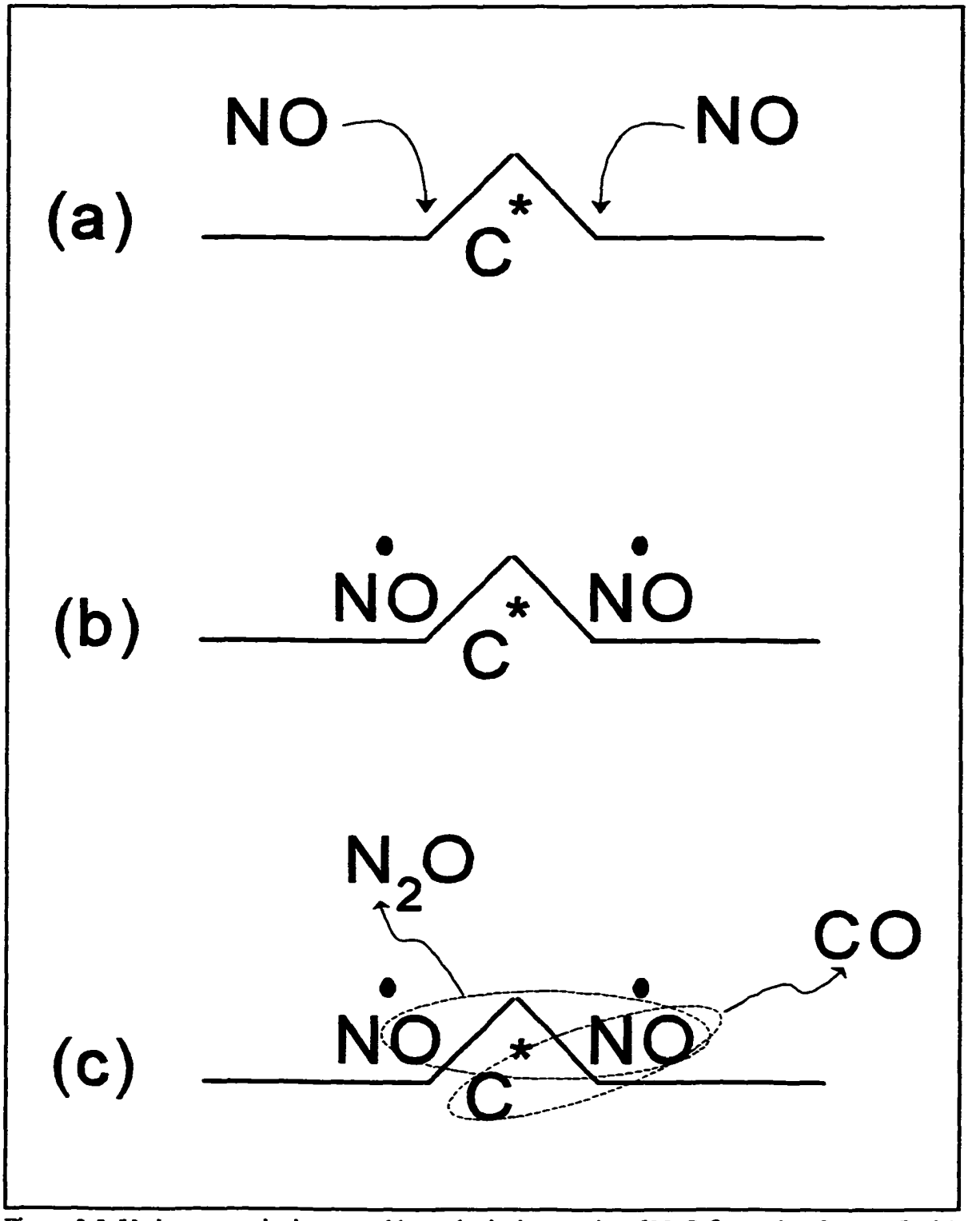


Figure 3.5 Various steps in the second hypothetical scenario of $N_2O$ formation from NO. (a) Two NO molecules attack an active carbon site, (b) NO molecules are adsorbed onto the active carbon site and therefore are excited, and finally (c) one of the excited NO molecules reacts with the oxygen of the other site forming $N_2O$ and, simultaneously, CO.

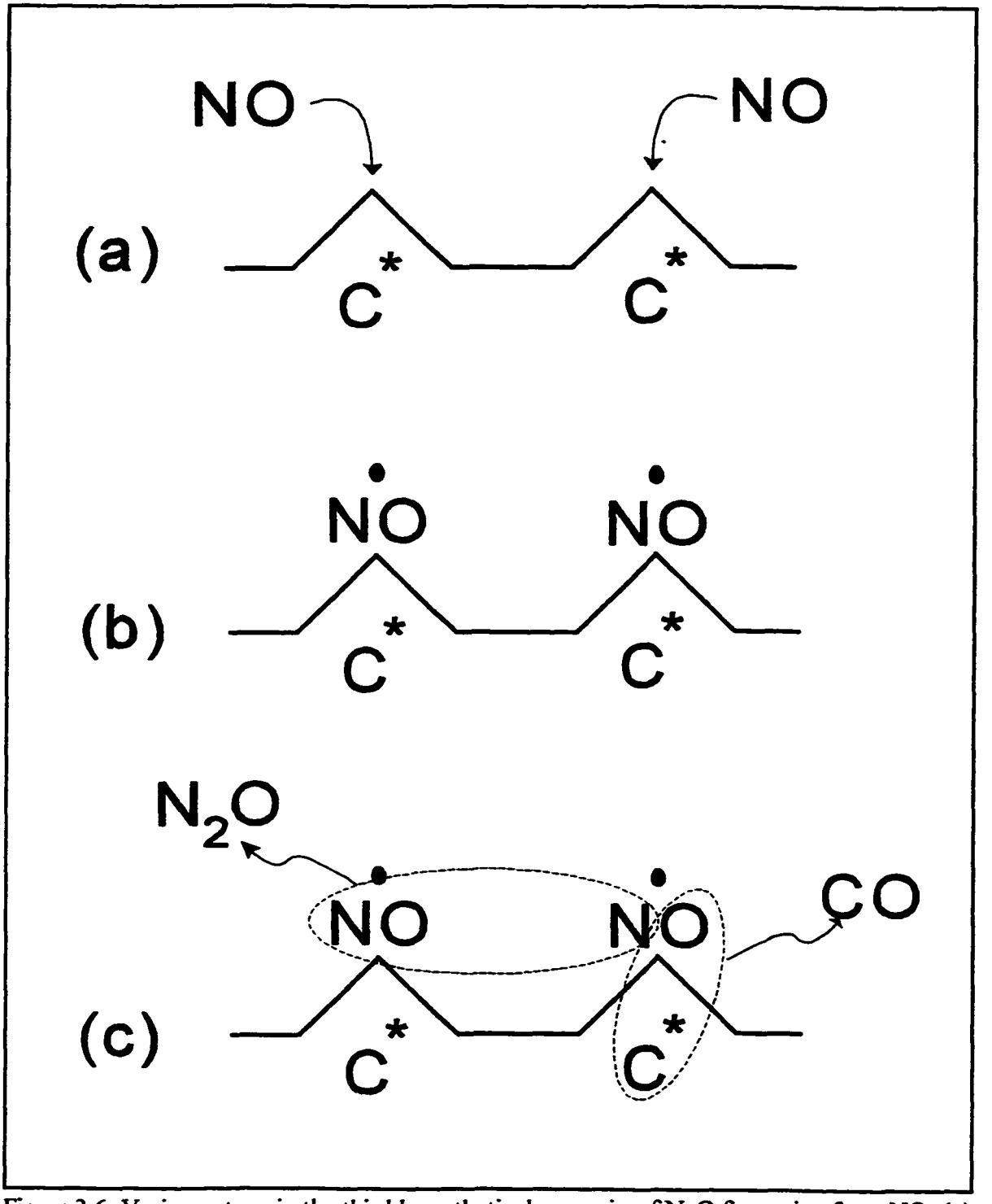


Figure 3.6 Various steps in the third hypothetical scenario of $N_2O$ formation from NO. (a) Two NO molecules attacking two neighboring active carbon sites, (b) NO molecules are adsorbed onto the active carbon sites and therefore are exited, and finally (c) one of the exited NO molecules reacts with the oxygen of the neighboring exited NO thereby forming $N_2O$ and, simultaneously, CO.

provided for the reaction. From 145 °C to almost 520 °C the NO profile shows a steadily lower trend than in the beginning; suggesting its continuing adsorption onto the active carbon sites. From 520 °C to 595 °C a dip in the profile suggests not only the ongoing adsorption of NO to the active carbon sites but also the capture of the bypassing NO molecules by the excited NO on the carbon sites and, ultimately, $N_2O$ formation. It is noteworthy that the appearance of a dip between 520 °C to 595 °C in the NO profile suggests that the first scenario is the only one that is consistent with the reported NO trend. The dip appears simultaneously with the formation of $N_2O$ and directly prior to the sudden and abrupt release of NO. The dip indeed represents a consumption of NO following the argument presented for the first scenario. It should be further noted that the $N_2O$ profile appears in the same time window as the dip in the NO profile. Finally, the last hump in the NO profile signals the inevitable release of all captured NO moieties from the active carbon sites due to the complete consumption of carbon by oxygen to form $CO_2$ and CO. It should be noted that the last NO hump appears right after the $CO_2$ and CO humps started to fade away.

In order to investigate the effect of NO concentration on overall $N_2O$ production the same experiment was performed at 400 ppm instead of 20,000 ppm NO (Figure 3.7). No $N_2O$ formation was observed, leading to the conclusion that $N_2O$ formation from NO is concentration dependent. The only similarity between the results from this experiment and those with higher NO concentration levels (20,000 ppm) was the late release of NO after $CO_2$ and CO formation started to taper off. This effect was also observed by Krammer et al.[41] who reported $N_2O$ formation in amounts that increase with increasing NO

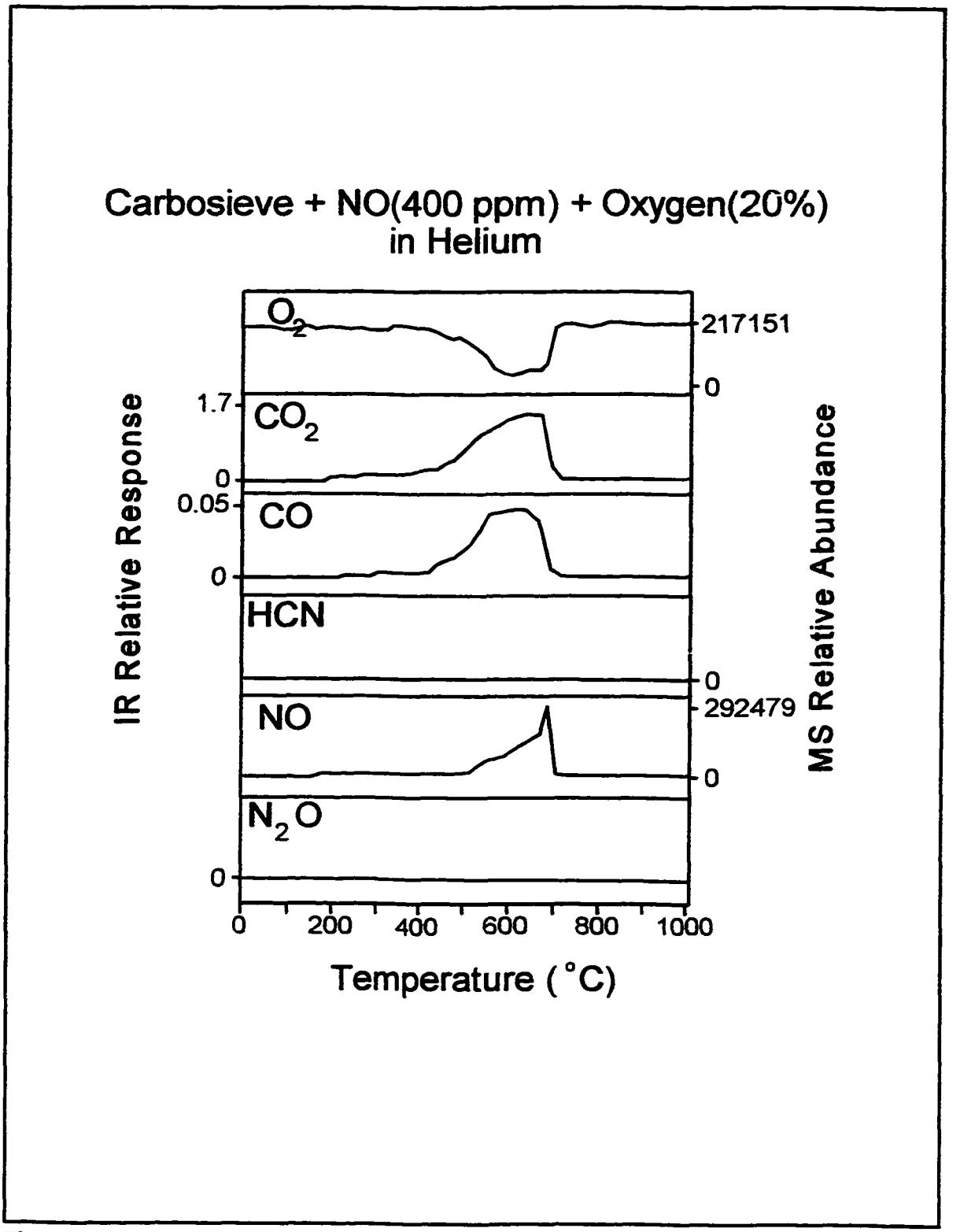


Figure 3.7 Temperature-resolved FTIR and MS profiles of $O_2$, $CO_2$, CO, HCN, NO and $N_2O$. Carbosieve was exposed to 400 ppm (v/v) of NO in the presence of 20% (v/v) $O_2$ in He.

concentration showing the importance of NO level for $N_2O$ formation.

As mentioned earlier, oxygen is assumed to be the key factor in the formation of active sites on the Carbosieve. To systematically examine the validity of this hypothesis an experiment with Carbosieve exposed to 2% (v/v) NO in the presence of a lower concentration of $O_2$ (5% (v/v)) in helium was conducted (Figure 3.8). Similar to the experiment with 20% (v/v) $O_2$, the temperature-resolved profiles showed formation of $CO_2$ and CO starting simultaneously. The total duration of this oxidation process, however, was about 5 to 7 minutes longer, apparently due to the rate limiting effect of the low oxygen concentration. Investigation of the temperature-resolved $O_2$ profile showed a major uptake event during $CO_2$ and CO formation. The production trend observed in the temperature-resolved $N_2O$ profile agreed closely with that observed at 20% (v/v) $O_2$ except for a late shoulder. Based on our observations two hypotheses could explain the presence of this shoulder, namely: (1) lack of sufficient oxygen, causing slower oxidation of carbon; and (2) reduction of $N_2O$ by the carbon, which will be explained in detail later. The active carbon sites are depleted at a much slower rate resulting in less formation of $N_2O$ from NO. The temperature-resolved NO profile presents the same trend as in the 20% (v/v) $O_2$ experiment. However, at 5% (v/v) $O_2$ concentration a higher concentration of NO is being detected although the amount of NO introduced into the reactor was the same for both experiments. Consequently, presence of higher NO concentration in the reactor would indicate that fewer NO molecules were attached to active carbon sites. If so, the presence of active carbon sites is indeed oxygen dependent.

The possibility of homogeneous reactions between NO and $O_2$, e.g., leading to the

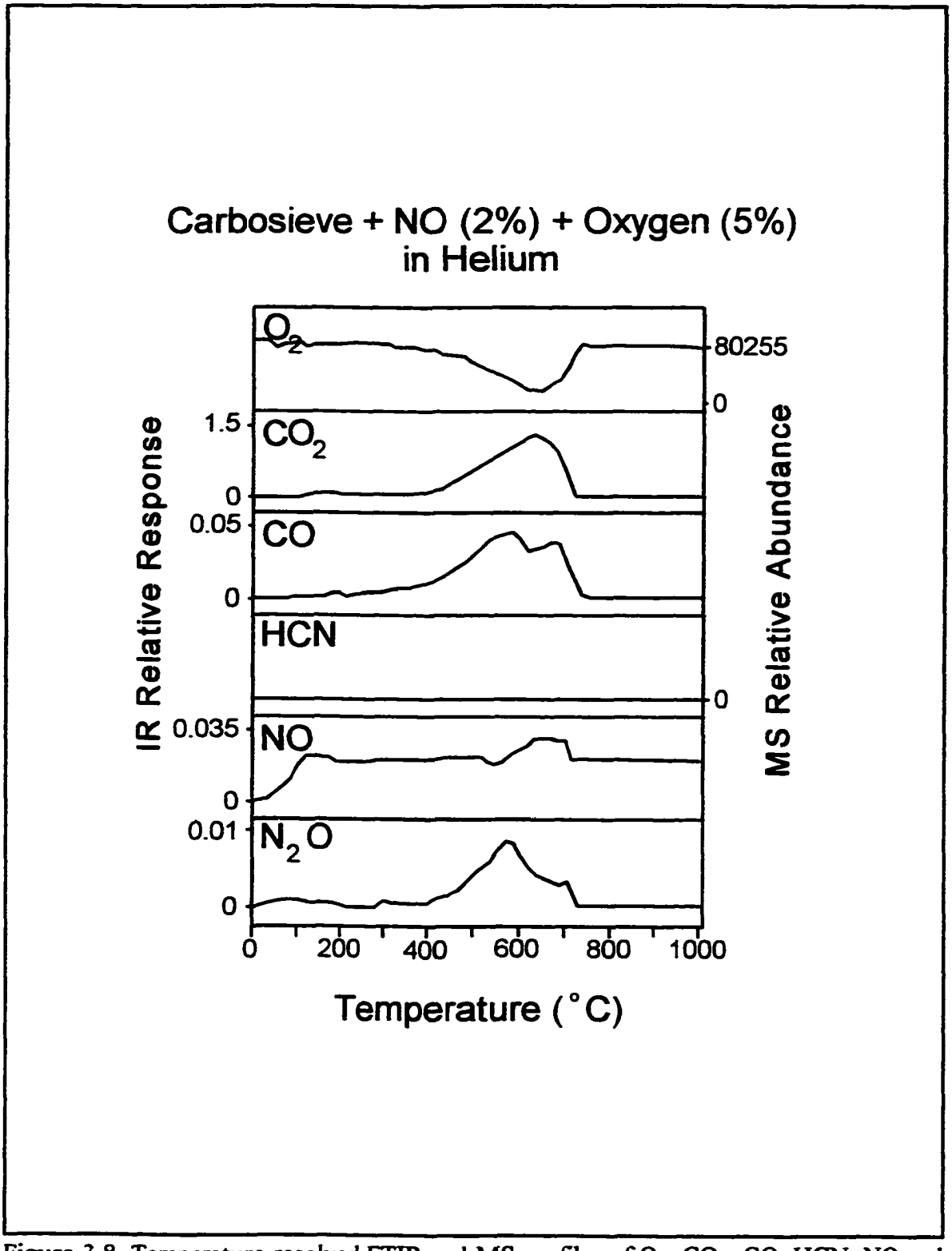


Figure 3.8 Temperature-resolved FTIR and MS profiles of $O_2$, $CO_2$, CO, HCN, NO and $N_2O$. Carbosieve was exposed to 2% (v/v) NO in the presence of 5% (v/v) $O_2$ in He.

production of $NO_2$, was also systematically examined. In this experiment 2% (v/v) NO was introduced into the reactor along with 20% (v/v) $O_2$ in helium in the absence of Carbosieve (Figure 3.9). No significant changes in NO and $O_2$ concentrations indicative of homogeneous reactions were observed under our experimental conditions.

To investigate the possible effect of nitrogen on the reaction pathways an experiment with Carbosieve exposed to 2% (v/v) NO in the presence of 20% (v/v) $O_2$ in $N_2$ was conducted (Figure 3.10). The trends of the temperature-resolved profiles for $CO_2$, CO, NO, $N_2O$, $O_2$ and $H_2O$ resembled those obtained in the prior experiment with helium as the carrier gas. This led to the conclusion that even the presence of very high concentrations of $N_2$ does not impose any mechanistic changes on the overall trends involved.

## 3.4 Reactions of HCN

In this study Carbosieve was exposed to 422 ppm of HCN in the presence of 20% (v/v) $O_2$ in helium (Figure 3.11). Temperature-resolved profiles of $CO_2$, CO, NO, $N_2O$, HCN, $O_2$ and $H_2O$ were evaluated. A prominent effect observed was that the profiles of NO and HCN follow exactly opposing trends. Around 520 °C the HCN level shows a gradual drop whereas the NO level experiences an increase at approximately the same rate. In other words, the formation of NO and the disappearance of HCN appear to be coupled. Thus, we concluded that NO is formed by a reaction, or reactions, involving HCN and $O_2$ even though the temperature-resolved profile of $O_2$ does not show any oxygen consumption.

It has been proposed by many investigators that, as seen here, HCN is the responsible precursor for the formation of NO. [20, 21, 43, 46 & 63] The char is gasified in the presence of

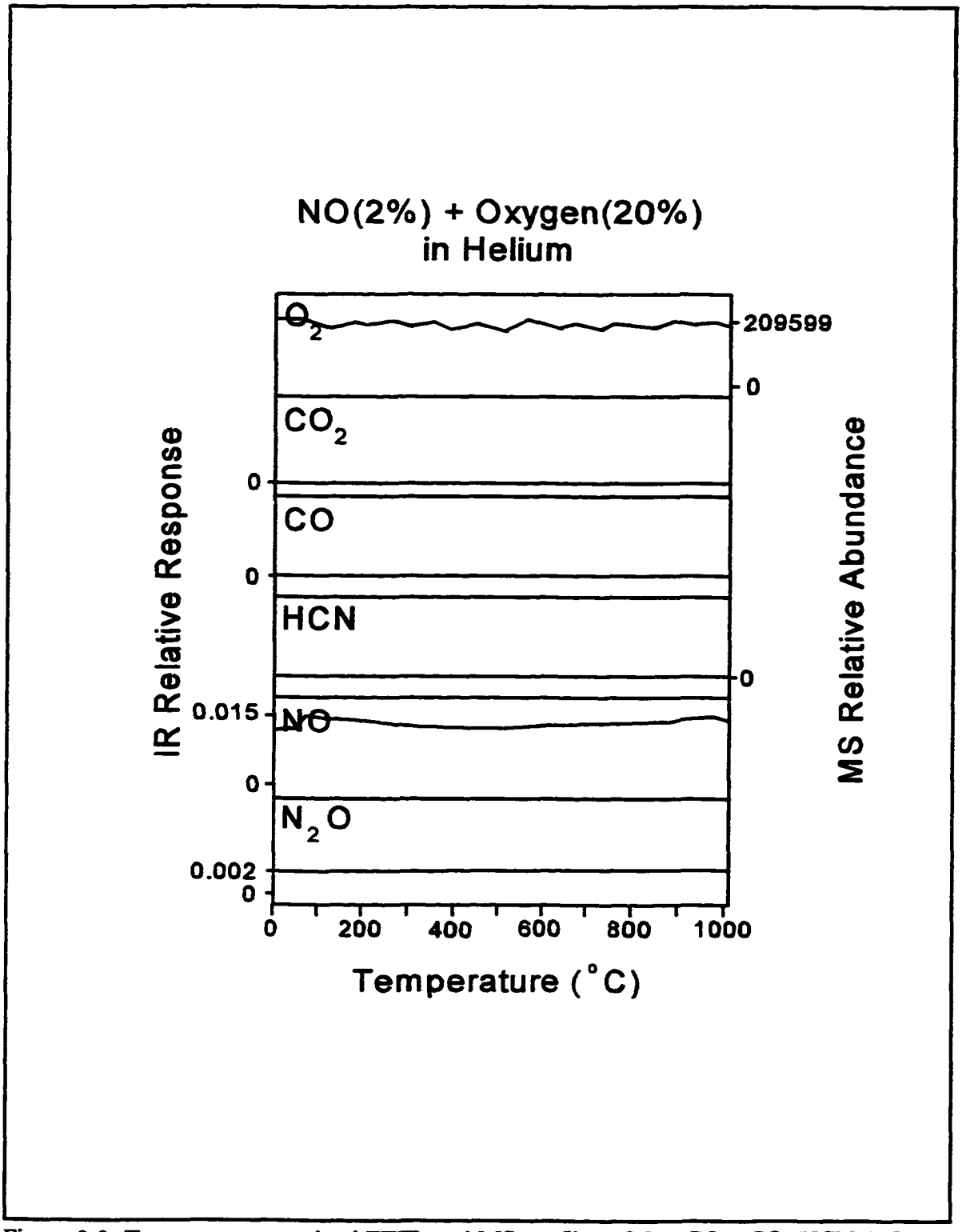


Figure 3.9 Temperature-resolved FTIR and MS profiles of $O_2$, $CO_2$, CO, HCN, NO and $N_2O$. 2% (v/v) NO and 20% (v/v) $O_2$ in He in the absence of Carbosieve. This experiment was performed to examine the possibility of any homogeneous reactions between NO and $O_2$.

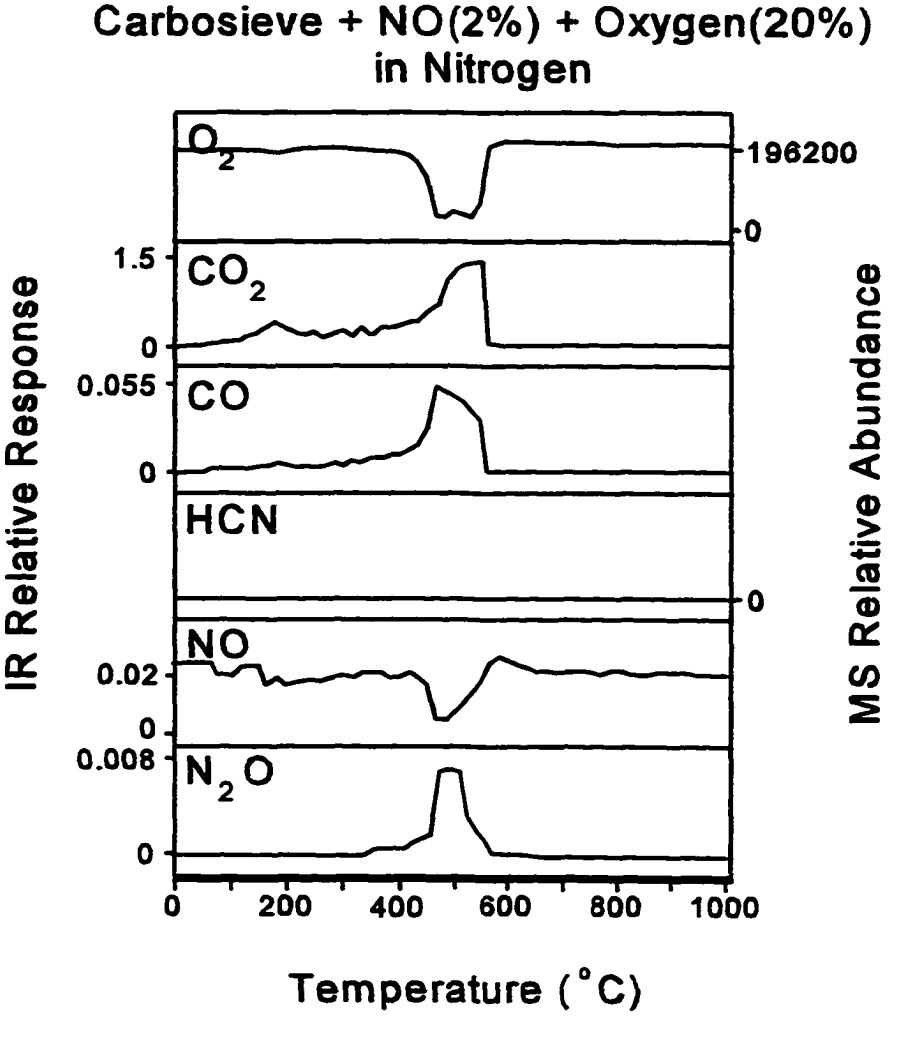


Figure 3.10 Temperature-resolved FTIR and MS profiles of $O_2$, $CO_2$, CO, HCN, NO and $N_2O$. Carbosieve was exposed to 2% (v/v) NO in the presence of 20% (v/v) $O_2$ in $N_2$.

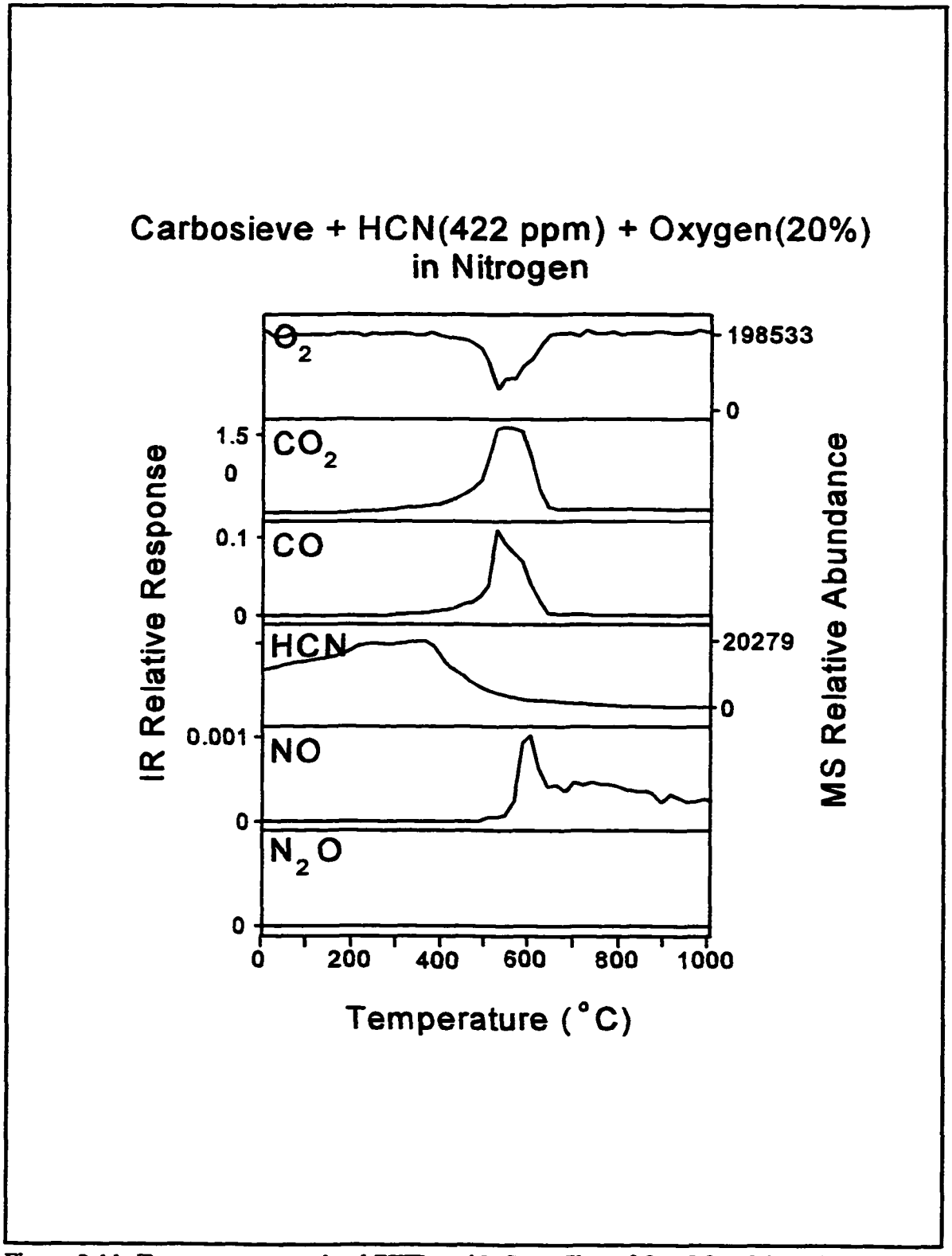


Figure 3.11 Temperature-resolved FTIR and MS profiles of $O_2$, $CO_2$, CO, HCN, NO and $N_2O$. Carbosieve was exposed to 422 ppm (v/v) HCN in the presence of 20% (v/v) $O_2$ in $N_2$.

$O_2$. Char-N is then converted to HCN, and further NO formation proceeds in the gas phase.

To examine the possible effects of Carbosieve another experiment was conducted under the same conditions but in the absence of Carbosieve (Figure 3.12). Similar effects are observed for NO and HCN as in the previous experiment suggesting that formation of NO from HCN involves homogeneous gas phase reactions. Only a relatively minor difference appears in the trends of both NO and HCN profiles. In the presence of Carbosieve, formation of NO is abrupt and strong, whereas in its absence NO release starts at a lower temperature and is more uniformly distributed over a range of temperatures.

In addition, the same effect discussed earlier was observed in this experiment as well. In the presence of Carbosieve, NO tends to get trapped by the available active carbon sites. This effect was discussed in detail in the previous section. During the oxidation process carbon is converted to $CO_2$ and CO. When carbon is on the verge of full consumption, NO moieties are released in a burst, appearing as a prominent hump in the NO profile. Although lack of $N_2O$ production might appear puzzling to some extent, the formation of $N_2O$ from NO is very much concentration dependent (as experimentally shown in the previous section) and, thus, at lower NO concentrations, no $N_2O$ is produced.

By careful evaluation of the observed profiles, and reconciliation with the available literatures the following reactions are thought to be responsible for formation of NO from the oxidation of HCN [46]:

$$HCN + O \approx NCO + H \quad (3.4)$$

$$NCO + O \approx NO + CO \quad (3.5)$$

$$CO + 1/2O_2 \approx CO_2 \quad (3.6)$$

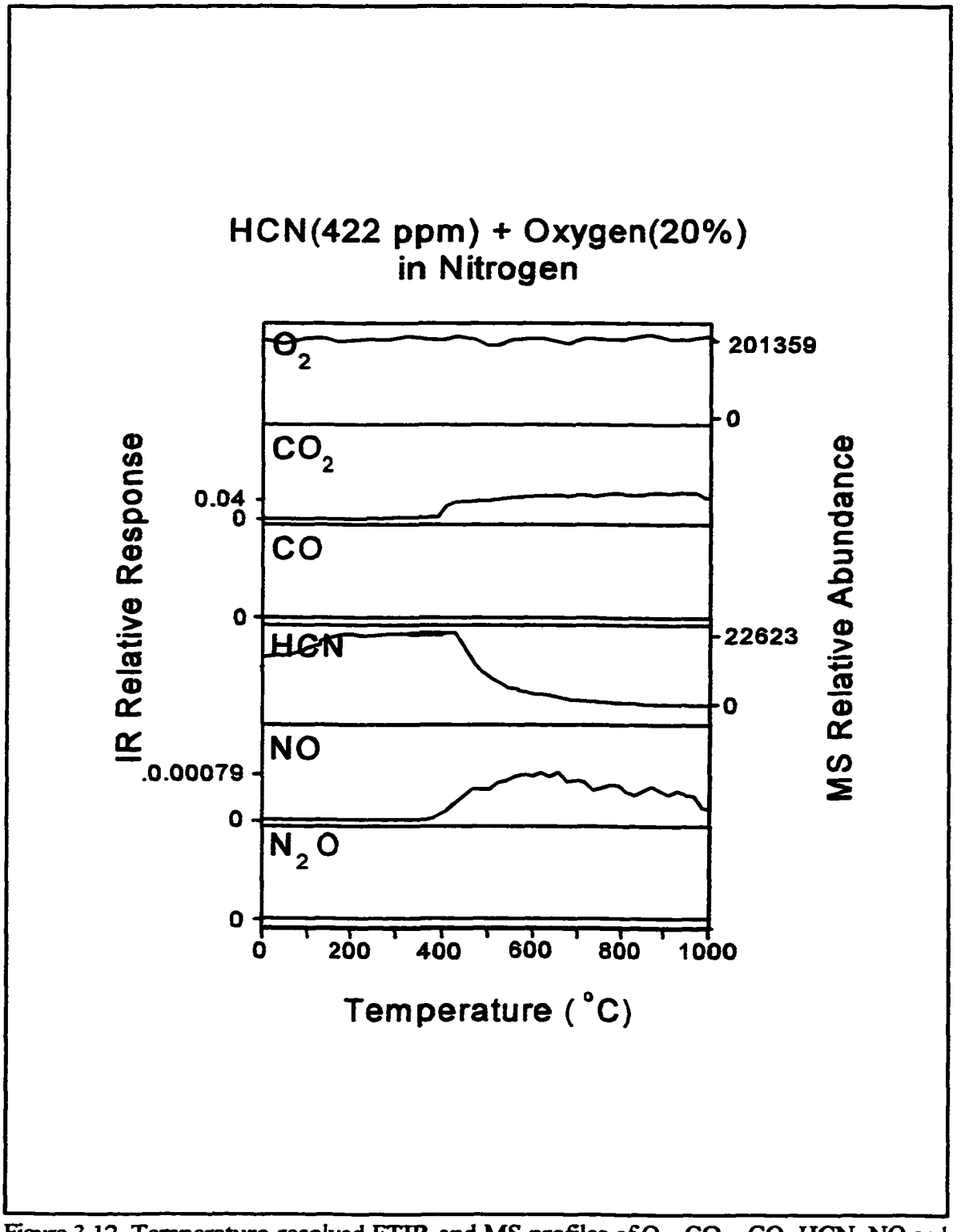


Figure 3.12 Temperature-resolved FTIR and MS profiles of $O_2$, $CO_2$, CO, HCN, NO and $N_2O$. 422 ppm (v/v) HCN in the presence of 20% (v/v) $O_2$ in $N_2$. This experiment was performed to examine the possibility of homogeneous gas phase reactions between HCN and $O_2$.

Reaction 3.6 is confirmed by the $CO_2$ profile obtained from the experiment in which Carbosieve was absent. It can be observed that the concentration profile of $CO_2$ closely follows that of NO.

It should be noted that, unlike the experiments discussed in the previous section, $N_2$ was the carrier gas in these experiments. Due to certain manufacturer-imposed-limitations the supplied HCN was available only in a nitrogen environment. Nitrogen did not appear to have any effect on the overall mechanisms involved as confirmed by the experiments discussed in the previous section. In these experiments Carbosieve was exposed to 2% (v/v) in 20% (v/v) $O_2$ in nitrogen. The temperature-resolved profiles of the products obtained were compared with the same profiles established from another experiment performed under exactly the same conditions with helium as the carrier gas. No measurable differences were observed in the profiles and their corresponding trends. From this it was concluded that the presence of nitrogen or helium as the carrier gas does not have any measurable effect on the underlying mechanisms involved in these experiments.

## 3.5 Reactions of $N_2O$

The overall effect of $N_2O$ was also investigated by a set of experiments similar to those described in the previous two sections. Carbosieve was exposed to 2% (v/v) $N_2O$ in the absence of $O_2$ in helium (Figure 3.13). The temperature-resolved profiles of $CO_2$, CO, NO, $N_2O$, $O_2$ and $H_2O$ were studied carefully. From the profile of $N_2O$ a decrease at 670 °C, followed by the occurrence of a minimum at 1020 °C, was observed. During this event CO seemed to be following an exactly opposite trend. This suggests that $N_2O$ was

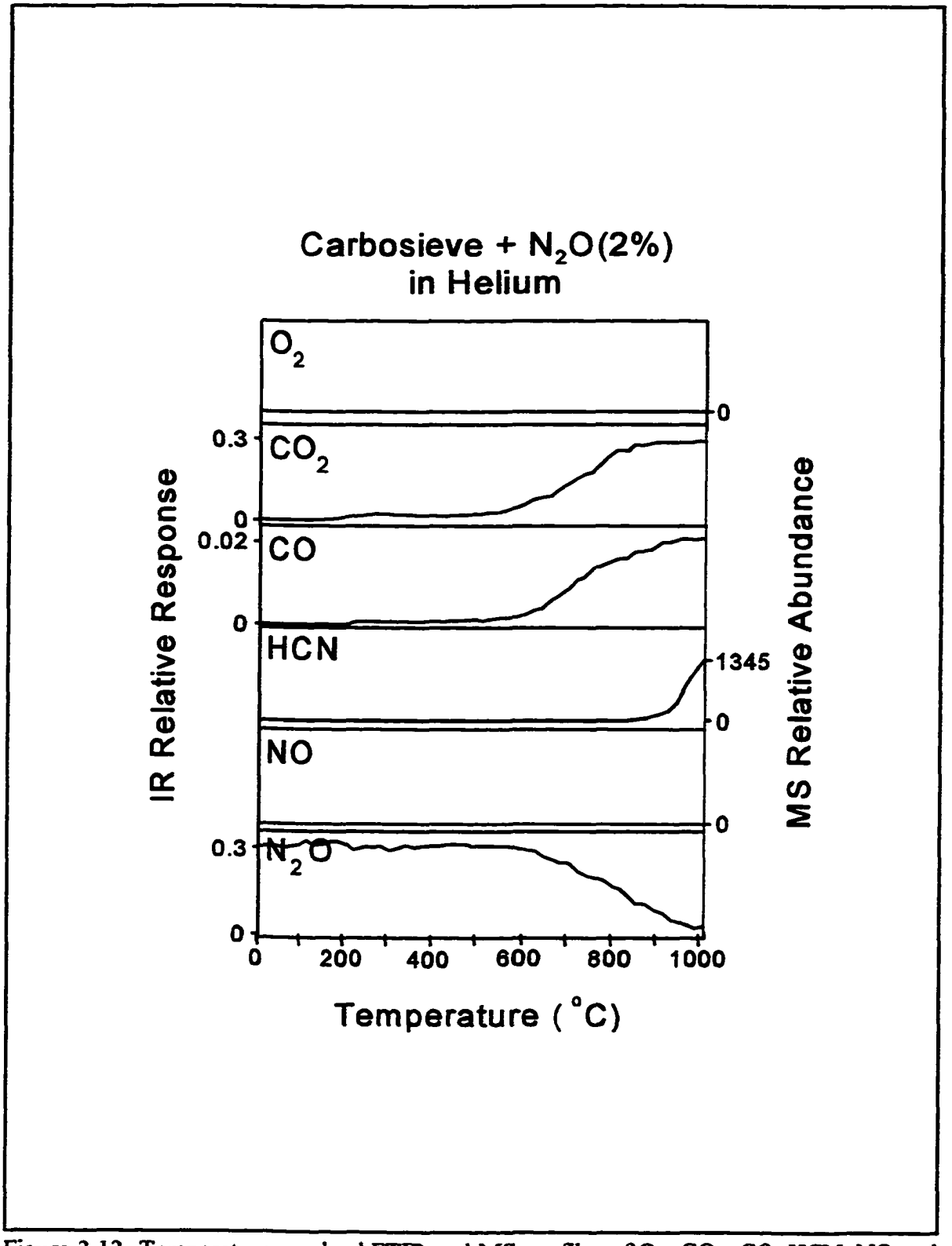


Figure 3.13 Temperature-resolved FTIR and MS profiles of $O_2$, $CO_2$, CO, HCN, NO and $N_2O$. Carbosieve was exposed to 2% (v/v) $N_2O$ in the absence of $O_2$ in He.

somehow being reduced, resulting in production of CO, e.g.,

$$N_2O + C = N_2 + CO \quad (3.7)$$

Results from combustion experiments with six coals and their chars reported by Pels et al.[45] also support the aforementioned finding. They reported that the gas phase reactions account for the majority of $N_2O$ emitted from a fluidized bed combustor. They explained this by the efficient heterogeneous reduction of $N_2O$ and $N_2$, which further occurs on the char surface immediately after $N_2O$ is formed from char-N. Based on these observations it can be proposed that around 520 °C $N_2O$ is being adsorbed onto active carbon sites. Once attached, the $N_2O$ moiety is excited and the oxygen part of this molecule becomes available for consumption by carbon to form CO. Consequently, the $N_2$ part of this molecule is released as a nitrogen molecule (Figure 3.14).

To further investigate this hypothesis an experiment with Carbosieve exposed to 2% (v/v) $N_2O$ in the presence of 20% (v/v) $O_2$ in helium was conducted (Figure 3.15). This was done with the notion that the presence of $O_2$ would increase the number of active sites on carbon molecular sieve as observed in the NO experiments described in section 3.2 of this chapter, and therefore would perhaps force the $N_2O$ oxidation to take place at a lower temperature. Unfortunately, carbon oxidation around 470 °C to $CO_2$ and CO did not allow for this effect to be observed. The absence of carbon at temperatures above 650 °C resulted in the absence of $N_2O$ reduction. By comparing these two experiments it can be concluded that carbon plays a major role in reducing $N_2O$ at temperatures above 650 °C.

This very same effect of $N_2O$ reduction was also observed when Carbosieve was exposed to NO in the presence of 5% (v/v) $O_2$ in helium. This experiment is described in

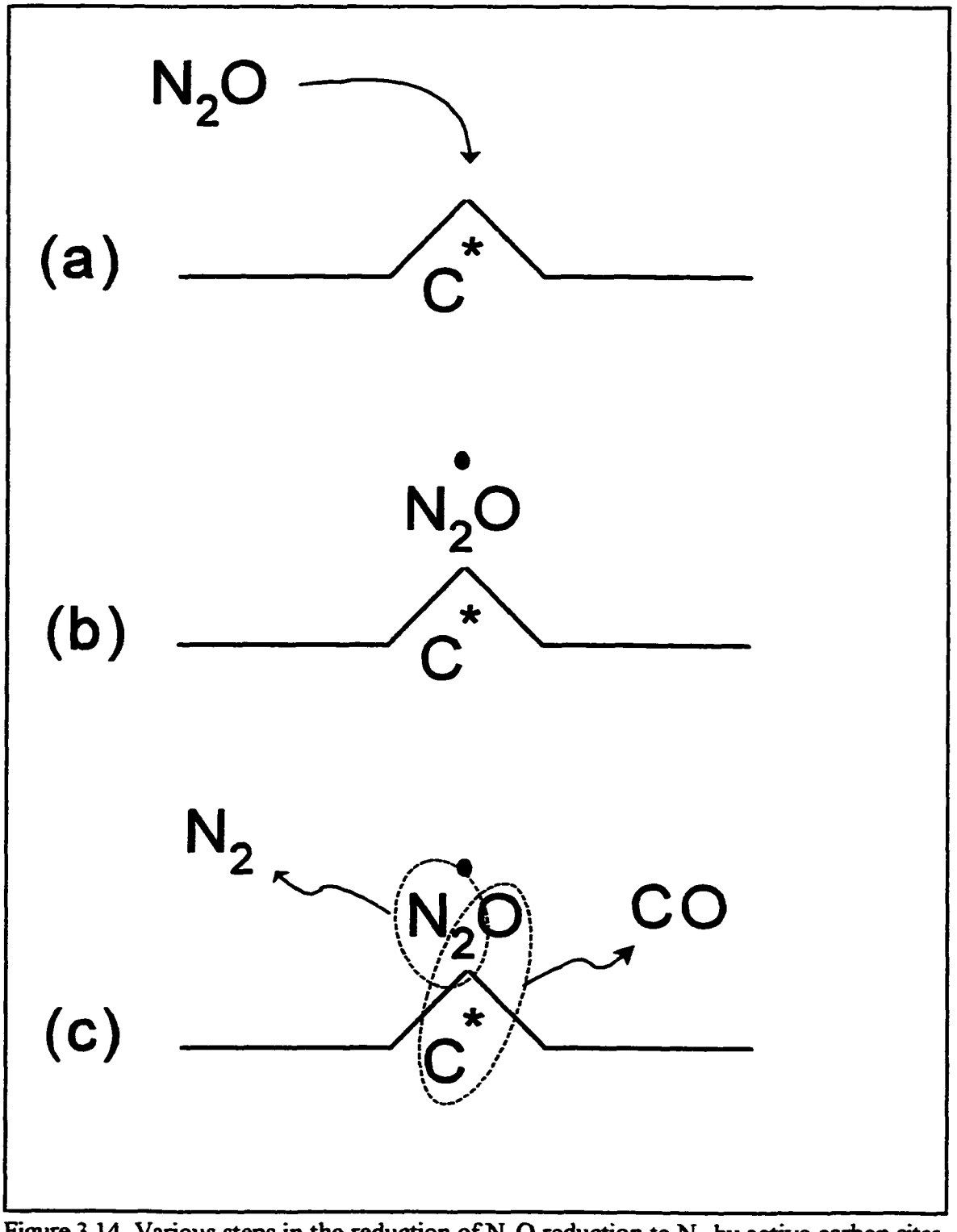


Figure 3.14 Various steps in the reduction of $N_2O$ reduction to $N_2$ by active carbon sites. (a) Bypassing $N_2O$ attacks the active carbon site, (b) $N_2O$ is then adsorbed onto the active site and therefore is excited, and finally (c) the excited $N_2O$ on the active site would react with the activated carbon to form $N_2$ and CO.

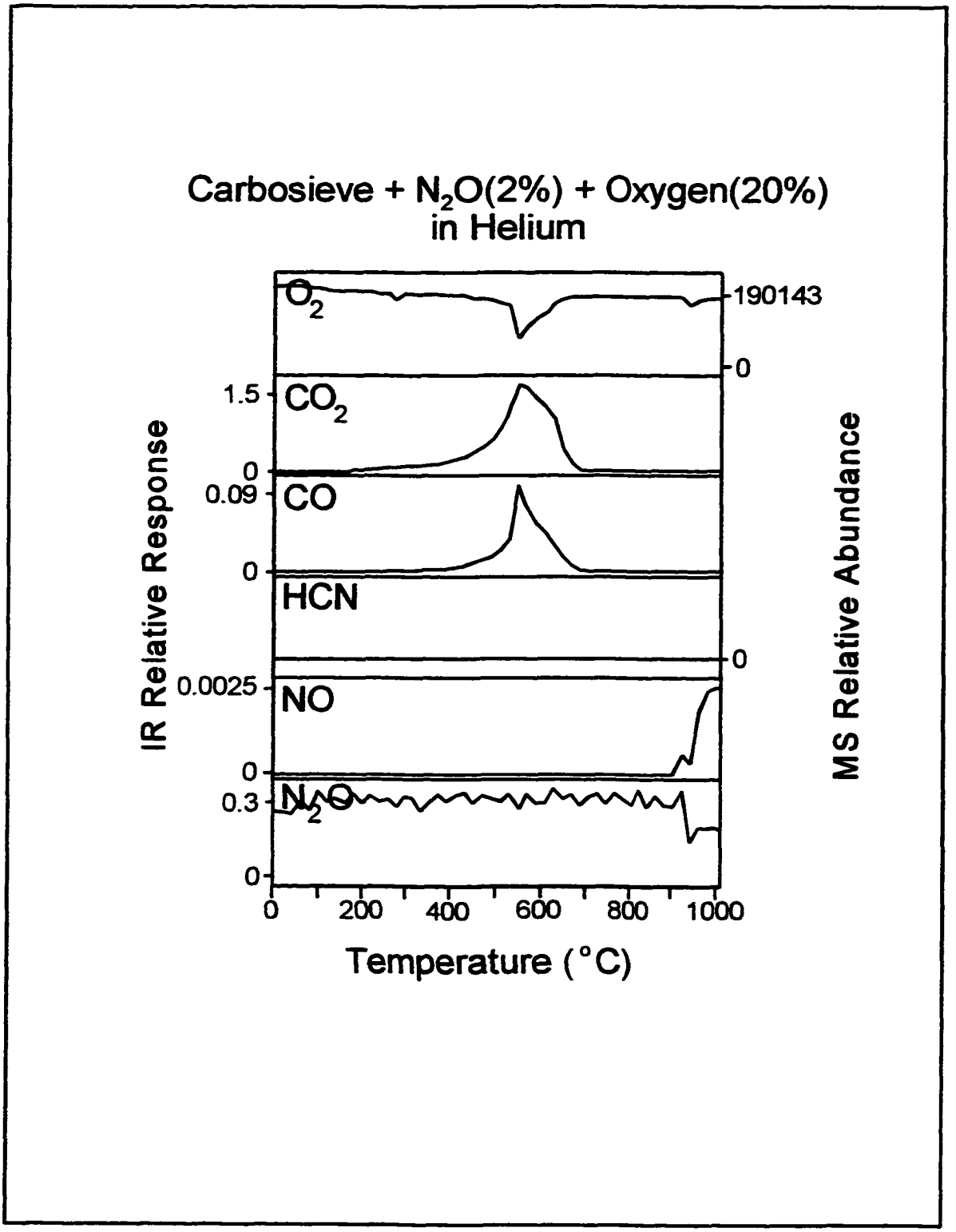


Figure 3.15 Temperature-resolved FTIR and MS profiles of $O_2$, $CO_2$, CO, HCN, NO and $N_2O$. Carbosieve was exposed to 2% (v/v) $N_2O$ in the presence of $O_2$ in He.

section 3.2. By carefully evaluating the temperature-resolved profiles for $N_2O$ and CO it is evident that $N_2O$ reduction is initiated at higher temperatures by the presence of an extended shoulder on the right hand side of the $N_2O$ "hump". In addition, during this event the simultaneous appearance of a second CO hump validates the occurrence of reaction 3.7.

The likelihood of homogeneous gas phase reactions between $N_2O$ and $O_2$ under our experimental conditions was also investigated. In this experiment 20% (v/v) $N_2O$ along with 20% (v/v) $O_2$ in helium in the absence of Carbosieve were fed into the reactor (Figure 3.16). The temperature-resolved profiles of $N_2O$, NO and $O_2$ presented rather interesting trends. At 920 °C $N_2O$ shows decreasing concentration levels reaching a minimum at 995 °C. The $O_2$ profile follows the same trend and precisely during this period NO production is evident. No formation of $N_2O$ has been reported at temperatures in excess of 800 °C.[2 & 47] Based on the aforementioned observation this would appear to be due to the formation of NO from $N_2O$. In other words, as proposed by Miettinen et al.,[24] the following gas phase reaction can be responsible for destruction of $N_2O$ and, ultimately, the formation of NO at higher temperature regimes:

$$N_2O + O_2 \approx 2NO \qquad (3.8)$$

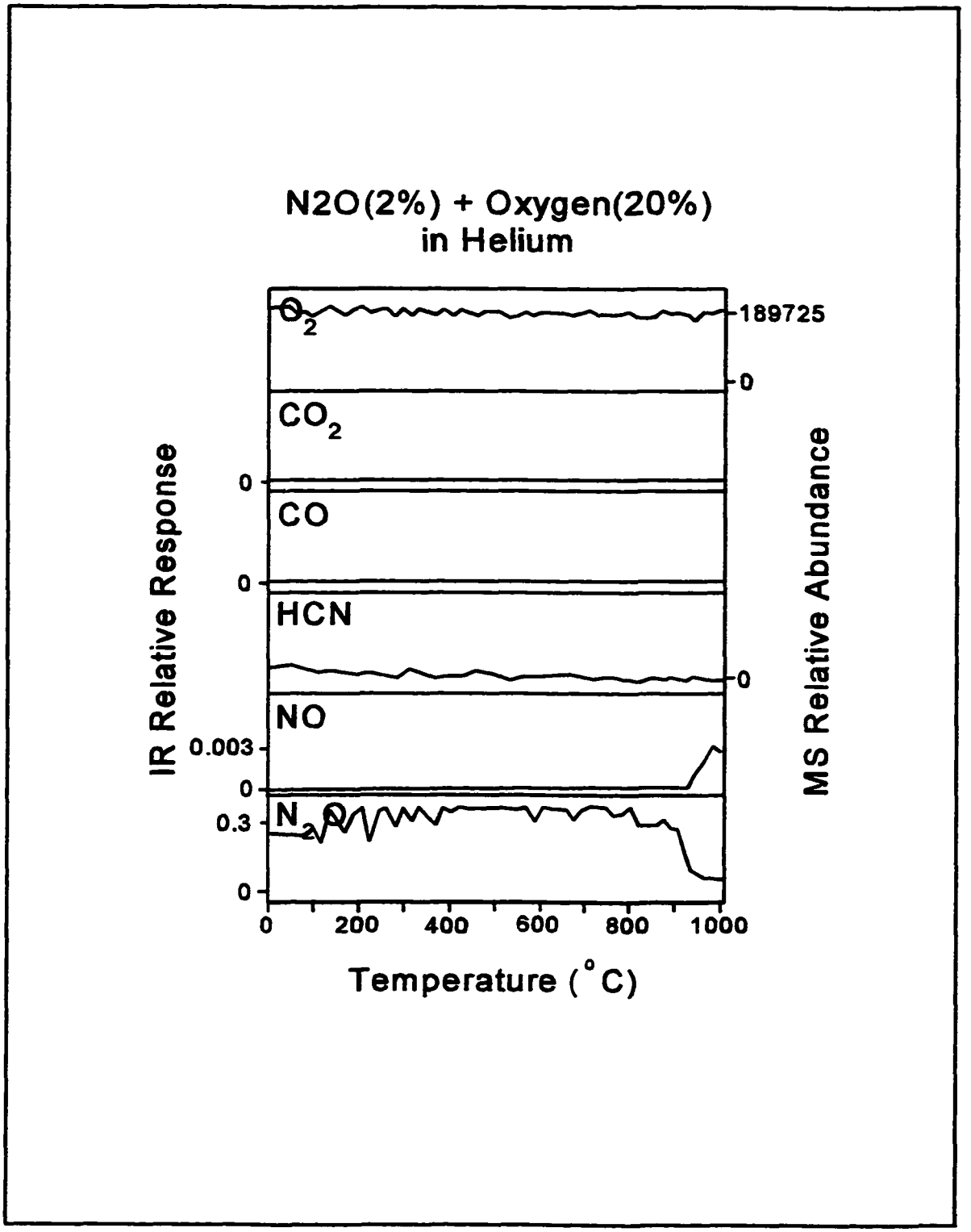


Figure 3.16 Temperature-resolved FTIR and MS profiles of $O_2$, $CO_2$, CO, HCN, NO and $N_2O$. 2% (v/v) $N_2O$ in the presence of 20% (v/v) $O_2$ in He. This experiment was performed to examine the possibility of any homogeneous reactions between $N_2O$ and $O_2$.

# CHAPTER 4

# MECHANISTIC STUDIES IN MODEL CHAR OXIDATION PROCESSES, EFFECTS OF OXYGEN LEVEL

## 4.1 Introduction

Formation of $NO_x$ from nitrogen moieties in coal char during combustion was perhaps among the least studied combustion reactions until the past 5 years or so when the effects of $NO_x$ on air quality gained more consideration and attention. The majority of nitrogen atoms in coal are known to be bound into aromatic organic structures which tend to become incorporated into the char residue during the initial devolatilization step of coal.[72] Investigations on solid coals and coal-derived materials have illuminated the fact that the organic nitrogen is mainly bound into five-membered pyrrolic and six-membered pyridinic ring structures.[35, 73 & 74] It has been shown by several investigators, e.g., Tullin et al.,[26] that char nitrogen contributes more significantly to the formation of NO and $N_2O$ than nitrogen in volatiles.

The complexity of the chemical structures in coals has given rise to challenging problems involving the characterization of mechanistic and kinetic aspects of $NO_x$ formation in combustion of coal and coal-derived char. To reduce experimental complexity many investigators have prepared and studied nitrogen-containing model compounds under

representative combustion conditions.[1, 13, 16, 27, 32, 61, 62 & 63] Hauser et al.[2] performed experiments with model compounds such as pyridine, HCN, and benzene/HCN. Wang et al.[63] studied the release of nitrogen species from model carbons derived from high pressure co-carbonization of carbazole and naphthol in argon. Thomas et al.[62] used nitrogen doped $^{13}C$ as model char in their gasification processes.

Our novel, combined TG/(GC)/IR/MS method was specially developed to produce mechanistic as well as kinetic data from a single analysis while achieving a closed mass balance. The system used for the experiments discussed in this chapter is described in detail in Chapter 2. Our initial intent was to perform kinetic studies with the TG measurements whereas the parallel IR and MS measurements would provide the capability for detailed mechanistic investigations. As noted earlier, a prerequisite for successful kinetic studies is a closed mass balance under chemically controlled reaction conditions.

However, since transport of oxygen into the sample bed within the TG crucible, as well as transport of reaction products out of the sample bed relies entirely upon slow diffusion processes, reaction rates measured with TG experiments are notoriously prone to transport limitations. Furthermore, the TG configuration in Figure 4.1 reveals an inherent design conflict in that it is desirable to sample the reaction products as close to the crucible as possible in order to minimize the effect of secondary reactions and/or sample losses at the hot reactor walls while it is also desirable to achieve nearly instantaneous mixing of the small reaction product flow with the reactor gas flow in order to obtain reliable, representative concentration measurements. In view of the anticipated shortcomings of the TG system in producing reliable concentration measurements under chemically controlled

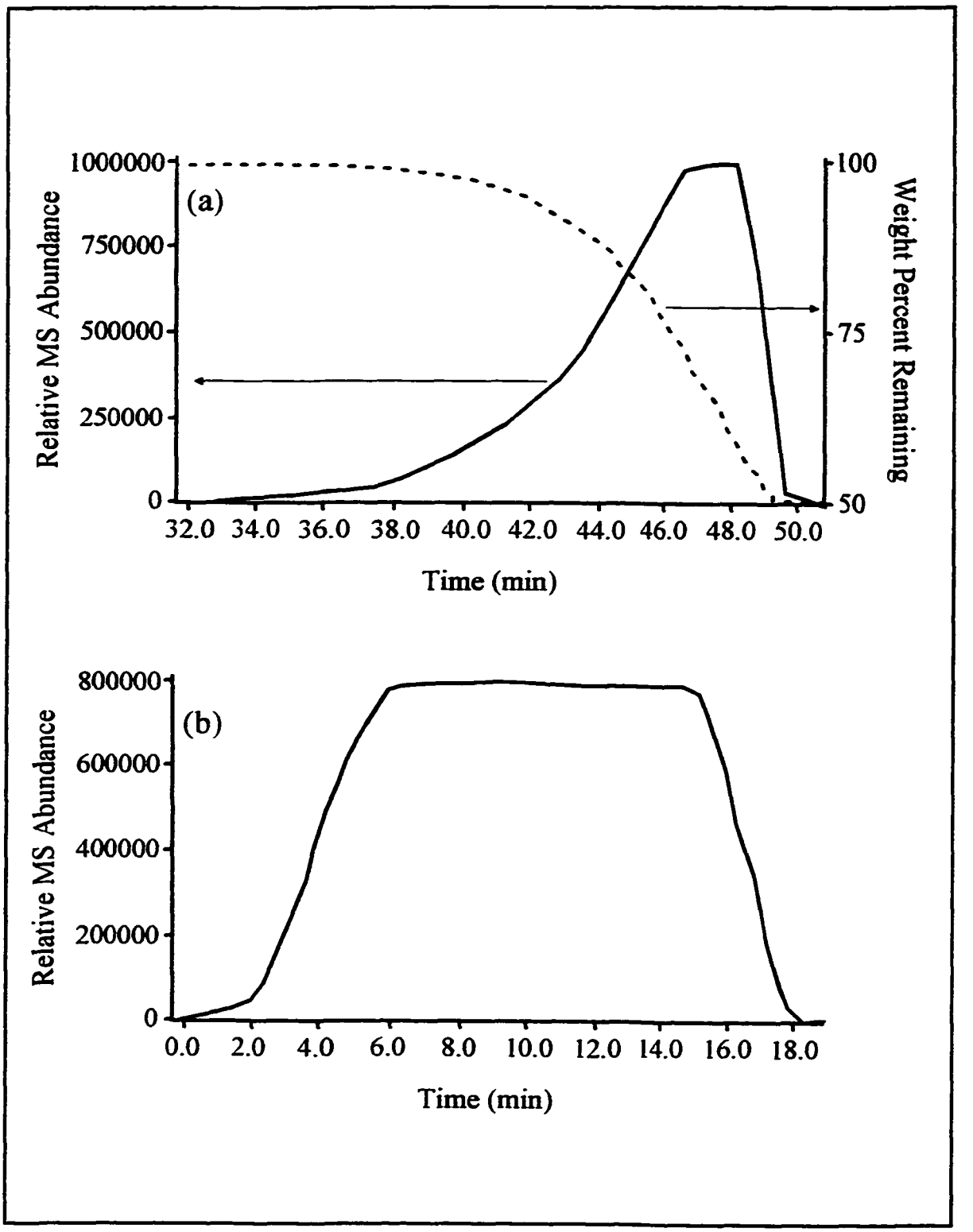


Figure 4.1 Schematic thermogravimetry reactor configuration. The system is composed of a fixed bed reactor crucible within a quartz furnace tube surrounded by a cylindrical heater block and equipped with a microbalance.

conditions a second reactor configuration (Figure 4.2) was designed in which the reactor gas flow percolates the sample bed, thereby greatly reducing the probability of transport limitations as well as promoting complete mixing of reaction products and reactor gas. It should be noted however that the tubular quartz reactor used in this configuration does not allow continuous weight loss determinations thereby making it more difficult to achieve a closed mass balance.

For the purpose of these studies two model compounds, tetrapyridyl porphine and tetraphenyl porphine were charified under conditions described in detail in Chapter 2. Next, these chars were oxidized in a controlled environment (Chapter 2) and the temperature-resolved evolution profiles of nitrogen-, carbon- and hydrogen-containing products of interest studied as a function of oxygen level. It should be noted that the experiments performed with these model chars also helped substantially in optimizing the experimental setup for coal char experiments which, will be presented and discussed in Chapter 5.

## 4.2 Reactor Configuration

The original Perkin Elmer TGA7 thermogravimetry furnace configuration is shown in Figure 4.1. In this configuration an alumina crucible hangs from an electronic micro-balance by means of a nichrome wire. A fixed sample quantity of 20 mg in the crucible was used for these experiments. In this design the crucible contains a sample bed and, therefore, the overall configuration can be thought of as a fixed bed reactor. The furnace tube has a large enough inner diameter that considerable spacing exists around the crucible for the purge gas to carry the evolved gaseous products away from the crucible. As discussed

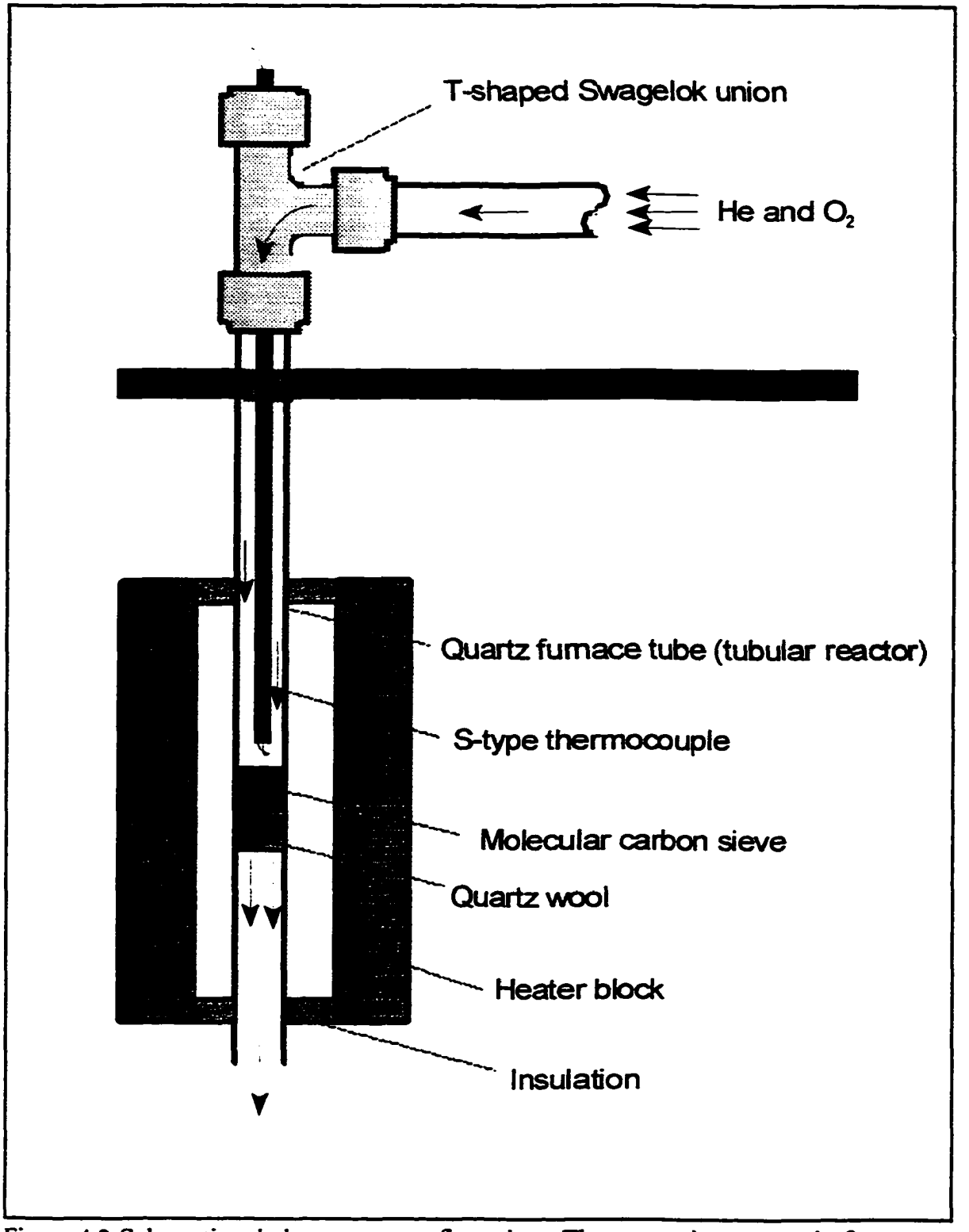


Figure 4.2 Schematic tubular reactor configuration. The system is composed of a reactor chamber (quartz furnace tube) surrounded by a cylindrical heater block and a molecular carbon sieve bed supported by a bed of quartz wool.

before, however, due to the poorly defined percolation behavior of oxygen and combustion products within the sample bed and the difficulty in achieving nearly instantaneous mixing of the evolved gaseous products within the main stream flow, the temperature-resolved evolution profiles of these products may be affected by mass transport limitations. As a result, the TG reactor configuration was used only to obtain information on the weight loss profiles during oxidation of the model compounds at various oxygen levels whereas the quartz tube reactor configuration shown in Figure 4.2 was used to measure chemically controlled product evolution rates as well as reliable product concentrations.

The furnace tube in the quartz tube reactor has a smaller inner diameter (0.5) than the TG reactor. The material of construction (quartz) and the length (15.5 cm) of the new furnace tube were chosen to be the same as the original tube in order to satisfy the dimensions and materials properties of the original thermogravimetry system. Quartz wool was selected as the bed support material in order to hold the powdered samples used and effectively replace the crucible. In order to eliminate the effect of sample size on the overall outcome of these experiments similar sample quantities (20 mg) were used. When an experiment is in progress, the carrier gas and the evolved gaseous products that have traveled through the sample as well as the quartz wool (60 ml/min) experience a more efficient mixing process. To facilitate complete mixing, the sampling probe inlet was set at a distance of 1 cm below the bed, thereby allowing longer gas phase residence times in the tube before sampling. It should be noted that due to the replacement of the crucible by the quartz wool plugs the micro-balance module of the TG system was not used any further.

## 4.3 Nitrogen Mass Balance in the Thermogravimetry Reactor Configuration

As pointed out earlier, the original reactor design of the Perkin Elmer TGA7 thermogravimetry system anticipated to pose problems due to incomplete mixing of products and carrier gas during the char oxidation process. To investigate this, an attempt to obtain a closed nitrogen mass balance from the oxidation of tetrapyridyl porphine char in 20% $O_2$ in He at 25 °C/min was made. NO, $N_2O$ and HCN gas standards (at known concentrations) were introduced into the reactor tube and, subsequently, into the infrared detector and the mass spectrometer by means of the AVS technique described in detail in Chapter 2. The areas under the curves obtained from both the IR and the MS chromatograms were then correlated to the concentrations of the corresponding calibration gases. The calibrations performed with the gas standards can also be used to compute the fraction of parent nitrogen (char nitrogen) contributing to the formation of the desired nitrogen end products (NO, $N_2O$ and HCN). The percentages of char nitrogen released as NO, $N_2O$ and HCN were determined to be 4.8, 1.1 and 12.0, respectively, together accounting for only approximately 18% of the overall char sample nitrogen.

At this point, two hypotheses had to be evaluated. The first being that the obtained product nitrogen values really represent the actual percent of char nitrogen contribution to each of the aforementioned three nitrogen end products with the remainder contributing to nitrogen products not detected by our analytical system. Lack of support for this hypothesis from the reviewed literature led us to consider the possibility that the existing thermogravimetry furnace tube configuration results in a poor percolation of oxygen and

combustion products within the sample bed and insufficient mixing of the evolved gases within the main stream flow.

In order to investigate the latter hypothesis, 3 mg of calcium carbonate ($CaCO_3$) were placed in the crucible and exposed to a constant heating rate of 25 °C/min in helium for about 50 min. The weight loss profile as well as the MS selected release profile for $CO_2$ were registered (Figure 4.3). Since $CO_2$ was the only gas expected to evolve form the thermal decomposition of $CaCO_3$ ($CaCO_3 \rightarrow CaO + CO_2$) the weight loss profile could be directly correlated to the $CO_2$ release profiles. The area under the $CO_2$ profile (i.e. 6,255,496) was then calculated and its corresponding mass (1.43 mg) was obtained from the weight loss data. This profile and its corresponding mass were then compared against the values obtained from another experiment involving a $CO_2$ gas standard. In this experiment a 3200 ppm $CO_2$ standard gas in He was introduced into the thermogravimetry furnace tube for a period of 18 min (similar to the $CO_2$ release period during the $CaCO_3$ experiment). The total mass of $CO_2$ was calculated to be 6.44 mg and compared with the MS $CO_2$ profile (area under the profile = 10,856,789). It is clear that the ratio of the $CO_2$ areas obtained from both experiments (1.74) is in no agreement with the ratio of their weights (4.5). The scenario was evaluated carefully and it was concluded that poor percolation and lack of mixing were the primary reasons for the observed discrepancies. Consequently, it was decided to repeat the nitrogen mass balance experiments in the tubular reactor configuration.

## 4.4 Nitrogen Mass Balance in the Tubular Reactor Configuration

Just as for the TG reactor configuration, an attempt was again made to achieve a

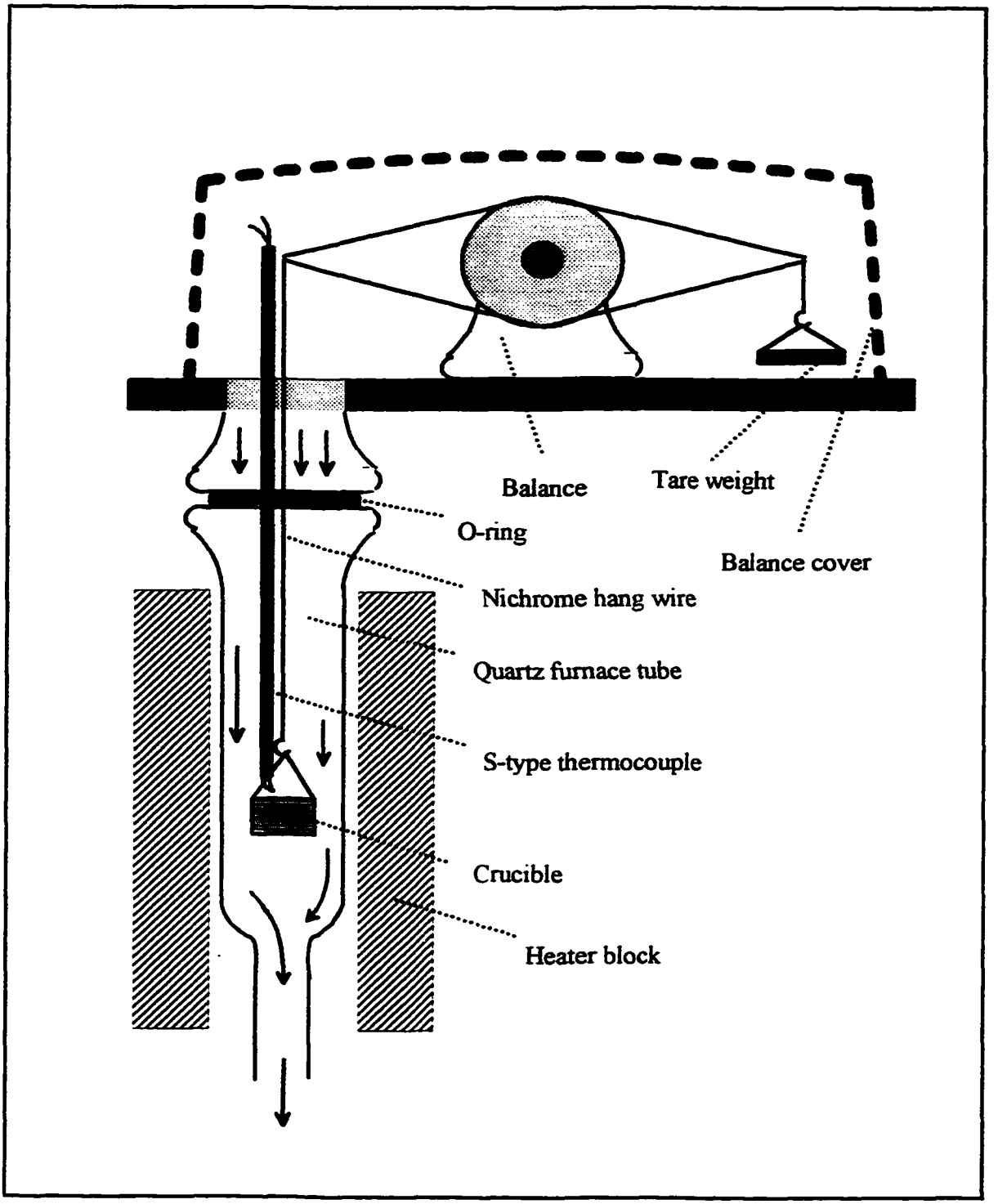


Figure 4.3 (a) The weight loss profile of $CaCO_3$ during exposure to a constant heating rate of 25 °C/min in He and its corresponding MS selected $CO_2$ release profile and (b) the selected release profile of a 3200 ppm $CO_2$ gas standard introduced for 15 min. (Note a 6 min delay in reaching full $CO_2$ concentration due to dilution in reactor and gas transport tubing.

closed nitrogen mass balance in order to investigate the efficiency of mixing and percolation in the tubular reactor design. As shown in Table 4.1 the total nitrogen contributing to the formation of the three nitrogen end products of interest (NO, HCN and $N_2O$) accounted for about 85% of the total char nitrogen. At this point, to further evaluate and understand the kinetic and mechanistic aspects of NO, HCN and $N_2O$ formation as well as to investigate the physical limitations versus the chemical factors involved during the model char oxidation processes, experiments at 5%, 10%, 20% and 40% $O_2$ in He were conducted.

Table 4.1 presents the percent of the char nitrogen released as NO, $N_2O$ and HCN in the oxidation of the tetraphenyl porphine and the tetrapyridyl porphine chars at various oxygen levels. An interesting observation is the accounted total amount of nitrogen at the end of every process. The nitrogen in NO, $N_2O$ and HCN accounts for about 80% of the initial amount (parent nitrogen in the char). There are good reasons to believe that the rest may represent $N_2$. In a study of the effects of pyrolysis conditions on the release of nitrogen

Table 4.1 The percent of released char nitrogen in NO, HCN and $N_2O$ forms during tetraphenyl porphine char and tetrapyridyl porphine char oxidation in various oxygen concentrations at 25 °C/min.

| % Oxygen in Helium | % char-N in NO | | % char-N in HCN | | % char-N in $N_2O$ | | % total char nitrogen | |
|---|---|---|---|---|---|---|---|---|
| | T-Ph-P | T-Py-P | T-Ph-P | T-Py-P | T-Ph-P | T-Py-P | T-Ph-P | T-Py-P |
| 5 | 31.2 | 4.1 | 39.6 | 86.7 | 8.3 | 2.0 | 79.1 | 92.8 |
| 10 | 13.5 | 9.8 | 70.8 | 106.3 | 5.4 | 2.4 | 89.7 | 118.5 |
| 20 | 19.0 | 21.9 | 61.1 | 60.8 | 2.8 | 2.0 | 82.9 | 84.7 |
| 40 | 23.0 | 50.0 | 55.6 | 17.5 | 2.0 | 3.0 | 80.6 | 70.5 |

during char combustion processes Làzaro et al.[6] noted that a substantial portion of the char-N is released in the form of $N_2$. Unfortunately, due to reasons explained in Chapter 2 a sufficiently accurate and error free detection of $N_2$ is not yet possible with the present system. As shown in Table 4.1 the HCN values obtained at 10% $O_2$ in He during the tetrapyridyl porphine char oxidation appear to be erroneous and are therefore not used in any mechanistic studies. It should also be noted that the values obtained are in reasonable agreement with those extracted from literature. Brown et al.[10] and Tullin et al.[26] reported that 14% to 47% of the char nitrogen contribute to the formation of NO during char oxidation processes. Tullin and coworkers have also shown that the total char nitrogen contributing to the formation of $N_2O$ is only 4% to 18%.

For both model char oxidation processes it is evident that the HCN formation decreases and the NO formation increases with increasing oxygen level (Figure 4.4). The opposite trend of HCN with respect to that of NO is suggestive of a series of reactions resulting in formation of NO from HCN. Note that the corresponding possible mechanisms will be discussed in detail in the following section. At higher oxygen levels, HCN molecules have a higher probability of becoming involved in oxidation reactions to form NO. In fact, the summed nitrogen contributions to the formation of NO and HCN (accounting for almost all of the nitrogen) is fairly constant over all oxygen levels. This clearly supports the assumption that the nitrogen in HCN ends up in NO as the oxygen level is increased. Due to the porous nature of the tetrapyridyl porphine char, the above mentioned effects appear to be much more pronounced here than for the tetraphenyl porphine char.

In contrast to HCN and NO formation, contributions of nitrogen to the formation of

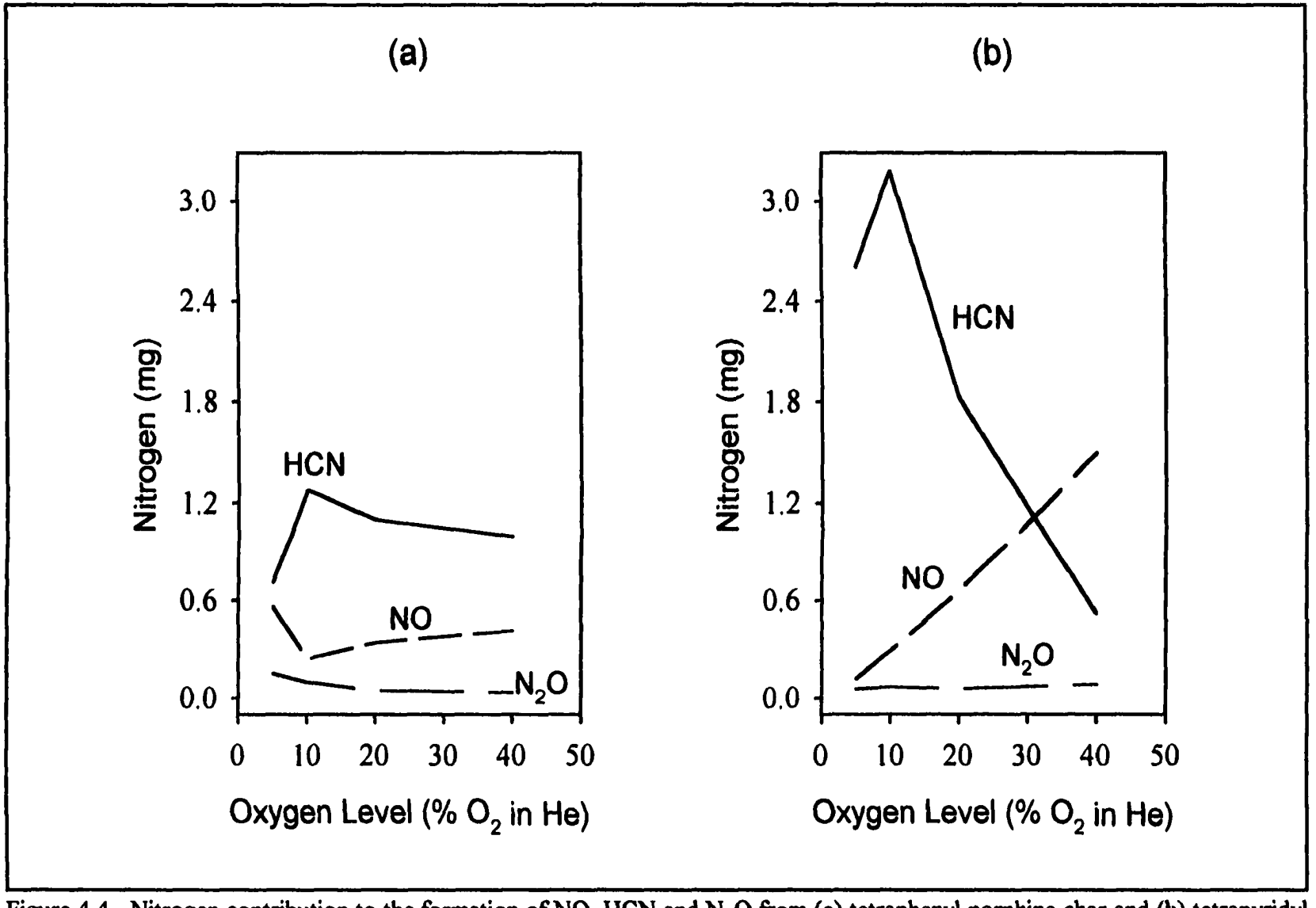


Figure 4.4 Nitrogen contribution to the formation of NO, HCN and $N_2O$ from (a) tetraphenyl porphine char and (b) tetrapyridyl porphine char oxidation at 25 °C/min as a function of oxygen concentration (tubular reactor configuration).

$N_2O$ as a function of oxygen level for both model chars do not follow the same trends. Tetrapyridyl prophine char oxidation illustrates a slightly increasing $N_2O$ trend with oxygen whereas the tetraphenyl porphine char oxidation presents an opposite trend. It is quite possible, that due to the less porous nature of tetraphenyl porphine, the rate of destruction of the active sites on the char surface by oxygen increases as the oxygen concentration is increased. Since, as proposed in Chapter 3, the formation of $N_2O$ from NO is thought to take place primarily on active carbon sites, the lower the population of these sites the lower the formation rate of $N_2O$. Thus, an increase in the level of oxygen could directly reduce the formation of $N_2O$. In the oxidation of tetrapyridyl porphine char a different factor controls the formation of $N_2O$ since, due to higher porosity, some of the NO molecules formed inside the pores could remain attached to these active sites. Meanwhile, evolution of other products inside the pores may produce a diffusion barrier for oxygen to enter the pores and attack and ultimately destroy the active sites. This could explain why the formation rate of $N_2O$ from the tetrapyridyl porphine char oxidation does not vary much with oxygen level.

## 4.5 Effects of Oxygen Level in the Thermogravimetry Reactor Configuration

Both model chars were oxidized in 5%, 10%, 20% and 40% $O_2$ in He at 25 °C/min in the original thermogravimetry furnace configuration. The corresponding differential weight loss profiles (DTG) are presented in Figures 4.5 and 4.6. By investigating these profiles at 95% weight remaining it is clear that the weight loss (or product evolution)

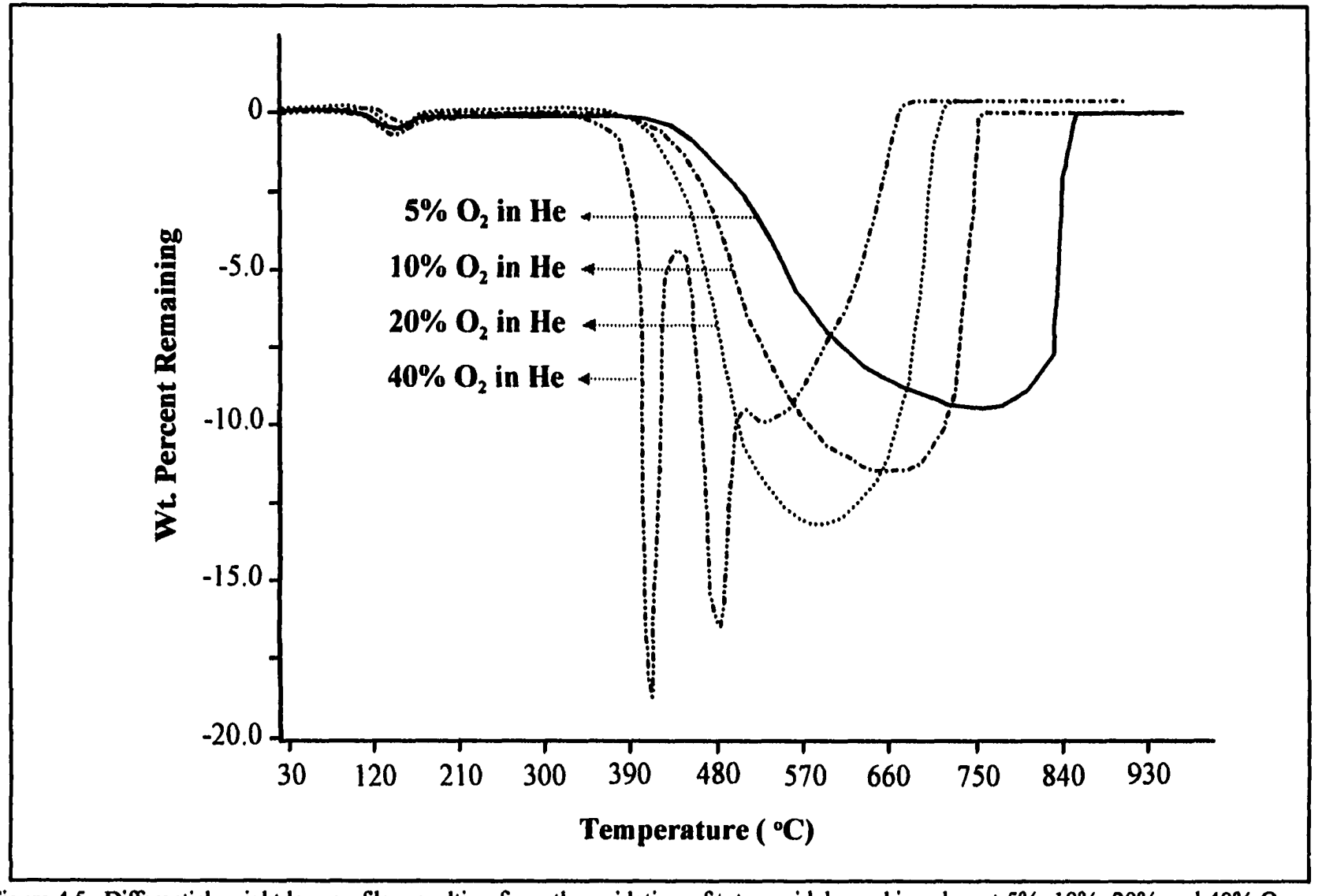


Figure 4.5 Differential weight loss profiles resulting from the oxidation of tetrapyridyl porphine char at 5%, 10%, 20% and 40% $O_2$ in He at 25 °C/min (thermogravimetry furnace reactor configuration).

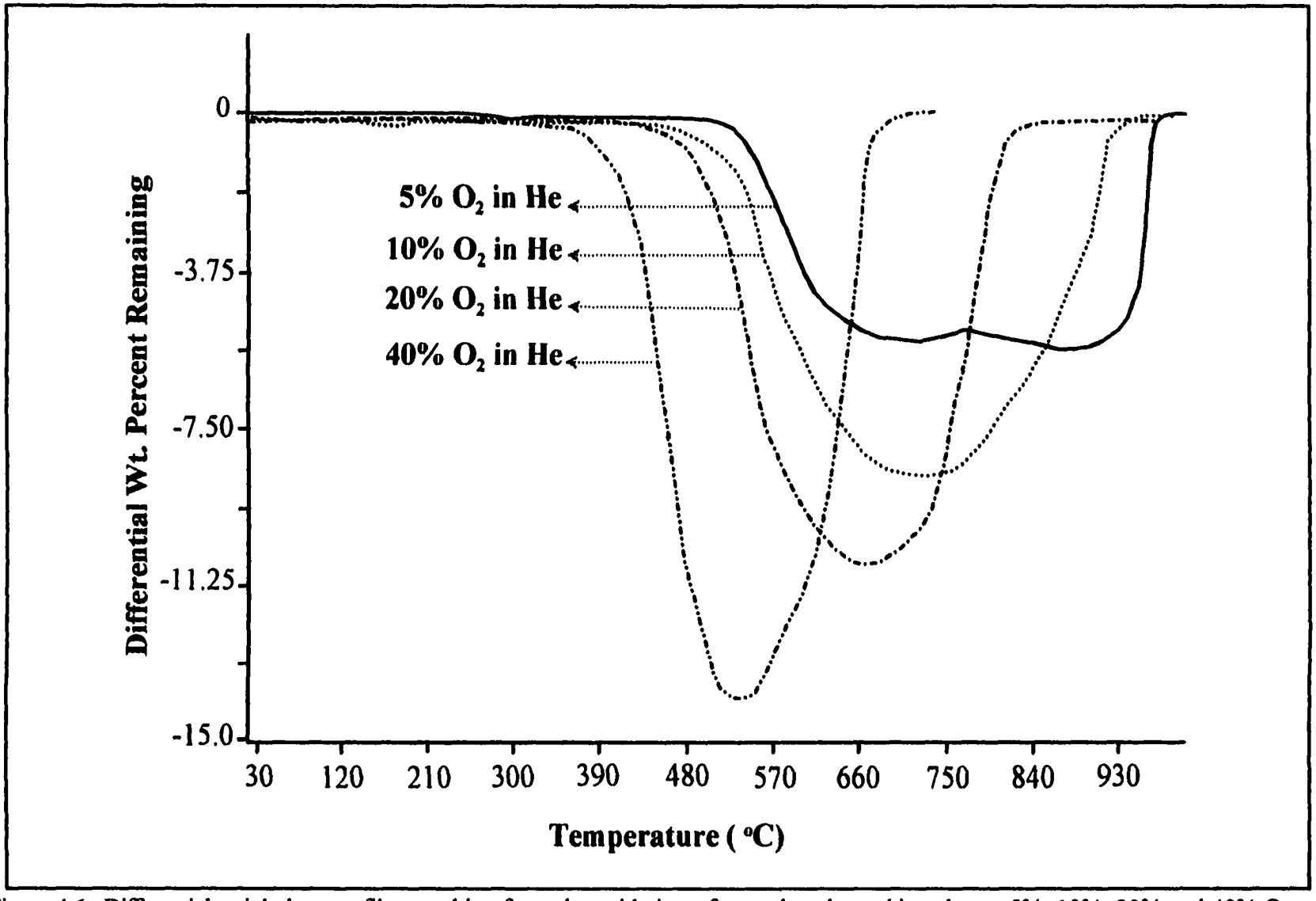


Figure 4.6 Differential weight loss profiles resulting from the oxidation of tetraphenyl porphine char at 5%, 10%, 20% and 40% $O_2$ in He at 25 °C/min (thermogravimetry furnace reactor configuration).

starting temperature decreases with increasing oxygen level (Table 4.2). The 5% weight remaining (i.e., 95% conversion) values indicate a similar trend. Note that the differential weight loss profiles tend to widen with decreasing oxygen level suggesting product formation and release over a longer temperature range. In addition to the lack of sufficient oxygen at lower oxygen levels, the cloud of evolved gases from the oxidation process (plus residual devolatilization) can limit the transport of oxygen into the crucible for further oxidation reactions. By comparing the differential weight loss profiles of both model chars it is readily seen that the overall reaction termination temperatures for tetrapyridyl porphine char are closer to one another than those of tetraphenyl porphine char. This can be again explained by the more highly porous nature of the tetrapyridyl porphine char. The char with the higher porosity exhibits a larger surface area for the oxygen to further react with the char whereas the less porous char presents a smaller surface area.

An interesting phenomenon appears in the weight loss profile of tetrapyridyl porphine oxidation in 40% $O_2$ in He. The profile illustrates a sudden drop in the weight of the char at

Table 4.2 Temperatures corresponding to 5% and 95% consumption of tetrapyridyl porphine and tetraphenyl porphine chars from oxidation at various oxygen levels.

| Percent Oxygen in He | Tetrapyridyl Porphine Char | | Tetraphenyl Porphine Char | |
|---|---|---|---|---|
| | $T_{5\%}$ (°C) | $T_{95\%}$ (°C) | $T_{5\%}$ (°C) | $T_{95\%}$ (°C) |
| 5 | 350 | 805 | 570 | 1060 |
| 10 | 325 | 710 | 525 | 840 |
| 20 | 310 | 690 | 480 | 720 |
| 40 | 300 | 660 | 458 | 665 |

the beginning of the oxidation process. This is thought to be the result of ignition on the char surface, either caused by the char itself or by the gaseous products in the pores of the char. The presence of ample oxygen for oxidation reactions as well as a large surface area (high porosity) can provide the right environment for ignition at the surface.

Although it is tempting to try to interpret the TG reactor profiles shown in Figures 4.5 and 4.6 further, e.g., with regard to possible underlying reaction mechanisms, the lack of a reliable mass balance as well as the mass transport limitations noted in the previous paragraphs prompted us to switch over to the quartz tube reactor configuration instead.

## 4.6 Effects of Oxygen Level in the Tubular Reactor Configuration

By investigating the total response chromatograms obtained with the infrared spectroscopy module and the mass spectrometry detector it can be seen that the overall product formation in the tetrapyridyl porphine char and the tetraphenyl porphine char oxidation processes starts at about 150 °C and 140 °C, respectively, regardless of the oxygen level (Figures 4.7 and 4.8). The product formation appears to happen over a broader temperature range at lower oxygen levels. In other words, at the heating rate used (25 °C/min) the level of oxygen dictates the temperature at which the product formation is completed. From the overall response chromatograms the completion temperature can be seen to decrease with increasing oxygen concentration clearly signaling the effect of mass transport limitaitons. Presence of high levels of oxygen at a given temperature would increase the chance of surface oxidation at higher rates resulting in a faster consumption of the char material and thus faster completion of gaseous product evolution.

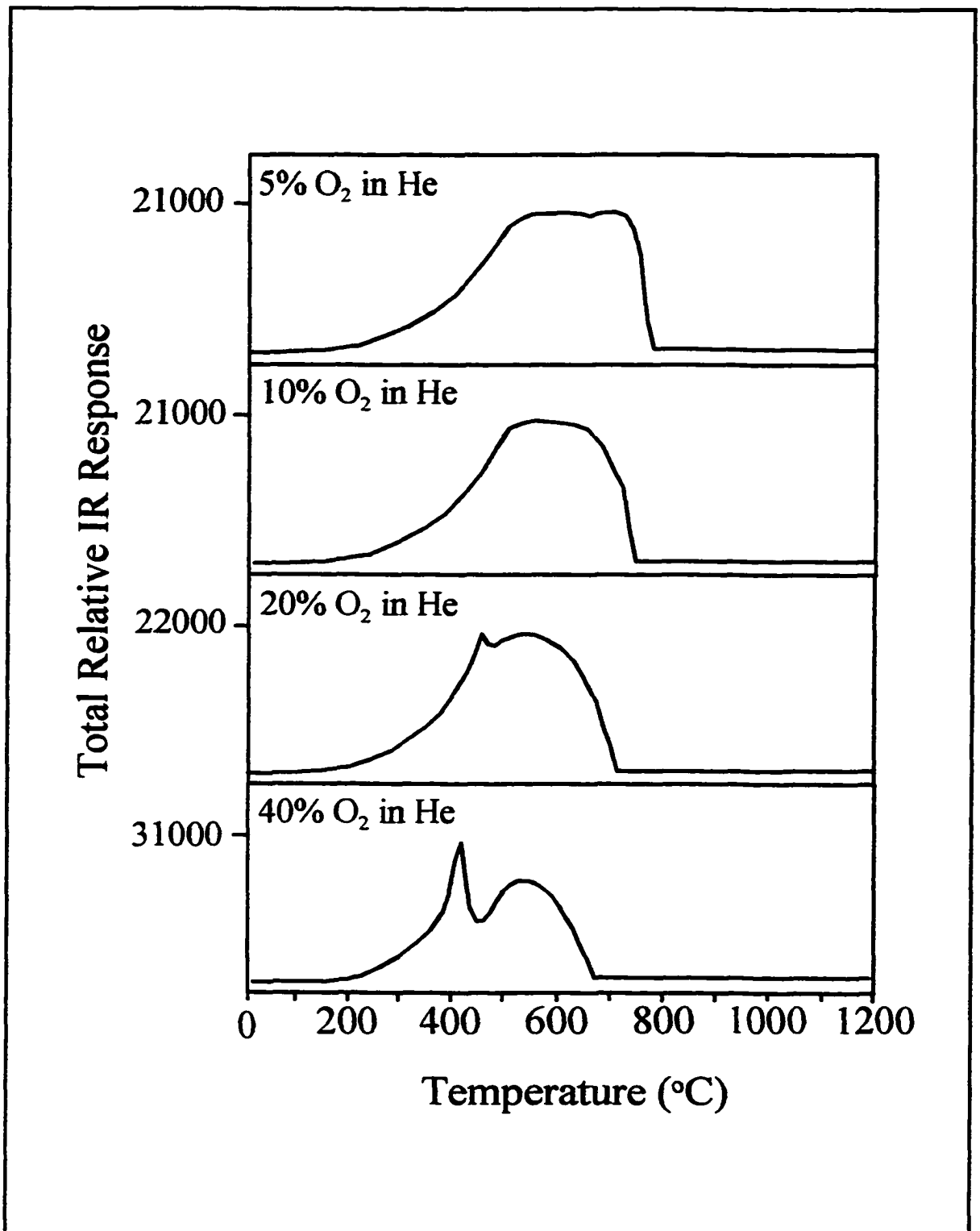


Figure 4.7 Total relative IR response chromatograms from the oxidation of tetrapyridyl porphine char in 5%, 10%, 20% and 40% $O_2$ in He at 25 °C/min (tubular reactor configuration).

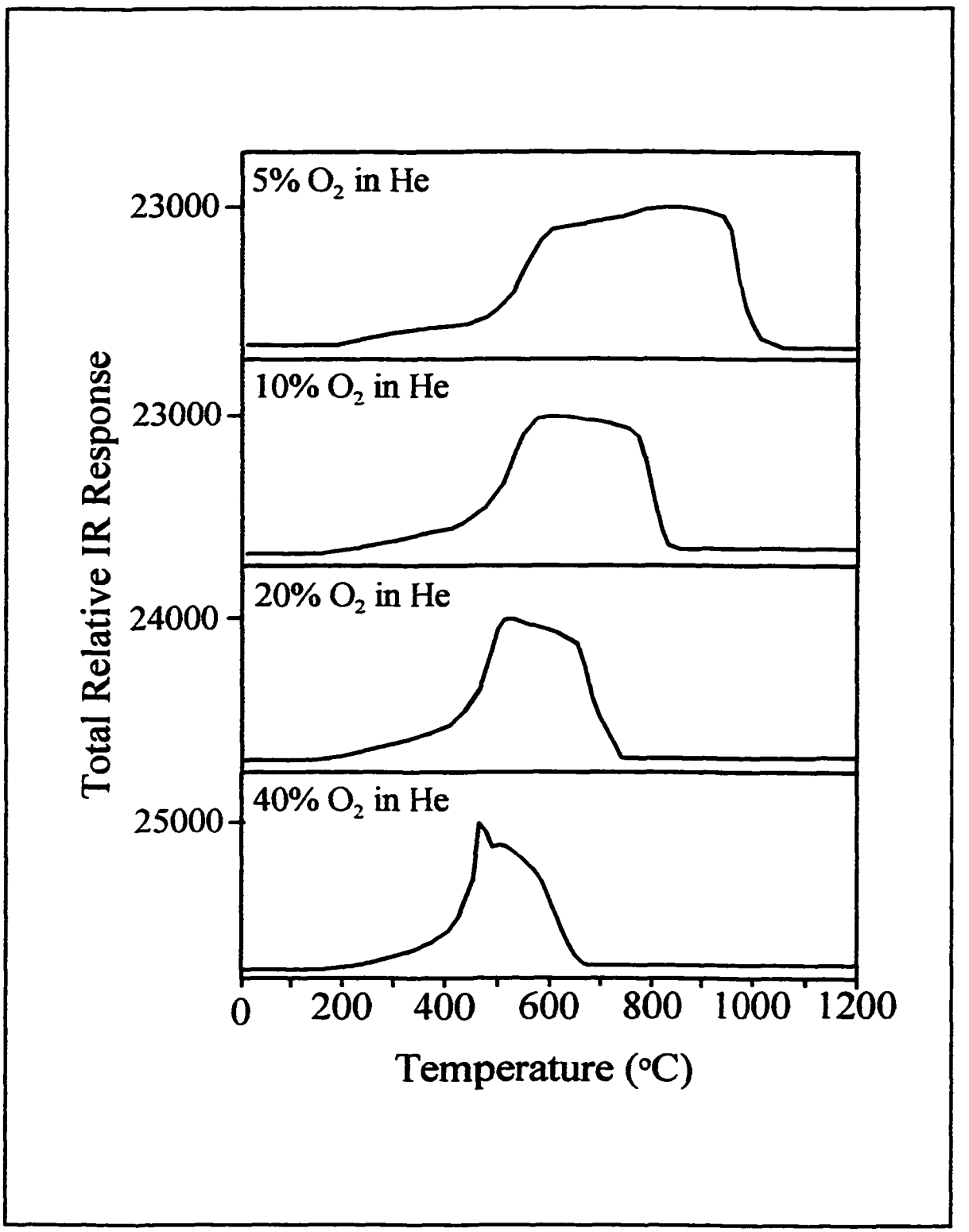


Figure 4.8 Total relative IR response chromatograms from the oxidation of tetraphenyl porphine char in 5%, 10%, 20% and 40% $O_2$ in He at 25 °C/min (tubular reactor configuration).

A rather intriguing phenomenon is observed at higher oxygen levels in both model char oxidation processes. At 20% and 40% oxygen concentrations a sharp and abrupt release of products is detected at about 430 °C (Figures 4.7 and 4.8). A possible explanation is that at higher oxygen levels (20% and 40% $O_2$ in He) the exothermic char oxidation process produces runaway sample bed heating. As a result, oxygen is consumed at a rapid pace while a cloud of gaseous combustion products forms around the surface of the char particles. The cloud of the gaseous products, in turn, can play the role of a barrier for the oxygen to reach the surface of the char for further oxidation. In other words, at the beginning of the oxidation process high levels of product formation are caused by a runaway exothermic reaction, probably involving highly active sites. This causes the relatively sharp increase on the left-hand shoulder of the profile. At this point oxygen levels within the char bed drop steeply while gaseous combustion products around the particles help create a diffusion barrier. This causes the runaway exothermic reaction to stop, resulting in the sudden drop on the left-hand shoulder of the profile. As the cloud of gaseous products gradually disappears, the concentration of oxygen at the char surface increases again. During this process oxidation increases, though at a somewhat slower rate since most active sites have now reacted out. This would result in a maximum in the profile, followed by a gradual shoulder on the right-hand-side corresponding to the gradual disappearance of the char. It is also conceivable that the sudden product release is due to secondary homogeneous reactions of the gaseous products. Due to the presence of ample amounts of oxygen the evolved gaseous products from the primary oxidation reactions could undergo a secondary gas-phase oxidation process (ignition), appearing as the sharp release of products on the left-hand-side shoulder. It should

be noted that the same effect was also observed in the oxidation of the tetrapyridyl porphine char in 40% oxygen in helium in the thermogravimetry furnace tube reactor. However, the presence of two peaks in the dTG profile of that experiment argues against the possibility of gas cloud ignition, unless as explained before, caused by sudden buoyancy changes.

Another interesting effect observed in both model char oxidation processes is the overall shape of the product release profiles (total response chromatogram) (Figures 4.7 and 4.8). From these profiles it is evident that, prior to reaching a maximum, the product formation shoulder on the left-hand-side is virtually identical for all oxygen levels (except for the sudden product release at higher oxygen levels). On the right-hand-side, however, the formation of products tends to vary from a sudden disappearance to a gradual termination in production as the oxygen level increases. In addition, at low oxygen levels (5% and 10% $O_2$ in He) the overall product formation increases until it reaches a plateau, apparantly as a result of detector saturation.

For mechanistic and kinetic studies the evolution profiles of $O_2$, $CO_2$, CO, HCN, $H_2O$, NO and $N_2O$ from the oxidation of both model chars in 5%, 10%, 20% and 40% $O_2$ in He were studied (Figures 4.9 and 4.10). By examining the time profiles of these products it is clear that due to the carbonaceous nature of these chars the profiles of $CO_2$ and CO appear first and follow the total response chromatograms very closely. The formation of water takes place almost simultaneously with $CO_2$ and CO regardless of the oxygen level. It should be noted that the first hump in the $H_2O$ profile at the initial stages of char oxidation corresponds to the evaporation of adsorbed moisture onto the char surface. Formation of

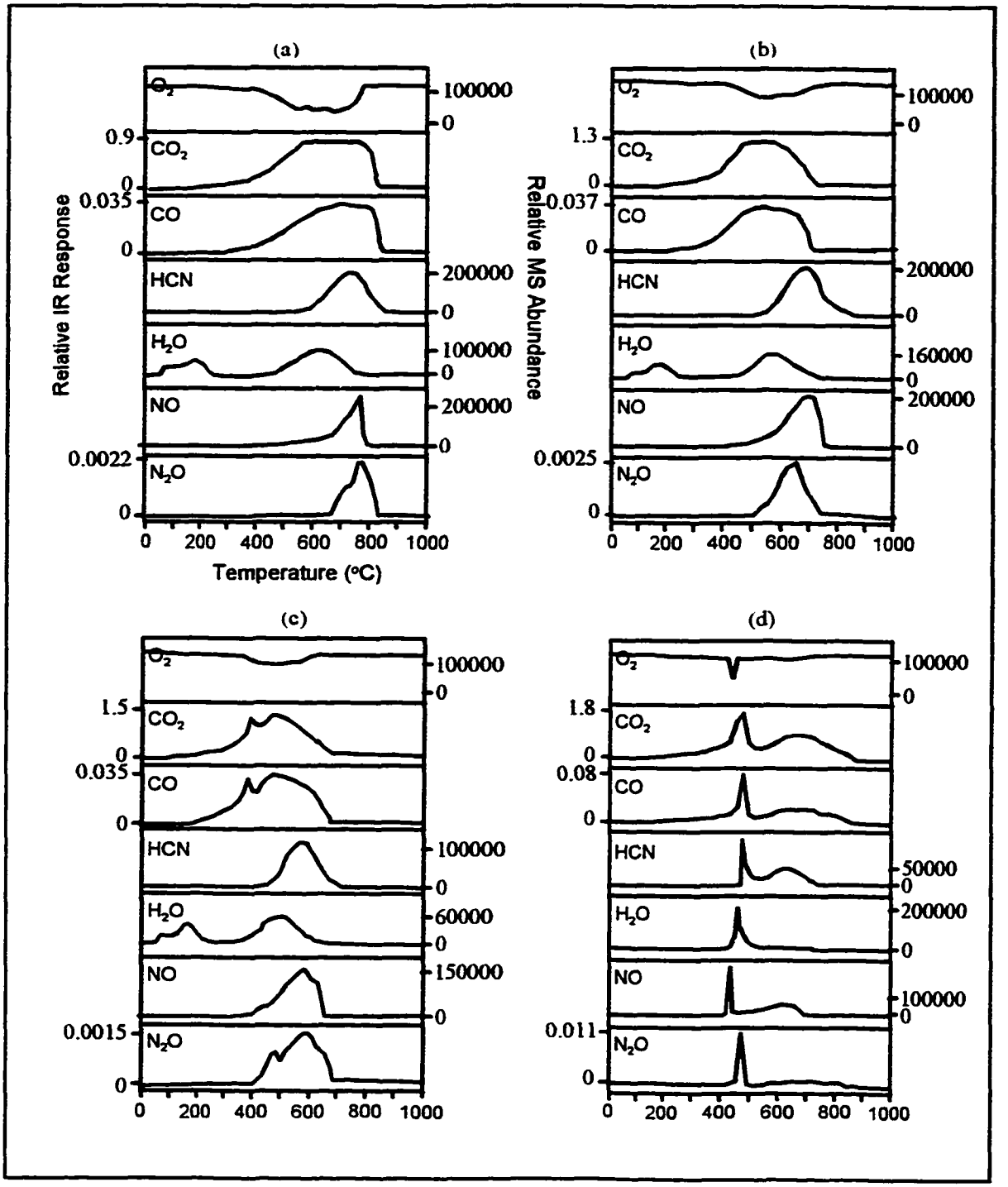


Figure 4.9 Temperature-resolved evolution profiles of $O_2$, $CO_2$, CO, HCN, $H_2O$, NO and $N_2O$ from the oxidation of tetrapyridyl porphine char in (a) 5%, (b) 10%, (c) 20% and (d) 40% $O_2$ in He at 25 °C/min (tubular reactor configuration). Note that figures (a), (b), (c) and (d) all posses similar axes but only (a) has been labeled. All left hand vertical axes ($O_2$, HCN, $H_2O$ and NO) represent relative IR response whereas all right hand axes ($CO_2$, CO and $N_2O$) show relative MS response.

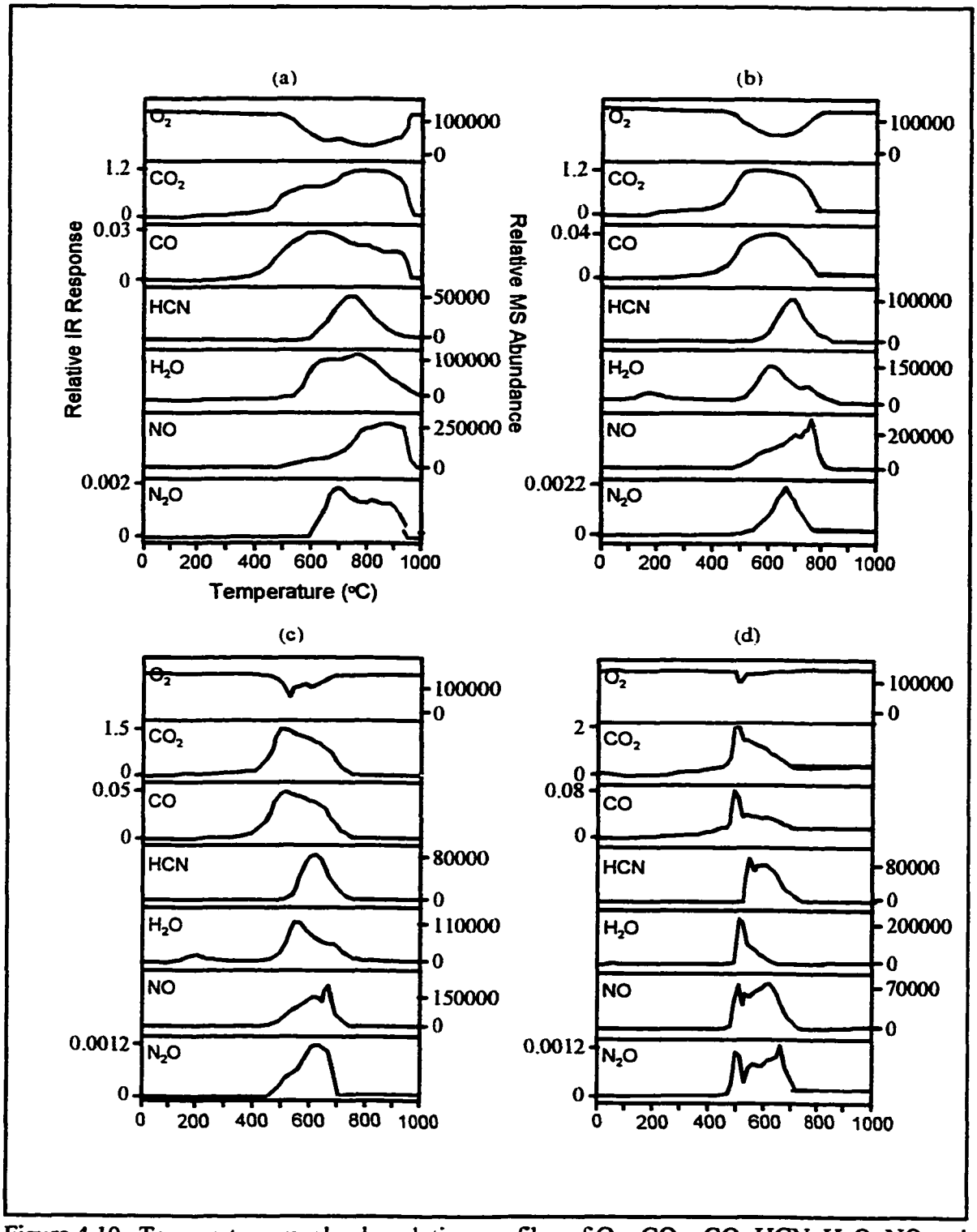


Figure 4.10 Temperature-resolved evolution profiles of $O_2$, $CO_2$, CO, HCN, $H_2O$, NO and $N_2O$ from the oxidation of tetraphenyl porphine char in (a) 5%, (b) 10%, (c) 20% and (d) 40% $O_2$ in He at 25 °C/min (tubular reactor configuration). For axes definitions refer to Figure 4.9.

NO starts earlier than HCN, but the profile shows a maximum at a lower temperature than NO. Formation of $N_2O$ starts almost at the same time as NO but reaches a maximum slightly prior to NO. The $O_2$ profile follows an inverse trend with respect to the $CO_2$ and CO suggesting that the most of the oxygen consumed was used for the oxidation of char carbon.

The HCN profile maximizes at a slightly higher temperature than the $H_2O$ profile, suggesting that $H_2O$ is perhaps the precursor to the formation of HCN. To further support this argument the $H_2O$ profile of tetraphenyl porphine char oxidation illustrates a bimodal behavior. By a close comparison of the $H_2O$ profiles with those of HCN at every oxygen level it is readily observed that the maximum in the HCN profiles lays right between the two humps of the $H_2O$ profiles. The trend is such that $H_2O$ formation starts at a certain temperature (depending upon the char and the oxygen levels) and increases until the HCN profile picks up. At this point the $H_2O$ formation slows down and in some cases even decreases (10% and 20% $O_2$ in He) until the HCN takes upon a decreasing trend after which the $H_2O$ profile picks up again. The relative MS abundances of HCN are about 10 times larger than those registered during the oxidation of both chars in the other reactor configuration. This indeed notes the fact, that in addition to $H_2O$ dependency, HCN formation is also oxygen dependent. This also supports the argument that the level of oxygen inside the forced percolation char bed, unlike the diffusion controlled crucible bed in the thermogravimetry tube reactor configuration, is very close to the oxygen concentration in the main stream flow. This is an indication of adequate mixing and sufficient percolation of oxygen in reactor tube and char bed, respectively.

Another interesting phenomenon are the relative MS abundance levels of $H_2O$ at each

oxygen level. It is rather obvious that at every oxygen concentration, irrespective of the char, the relative MS abundances of $H_2O$ are very much the same except at 20% $O_2$ in He. In other words, although the $H_2O$ formation level appears to change with $O_2$, the porosity does not seem to play a major role in its level. This is perhaps due to the fact that the $H_2O$ formed in the pores of the char during the oxidation process undergoes a secondary reaction resulting the formation of another product (HCN). As a result, the only surviving $H_2O$ molecules are the ones that are formed on the surface of the char and are not exposed to any secondary reaction pathways.

As pointed out earlier, the NO profile maximizes right after that of HCN regardless of the char type or oxygen level. Many investigators have proposed that HCN is the precursor responsible for the formation of NO. [15, 20, 21, 43 & 46] Galborg et al.[43] investigated the oxidation of hydrogen cyanide under flow reactor conditions. They proposed that the main oxidation reaction pathway for HCN proceeds through NCO:

$$HCN + OH \rightarrow CN + H_2O \qquad (4\text{-}1)$$

$$CN + O_2 \rightarrow NCO + O \qquad (4\text{-}2)$$

Further, depending on the gas composition and temperature, NCO would form HNCO by reacting with $H_2O$ or HCN, $N_2O$ or $N_2$ by reacting with NO, or NO by reacting with O.

For both model chars the relative MS abundances for NO show a decreasing trend with increasing oxygen level except for tetrapyridyl porphine char at 40% $O_2$ in He. The ratio of HCN to NO vary from 0.2 to 1.14. It should be noted that the HCN/NO ratio obtained from the gas phase oxidation experiment explained in Chapter 3 was 0.4. The HCN/NO ratio illustrates a decreasing trend with increasing oxygen in the tetrapyridyl porphine char

oxidation whereas the tetraphenyl porphine char shows an exactly opposite trend. These observations indicate that the porosity of the chars also plays an important role in the level of NO formed. It is very possible that the NO molecules are reduced inside the pores before having a chance to escape. [19, 26 & 37] Tullin et al.[19] proposed a model explaining the NO and $N_2O$ emissions by the nitrogen bound in the char conversion to NO and $N_2O$ on oxidation within pores. They also noted that the NO and $N_2O$ formed are subsequently reduced as they diffuse out of the pores. With higher porosity the possibility of a higher number of active carbon sites increases. This, in fact, could be the factor that reduces the NO molecules before they leave the pores of the tetrapyridyl porphine char.

The bimodal behavior of NO is only observed in the oxidation of tetraphenyl porphine char at 10%, 20% and 40% $O_2$ in He. It should be noted that at 40% $O_2$ in He the bimodal behavior is mainly due to the sudden product release which was explained earlier. In contrast to the common belief that bimodality in the NO profile is caused by two different nitrogen functionalities in char, [6, 9, 16, 31, 62 & 63] the results obtained from the experiments discussed in Chapter 3 clearly indicate that the bimodality is mainly caused by formation of the NO moiety (first peak) followed by the release of the chemisorbed NO form the active sites (second peak) due to the oxidation (and ultimately full consumption) of all the char carbon moieties. An observation that supports this argument is the formation of the second NO peak and its relationship with the disappearance trends of $CO_2$ and CO.

Irrespective of the char and the oxygen levels the $N_2O$ and NO profiles follow each other very closely with $N_2O$ maximizing prior to NO (Figure 4.9 and 4.10). This suggests that $N_2O$ is formed from NO. The same observation has also been reported by other

investigators.[15, 22, 26 & 41] Lu[22] in a laboratory-scale batch reactor under well-defined operating conditions observed both homogeneous and heterogenous reactions contributing to the formation of $NO_x$ and $N_2O$. He reported that the reaction of NO with char-N is the principle path for $N_2O$ formation in the presence of oxygen. Based on the results of the experiments discussed in Chapter 3 formation of $N_2O$ results from the reaction between an activated NO complex and a passing by NO molecule. In this scenario the activated NO loses the oxygen and reacts with the passing by NO to form $N_2O$. The oxygen is then consumed by the activated carbon to form CO:

$$NO + C \rightarrow CNO^* \quad (4\text{-}3)$$

$$CNO^* + NO \rightarrow N_2O + CO^* \quad (4\text{-}4)$$

To investigate the contribution of NO to the formation of $N_2O$, Miettinen et al.[24] used an $^{15}N$-isotope-marked NO in the inlet gas during a char oxidation process. They discovered that the addition of $^{15}NO$ to the inlet gas led to the formation of $^{15}N^{14}NO$ and $^{15}N_2O$, and the formation of these species increased with increasing concentration of $^{15}NO$ in the inlet gas, especially the formation of $^{15}N_2O$. These investigators suggested a two-step mechanism for $^{15}N_2O$ formation. The first step involves simultaneous reduction of $^{15}NO$ on the char surface and formation of a cyano compound. The second step is the reaction between $^{15}NO$ and the released and partly oxidized char compounds forming $^{15}N_2O$.

It should be noted that, formation of $N_2O$ from NO is a direct function of the concentration of NO as shown in Chapter 3. It was illustrated that at low NO concentrations (fed onto the Carbosieve) no $N_2O$ was formed. As noted in Chapter 3 Carbosieve is pure carbon and contains no nitrogen. It has been observed that in the model char oxidations even

at lower NO concentrations $N_2O$ has appeared as one of the prominent nitrogen products. It is possible that it is the char nitrogen that reacts with the activated NO to form $N_2O$. The other possibility is that during the carbosieve experiments the NO could not fully diffuse into the pores of the carbosieve to further react and form $N_2O$. In the model char oxidation processes the NO formation partly happens inside the pores of these chars and reacts in there to form $N_2O$.

It was mentioned earlier that $N_2$ is perhaps the other nitrogen compound formed during the oxidation of these model chars. In fact, it is likely the responsible species in consuming the unaccounted 10%-15% of the char nitrogen. It is possible that a considerable part of $N_2O$ is reduced on the char surface after formation, e.g.,

$$N_2O + C \rightarrow N_2 + CO^* \qquad (4\text{-}5)$$

Pels et al.[45] during an study on emissions of $N_2O$ and NO during fluidized bed combustion of six coals and their chars observed the efficient heterogenous reduction of $N_2O$ to $N_2$, which as they proposed, occurs on the char surface immediately after $N_2O$ is formed from char-N.

## 4.7 Effects of $O_2$ Level on the Maximum Product Evolution Rate Temperatures ($T_{max}$)

In order to investigate the physical and chemical effects of variation in oxygen levels on the overall char oxidation processes, a study was conducted on the temperatures at which the maximum nitrogen products of interest ($T_{max}$) were formed. The $T_{max}$ values of NO,

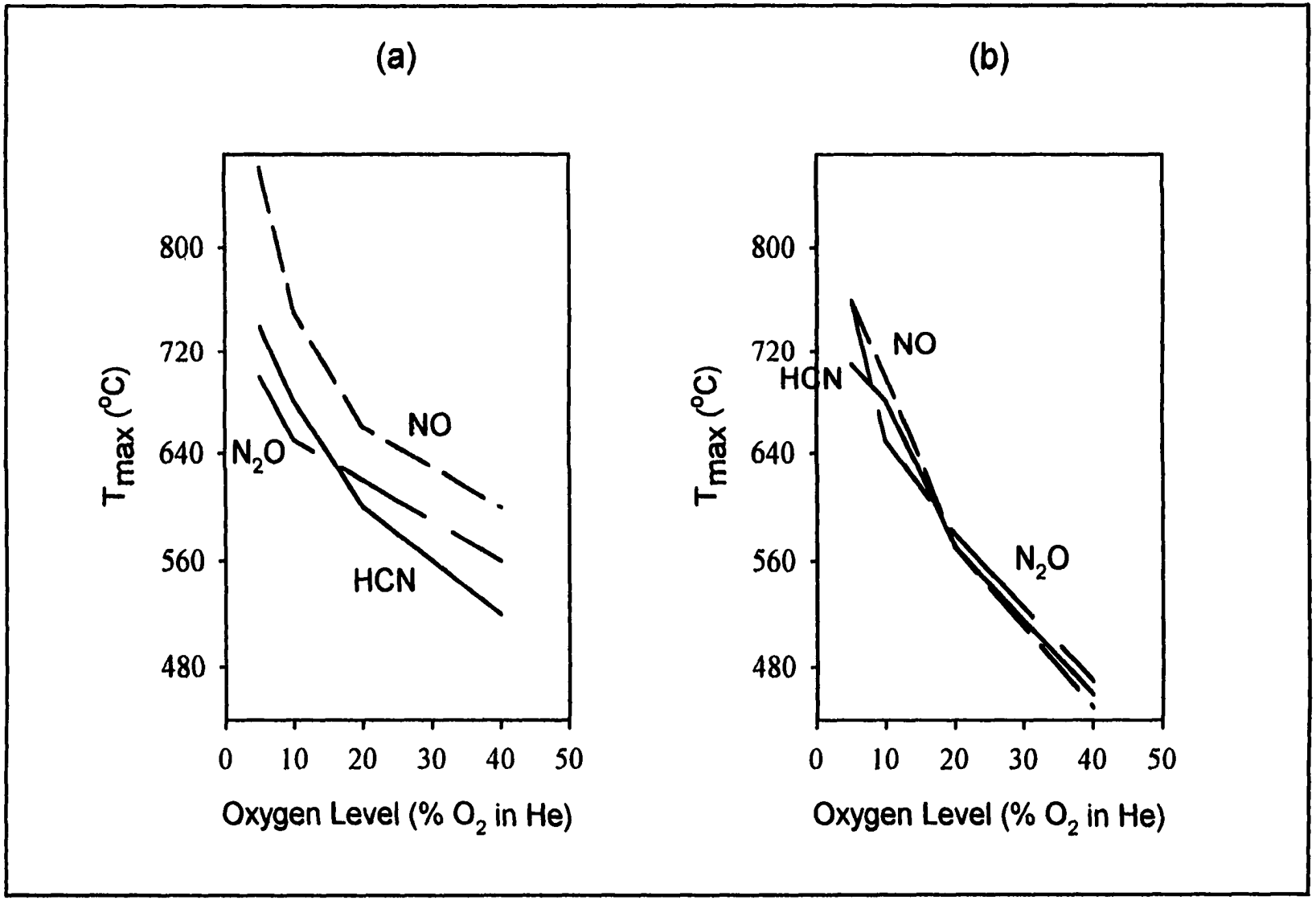


Figure 4.11 The maximum product release temperature versus oxygen level for NO, HCN and $N_2O$ during oxidation of (a) tetraphenyl porphine char (b) tetrapyridyl porphine char at 25 °C/min (tubular reactor configuration).

HCN and $N_2O$ versus oxygen levels for both model chars are presented in Figure 4.11. Note that the overall $T_{max}$ values for the tetrapyridyl porphine char are slightly lower than those of the tetraphenyl porphine char. This is due to the higher porosity of the tetrapyridyl porphine char compared to the other. Another phenomenon that is also affected by the porosity issue is the closeness of the $T_{max}$ profiles in the tetrapyridyl porphine char oxidation, as compared to the tetraphenyl porphine char. Since most of the reactions responsible for the formation of the NO, HCN and $N_2O$ are secondary reactions, the presence of porosity provides the right environment for these reactions to pursue. In other words, inside the pores the moieties responsible for the formation of any of the mentioned products have a better chance of meeting each other sooner whereas, in the less porous char the same effect takes place in a slightly longer time.

Another interesting phenomenon is the slope of the $T_{max}$ variation with respect to oxygen level. For both model chars, the $T_{max}$ slope of variation is relatively steep for oxygen concentrations below 20%. From 20% on the $T_{max}$ variation takes upon a milder slope. This can be explained by the fact at lower oxygen levels the overall process is chemically controlled and the reactions and their rates are the controlling factors during the oxidation processes. At higher oxygen levels (20% and 40% $O_2$ in He) a physical factor, namely transport limitation, overrides the chemical control. In this scenario, at the initial stages of the process the evolution of products take place at such a high rate that a the diffusion of the oxygen onto the char surface and into the pores is impeded by this phenomenon. This argument is also well supported by the ignitions observed in the overall release profiles of both tetrapyridyl porphine and tetraphenyl porphine chars.

# CHAPTER 5

# MECHANISTIC STUDIES IN COAL CHAR OXIDATION PROCESSES, EFFECTS OF OXYGEN LEVEL

## 5.1 Introduction

The experimental work discussed in Chapter 3 and 4 of this thesis demonstrated the existence of several different reaction pathways leading to the formation and/or destruction of HCN, NO and $N_2O$ when using various model chars and standard reference compounds. In this chapter we extend these studies to these coal-derived chars, representing different coal ranks (hvCb, hvAb and lvb). Two of these chars were produced by slow heating (10 °C/min) thermogravimetry (TG) techniques at relatively low temperatures ($T_{max}$ = 700 °C) whereas the third char was obtained with a high temperature (1200 °C), bench scale coal combustion reactor (Table 5.1).

In view of the difficulties encountered with slow diffusion of reaction products from the sample bed in a typical TG crucible, as well as incomplete mixing of products within the main carrier gas stream, we decided to use a quartz tube reactor configuration with small fixed sample bed and controlled percolation of known reactor gas flows, as described in Chapter 4.

The mechanisms and kinetics of $NO_x$ formation reactions during combustion of coal

Table 5.1 The rank and the elemental analysis of the selected coal chars. *Relative porosity rankings based on observed char densities (i.e., relative volume at selected char weight).

| Coal Chars | Coal Rank | C% | H% | N% | Porosity* |
|---|---|---|---|---|---|
| PSOC-1498 | hvCb | 82.32 | 2.08 | 1.70 | Low |
| PSOC-1521 | lvb | 81.22 | 2.26 | 2.03 | Medium |
| Pitt #8 | hvAb | 68.08 | 0.70 | 1.14 | High |

chars in small tube reactors have been investigated by Pels et al.[20] using mass spectrometry (MS) as a detection method and by Lázaro et al.[6] using infrared spectrometry (IR). Thus far, no studies appear to have been reported using combined IR and MS techniques, the advantages of which have been discussed in Chapter 2. Notwithstanding the sizeable numbers of coal char $NO_x$ formation studies reported in the literature, considerable uncertainties remain regarding the precise mechanisms of NO and $N_2O$ formation as well as the roles of HCN and of non-nitrogen-containing major combustion products, including CO, $CO_2$ and $H_2O$.

The present study attempts to establish the relevance of our findings for $NO_x$ formation during coal char combustion processes, by verifying and validating the results of these model char experiments with selected coal chars.

Due to the more than one magnitude lower nitrogen content of the coal chars (typically <1%) compared to the model chars (9-15%), on-line analysis attempts of nitrogen-containing TG reaction products severely test the lower detection limits of the MS and, particularly, the FTIR methods. Consequently, it is necessary to maximize product evolution rates, e.g., by using relatively large samples (20 mg) and high heating rates (25 K/min), thereby risking transport-controlled, rather than chemically-controlled, reaction conditions.

Although some degree of transport control of the primary heterogeneous reactions involved is practically unavoidable, e.g., with regard to pore diffusion rates of the oxygen reactant, the more serious transport limitations in terms of understanding the underlying reaction mechanisms are those affecting rate and residence time the evolution of nitrogen-containing reaction products, thereby possibly leading to a-typical secondary chemical reactions.

Finally, we need to have a reasonably complete ("closed") nitrogen mass balance in order to account for all major nitrogen containing reaction products. This requires a representative sampling strategy, i.e., measured sample concentrations should reflect the combined stoichiometries of the underlying chemical reactions. As discussed above, well-mixed representative samples can be difficult to obtain in a typical TG experiment. Consequently, most of the nitrogen product evolution monitoring experiments reported here were performed in a small QTR with well-percolated sample bed.

## 5.2 Reactor Configuration

The original Perkin Elmer TGA7 thermogravimetry furnace configuration is shown in Figure 5.1. In this configuration an alumina crucible hangs from an electronic micro-balance by means of a nichrome wire. Fixed sample quantities of 20 mg in the crucible were used for these experiments. In this design the crucible contains a small sample bed and, therefore, the overall configuration can be thought of as a micro-scale fixed bed reactor. The furnace tube has a large enough inner diameter that considerable spacing exists around the crucible for the purge gas to carry the evolved gaseous products away from the crucible. As discussed before (Chapter 4), however, due to the poorly defined percolation behavior

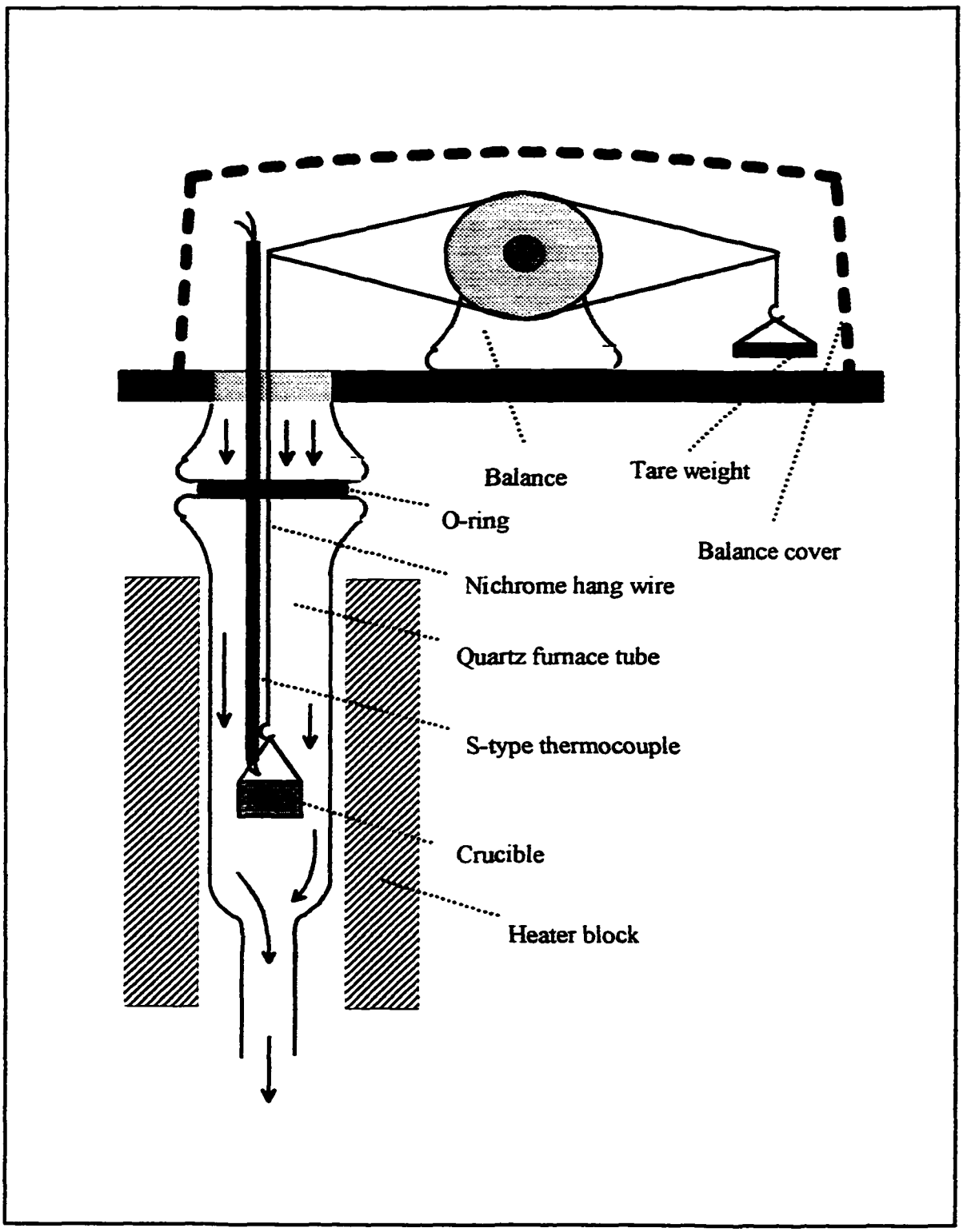


Figure 5.1 Schematic of the original Perkin Elmer TGA7 thermogravimetry furnace configuration. The system is composed of a reactor chamber (quartz furnace tube) surrounded by a cylindrical heater block and topped off with a microbalance.

of oxygen and combustion products within the sample bed and the difficulty in achieving nearly instantaneous mixing of the evolved gaseous products within the main stream flow, the temperature-resolved evolution profiles of these products may be affected by mass transport resistance. As a result, the TG reactor configuration was used only to obtain information on the weight loss profiles during oxidation of the model compounds at various oxygen levels whereas the quartz tube reactor configuration shown in Figure 5.2 was used to record time-resolved product evolution rates as well as determine product concentrations under chemically controlled conditions.

The furnace tube in the quartz tube reactor has a smaller inner diameter (0.5) than the TG reactor. The material of construction (quartz) and the length (15.5 cm) of the new furnace tube were chosen to be the same as the original tube in order to satisfy the dimensions and materials properties of the original thermogravimetry system. Quartz wool was selected as the bed support material in order to hold the powdered samples used and effectively replace the crucible. In order to eliminate the effect of sample size on the overall outcome of these experiments similar sample quantities (20 mg) were used. When an experiment is in progress, the carrier gas and the evolved gaseous products that have traveled through the sample as well as the quartz wool, experience a more efficient mixing process. To facilitate complete mixing, the sampling probe inlet was set at a distance of 1 cm below the bed, thereby allowing longer gas phase residence times in the tube before sampling. In the quartz tube configuration mode no weight loss profiles can be recorded.

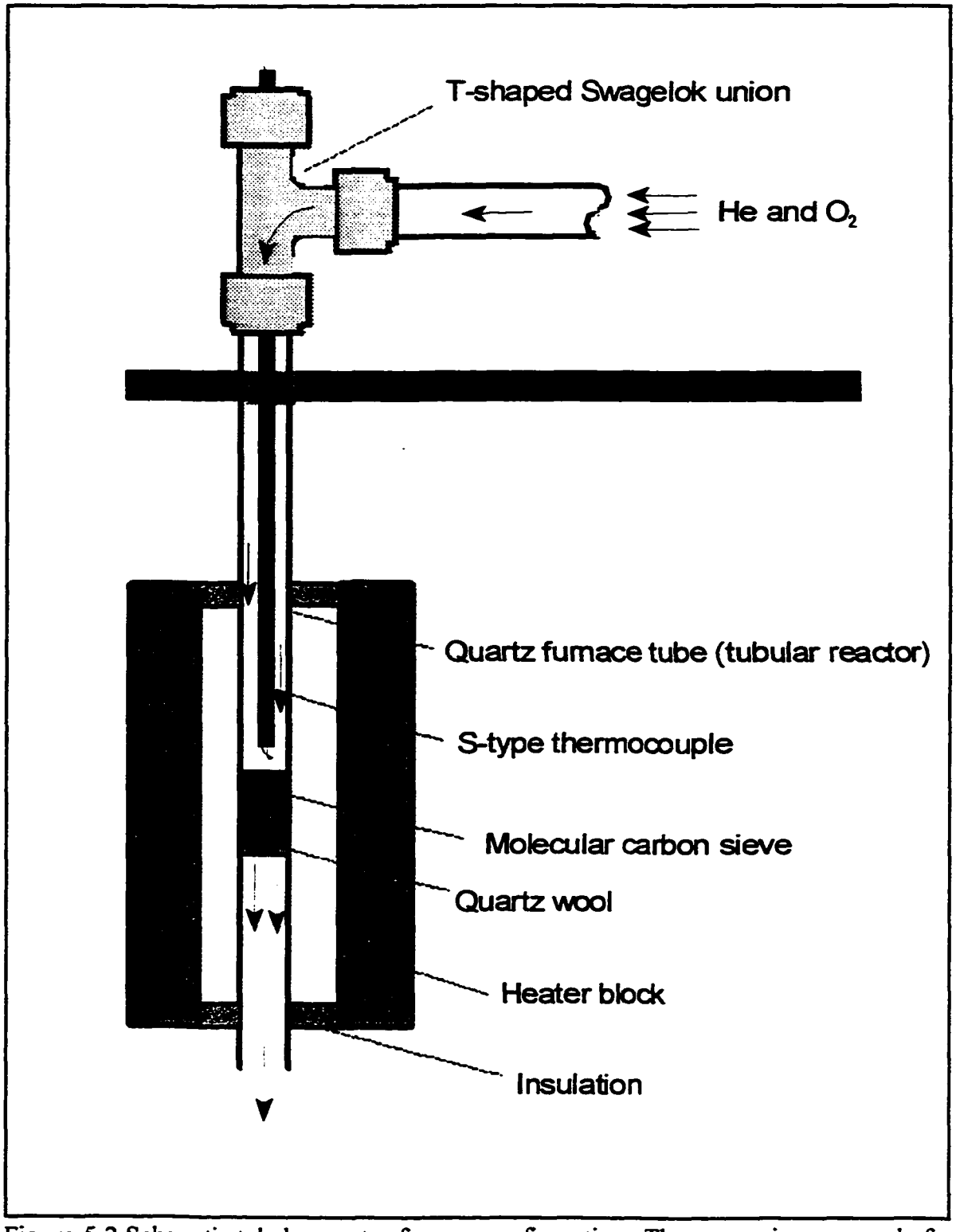


Figure 5.2 Schematic tubular reactor furnace configuration. The system is composed of a reactor chamber (quartz furnace tube) surrounded by a cylindrical heater block and a molecular carbon sieve bed supported by a bed of quartz wool.

## 5.3 Thermogravimetry Experiments

In order to determine whether the char oxidation rates observed in our experiments were consistent with chemically controlled conditions, TG weight loss rates were measured at the same heating rates (25 °C/min), oxygen levels (5%, 10%, 20% and 40% $O_2$ in He) and sample size (approx. 20 mg) as used in the flow-through QTR experiments, in which individual reaction product concentration profiles were measured.

The TG weight loss profiles in Figure 5.3 show the well-known positive correlation between char oxidation rate and oxygen concentration. Recent articles by Vàrhegyi et al.[75 & 76] report a first order dependence of reaction rate on oxygen level. Similar findings were reported by Alvarez et al.[77]

A more detailed view of the rate phenomena underlying weight loss measurements during temperature-programmed TG runs can be obtained by the procedure outlined by Maswadeh et al.[78] in which the observed weight loss and/or product evolution rates as a function of temperature are normalized for driving force (i.e., divided by the remaining weight loss elevated to a power equal to the reaction order) and then plotted in an Arrhenius plot format, as shown in Figure 5.4. Note that these are not formal Arrhenius plots obtained by drawing a straight line (i.e., assuming a single underlying rate law) through a series of rate constants measured at different temperatures, each representing a separate isothermal experiment. However, it should be pointed that as long as the underlying assumption is that at every point in time during the experiment (whether isothermal or temperature-programmed) the reacting sample has decomposed into a reacted and an unreacted part, there should be no difference between the results of a series of isothermal experiments at

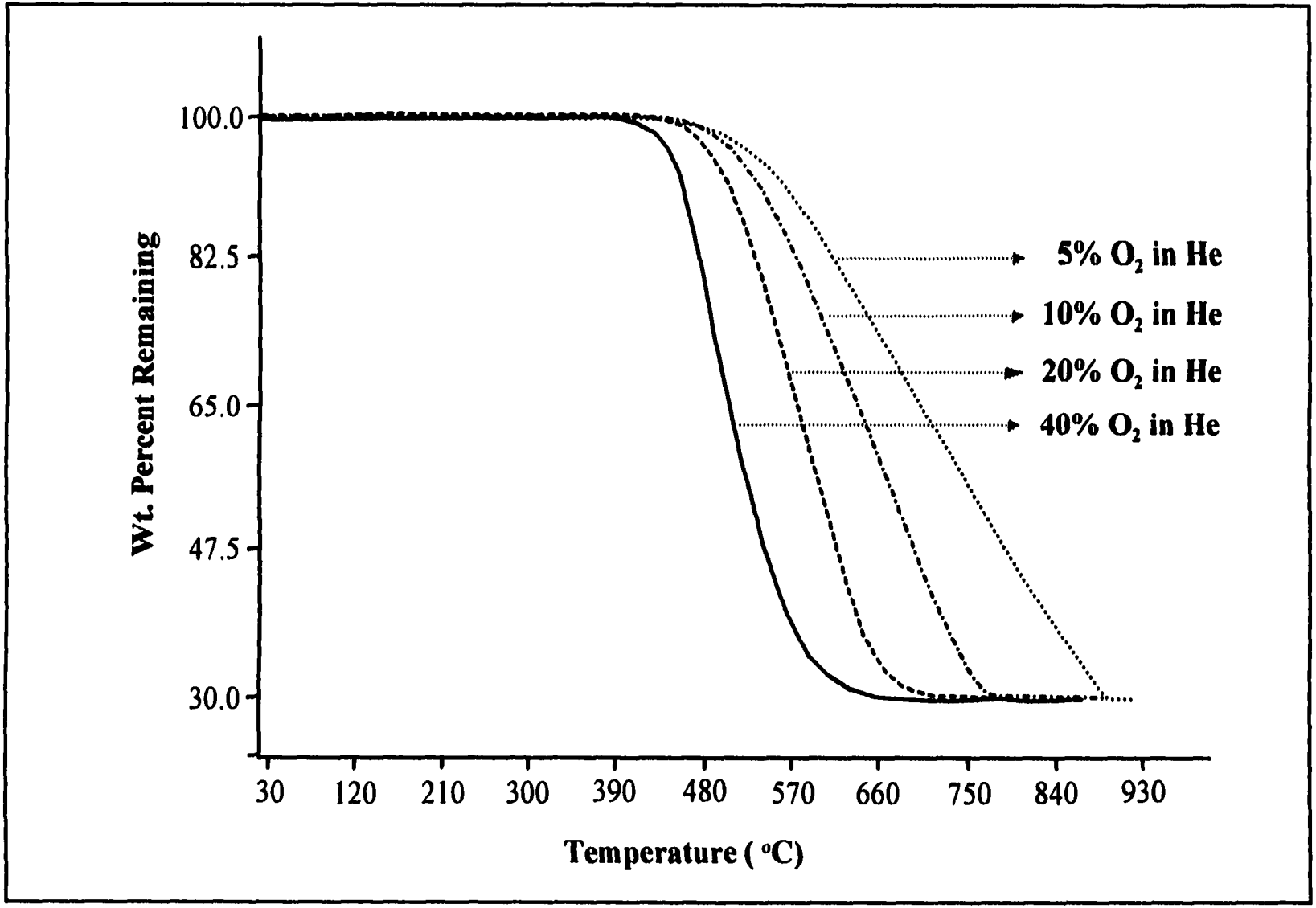


Figure 5.3 Weight loss profiles resulting from the oxidation of Pittsburgh #8 at 5%, 10%, 20% and 40% $O_2$ in He at 25 °C/min (thermogravimetry furnace reactor configuration).

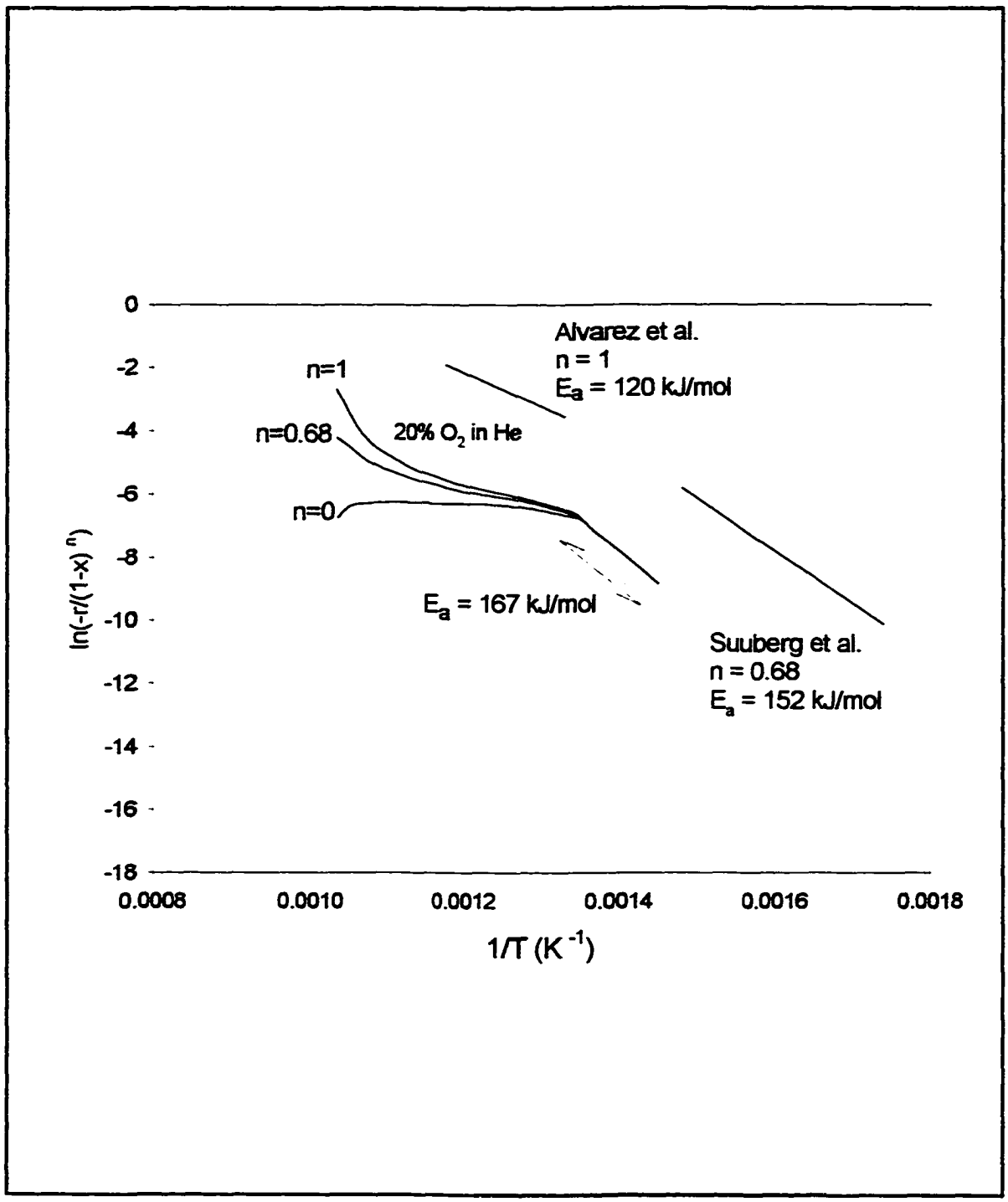


Figure 5.4 The observed weight loss and/or product evolution rates as a function of temperature normalized for driving force (i.e., divided by the remaining weight loss elevated to a power equal to the reaction order) and then plotted in an Arrhenius plot format. This is done for reaction orders of n=1, 0.68 and 0 in oxidation of Pittsburgh #8 char in 20% $O_2$. The resulting profiles are also compared to the ones reported by Alvarez et al.[77] and Suuberg et al.[79]

different sample temperatures x, y and z and a single experiment in which the sample temperature is changed from x to y to z in a stepwise manner, provided that (in both types of experiment) sample temperatures are maintained longer than the response time of the experimental system. Furthermore, as long as during a linear temperature-programmed TG run the response time of the experimental system is shorter than the time associated with the inherent temperature measurement error of the system, the error associated with rate measurements obtained during continuous, temperature-programmed weight loss experiments will not be measurably larger than the errors inherent in isothermal TG weight loss rate measurements. In summary, the errors associated with estimating rate constants during a single, temperature-programmed experiment are not necessarily larger than the errors associated with rate constant estimates obtained from consecutive isothermal experiments provided: (a) the reaction is chemically controlled; (b) the driving force is provided by unreacted sample; and (c) the response time of the experimental system is short relative to the time uncertainty caused by the sample temperature measurement error.

Suuberg et al.[79] reviewed the literature on char oxidation rates and found that the majority of studies reported fractional reaction orders in the 0.5 to 1.0 range for chars as well as graphite. In their own experiments they consistently observed a reaction order of 0.68. Várhegyi et al.[76], on the other hand propose an apparent reaction order of 1.0 under strictly chemically controlled reaction conditions. Viewed from the perspective of reaction order, a careful inspection of Figure 5.4 reveals that during the first 5%, or so, of the weight loss process the driving force-normalized measured rates form a single straight (or nearly straight) line independent of a particular reaction order assumption (viz. n=1, n=0.68 and n=0).

According to the foregoing discussion the slope of this line can be assumed to represent the apparent activation energy, $E_a$, whereas the (extrapolated) intersect with the ordinate determines the pre-exponential factor, A. The strong deviation of the measured reaction constants at conversion values well above 5% from the linear relationship observed at lower temperature (the cause of which will be discussed) makes it alas impossible to choose between the various reaction orders proposed in the literature.

Not only are the reaction temperatures in our experiments relatively low, also the density of active sites in the coal char samples used appears to approximately one or two orders of magnitude lower than that of the specially activated chars used in many experiments reported in the literature. This is illustrated in Figure 5.4 by comparing our measured rates with the measured rate plots reported by Suuberg et al.[79] and Alvarez et al.[77]

Before discussing the obvious deviation of the measured rates at higher temperatures seen in Figure 5.4 it should be noted that the observed insensitivity of the measured rate constants to the choice of reaction order during the earliest stages of the reaction is a well-known phenomenon in chemical kinetics.[80] In fact, this phenomenon is widely used to estimate the apparent activation energy of a reaction without having to establish a reaction order.[80] In this case, an activation energy, $E_a$, of 167 kJ/mole produce Arrhenius plots which are indistinguishable from all three normalized experimental rate curves plotted in Figure 5.4 at temperatures up to 1000 °C.

If we assume that the straight line segment at lower temperatures represents chemically controlled reaction rates at 20% oxygen it becomes readily possible to predict the reaction rates at 10% , 5% and lower oxygen levels using the reported linear dependence of

the reaction rate on the oxygen concentration. As shown in Figure 5.5, at the lowest temperatures the measured rates at 10% and 5% indeed approach the predicted rates.

Above this temperature, however, we observe a rapid loss of reaction rate. This corresponds to the point where a 20 mg char sample heated at 25 °C/min in a percolated flow of 50 ml/min of 20% oxygen in helium is starting to measurably reduce the measured concentration of oxygen exiting the bed, as shown in Figure 3.3 (Chapter 3). Note that in nonpercolated (i.e., diffusion-controlled) TG crucibles oxygen concentrations may be assumed to be reduced even further. As discussed before, the relatively large sample size (20 mg) and high heating rate (25 °C/min) were necessary in these experiments in order to permit time-resolved FTIR and MS measurements of low concentration, nitrogen-containing char oxidation products. Figure 3.3 in Chapter 3 shows that around 480 °C the oxygen concentration at the bottom of the bed can be estimated to be approximately 4%. This corresponds to an average estimated bed oxygen level of 12%.

Assuming a first order dependence of carbon weight loss rate on oxygen concentration, as reported by several investigators,[75 & 77] predicted normalized rate curves at 20, 10 and 5% $O_2$, using the previously estimated $E_a$ and A values, are shown in Figure 5.4 for reaction orders n=1, n=0.68 and n=0.

Due to well recognized differences between the quartz tube reactor and the TG crucible experiments no direct experimental verification of the predicted bed oxygen levels in the crucible is possible. Future experiments should focus on combining the advantages of percolated bed with those of direct weight loss measurements. However, a rough comparison of Figure 5.5 and Figure 3.3 in Chapter 3 shows that as oxygen levels start

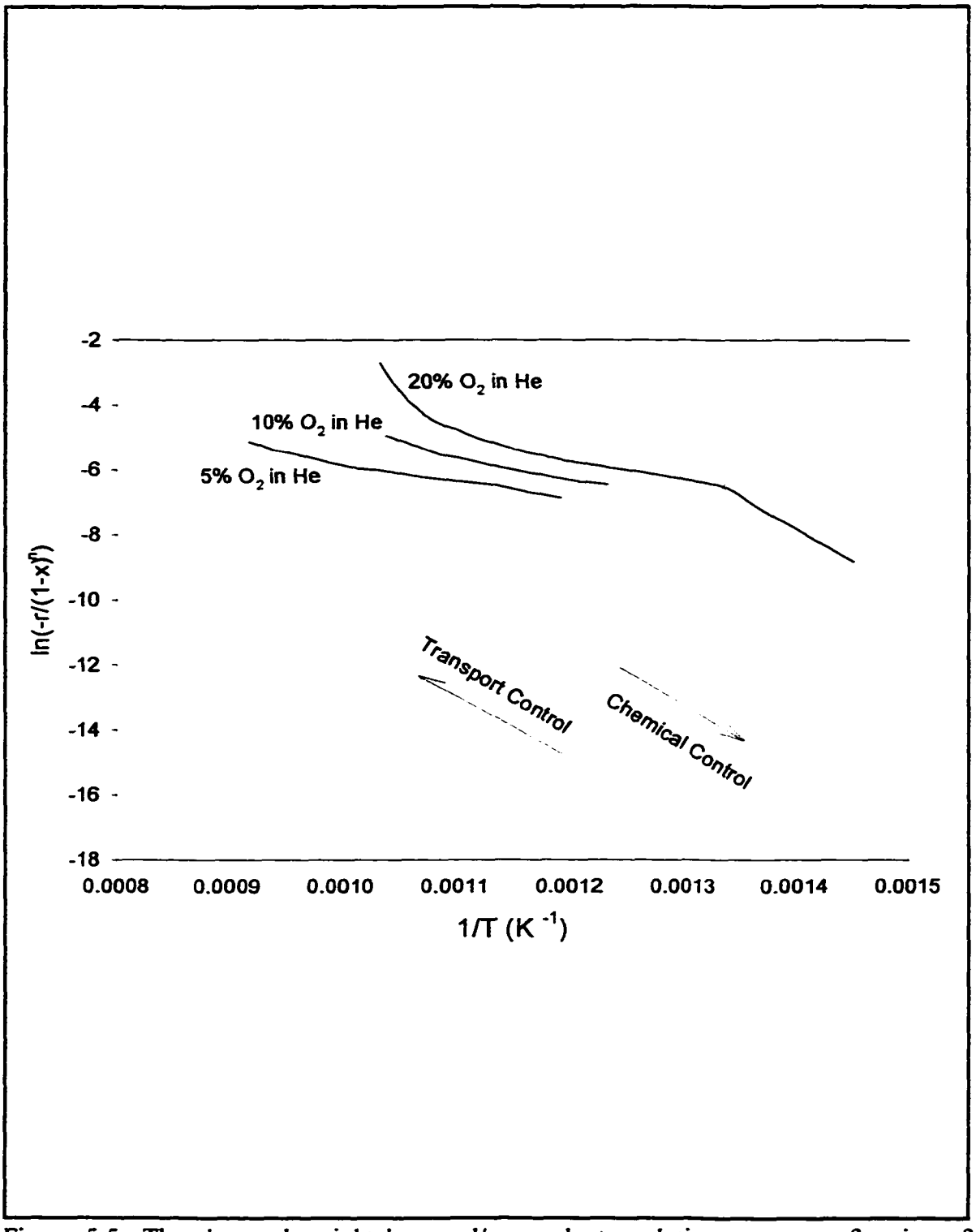


Figure 5.5 The observed weight loss and/or product evolution rates as a function of temperature normalized for driving force (i.e., divided by the remaining weight loss elevated to a power equal to the apparent reaction order; here assumed to be 1.0) and then plotted in an Arrhenius plot format.

recovering a slow return of the normalized measured rates to the predicted rates at 20% $O_2$ levels is observed. It should be remembered, however, that the measured oxygen levels in the well percolated quartz tube reactor may be assumed to have depleted less and recovered faster than the oxygen levels in the purely diffusion controlled TG reactor. Moreover, the possible effects of desorption losses of active sites at higher temperatures, a well-established phenomenon,[11, 12, 13, 29 & 32] on the observed rates have been ignored here.

As discussed previously, the primary purpose of the TG experiments shown in Figures 5.3-5.5 is not to contribute new data or understanding to the kinetics or mechanisms of carbon oxidation but to establish whether the experimental envelope within which we were able to perform our char nitrogen oxidation studies is conducive to the elucidation of chemical reaction mechanisms for nitrogen-containing char moieties. The conclusion that can be drawn cautiously is that the early stages of the carbon gasification reactions appear to be primarily under chemical control in that calculated kinetic parameters correspond well with literature values. During the middle portion of the gasification reaction falling oxygen levels within the reactor bed can be shown to strongly affect measured weight loss rates. Whether this should be regarded as a chemical effect (i.e., based on the first order relationship between oxygen concentration and char oxidation rate proposed in the literature) or as a transport limitation is largely a matter of definition. However, there appear to be no literature data to suggest that the variation in oxygen level during the experiment should be expected to affect not only the reaction rates but also the char nitrogen oxidation rates and mechanisms. Finally, towards the end of the carbon gasification process, oxygen levels within the char bed, as well as the corresponding weight loss rates, start to return towards the initial levels.

## 5.4 Tubular Reactor Experiments

### 5.4.1 Nitrogen Mass Balance

In order to determine whether major reaction pathways leading to the formation of nitrogen-containing combustion products could be overlooked nitrogen mass balances were calculated from the measured intensities of the HCN, NO and $N_2O$ signals. The results are shown in Figure 5.6 and reveal that between 48% and 94% of the nitrogen in all three char samples is accounted for by HCN, NO and $N_2O$. Note that, just as in the model chars shown in Chapter 4, the HCN and NO profiles for all three chars are mirror images suggesting that NO is again formed by homogeneous gas phase oxidation; a pathway clearly demonstrated in Chapter 2.

Obviously, the percentage of nitrogen explained is strongly affected by the experimental conditions as well as by char type. Surprisingly, in all three chars the highest explained nitrogen percentages are seen at lowest oxygen concentration values (i.e., 5%) with the lowest explained nitrogen percentages found at 20% $O_2$. This pronounced nonlinear behavior is either thought to indicate the presence of two or more competing mechanisms, or else the participation of an undetectable, nitrogen-containing intermediate. Based on the model char and model compound studies described in Chapters 3 and 4, a competitive reaction mechanism leading to pronounced losses of detectable nitrogen at intermediate oxygen levels could well involve the following hypothetical pathways: (1) at highest oxygen percentages (i.e., 40%) the relatively low average reaction temperatures lead to the highest

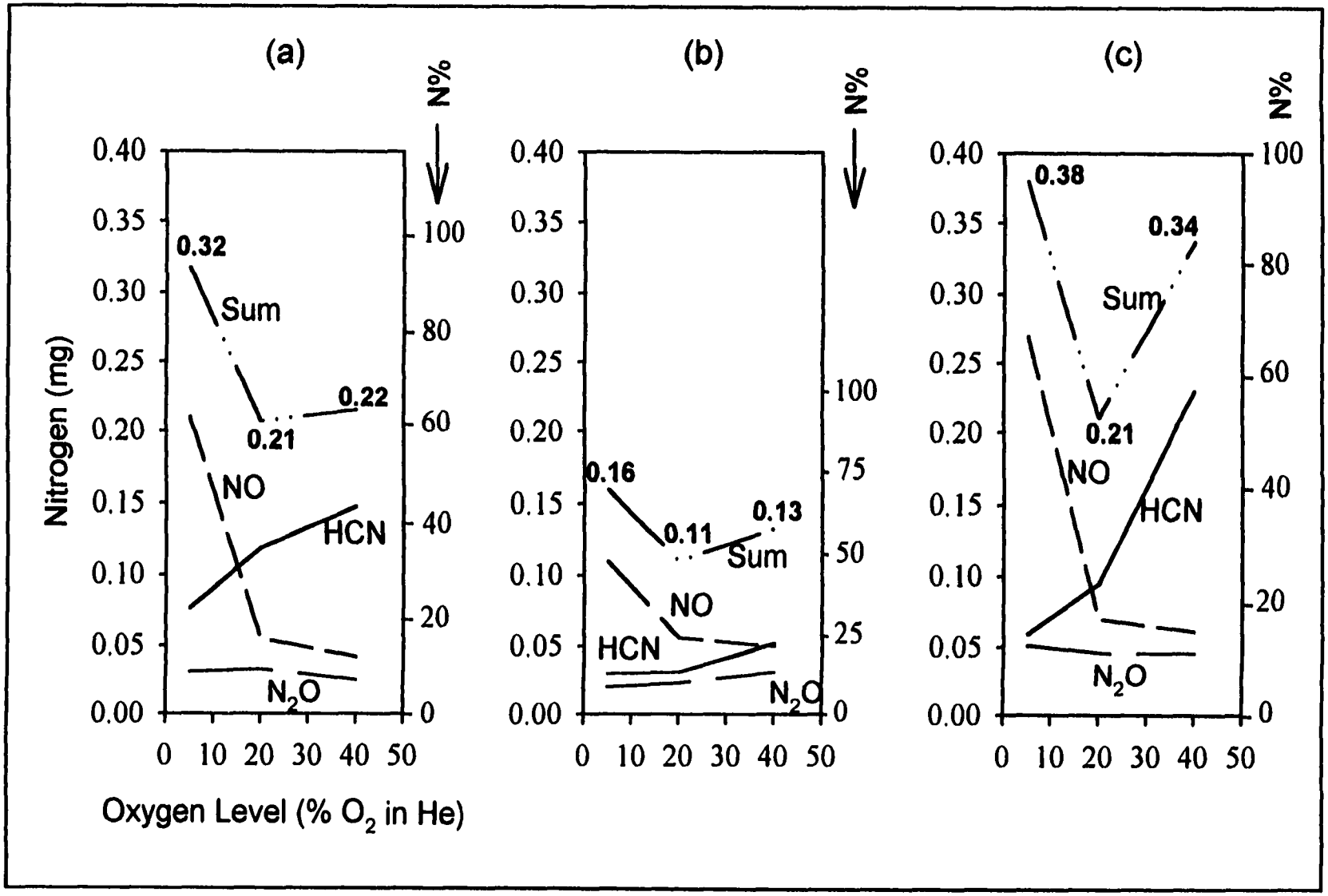


Figure 5.6 Nitrogen contribution to the formation of NO, HCN and $N_2O$ from (a) PSOC-1498, (b) Pittsburgh #8 and (c) PSOC-1521 chars at 25 °C/min as a function of oxygen concentration (tubular quartz reactor configuration).

percentages of, readily detectable, HCN which is only slowly being converted to equally readily detectable NO by gas phase oxidation at these temperatures and, apparently, is only partially, if at all, being lost to (nondetectable) $N_2$ by heterogeneous char reduction reactions.

At 20% oxygen levels, average reaction temperatures have gone up by 50 °C or so, thereby, conceivably promoting gas phase reaction to NO and subsequently to (non-detectable) $NO_2$ leading to the lowest detectable nitrogen percentages. At the very low oxygen levels encountered at 5% $O_2$ nearly all of the HCN formed is now transformed to (readily detectable) No by homogeneous gas phase oxidation (as shown in Chapter 3), thereby leading to the highest recorded N percentages. Relatively little NO is converted to $NO_2$ due to the very low oxygen levels in the reactor bed.

The high temperature char (Figure 5.6B: Pittsburgh # 8) can be seen to produce much less HCN, probably because of lower hydrogen content due to the more complete char devolatilization process. It should be noted again that this char was obtained at a high temperature (1200 °C) in a bench scale coal combustion reactor (Combustion Group, University of Utah). They reported no detection of HCN from the combustion of this char around 1500 °C.[81] The much lower detectable total nitrogen product percentages in the Pittsburgh #8 coal are not readily explainable. However, both its low nitrogen content (1.14%) and its low hydrogen content (0.70%) explain the low HCN yields observed, even at the lowest average reaction temperatures. Concievably, these low HCN concentrations may have promoted a more complete gas phase conversion to $NO_2$. Also, at all oxygen levels the average reaction temperatures of the Pittsburgh #8 char tend to hover between the more extreme low and high reaction temperatures observed in the two other chars, i.e., around

those temperatures that tend to produce the lowest total nitrogen yields.

Clearly, the experiments described here cannot provide the last word on the nitrogen mass balance question due to our inability to reliably measure $NO_2$ levels (too polar to pass through the capillary transfer lines and GC column without major losses) as well as $N_2$ levels (not detectable by absorption FTIR experiments and not reliably measurable by MS due to residual gas background interference problems). Also, the question should be asked whether nitrogen products other than $NO_2$ or $N_2$, e.g., $NH_3$ or HNCO, might have gone undetected in our experiments, thus causing the observed nitrogen mass balance deficits. With regards to $NH_3$, all available literature data suggest that the probability of high $NH_3$ concentration during char oxidation is quite small due to the hydrogen concentration in most chars.[25] Further, our FTIR and MS equipments should have had relatively little difficulty in detecting HNCO unless its limited stability might have confounded our experimental setup.

### 5.4.2 Evaluation of the Total Response Chromatograms

In order to study the effect of oxygen level on the oxidation processes, the aforementioned chars were oxidized in 5%, 10%, 20% and 40% $O_2$ in He at 25 °C/min. The total IR response chromatograms (i.e., overall product release profiles) resulting from the oxidations of these coal chars are presented in Figures 5.7-5.9. As evident from these figures the overall product formation takes place over a larger temperature range at lower oxygen levels. In other words, the overall product formation duration tend to decrease with increasing oxygen concentration. Overall formation of products starts at almost the same

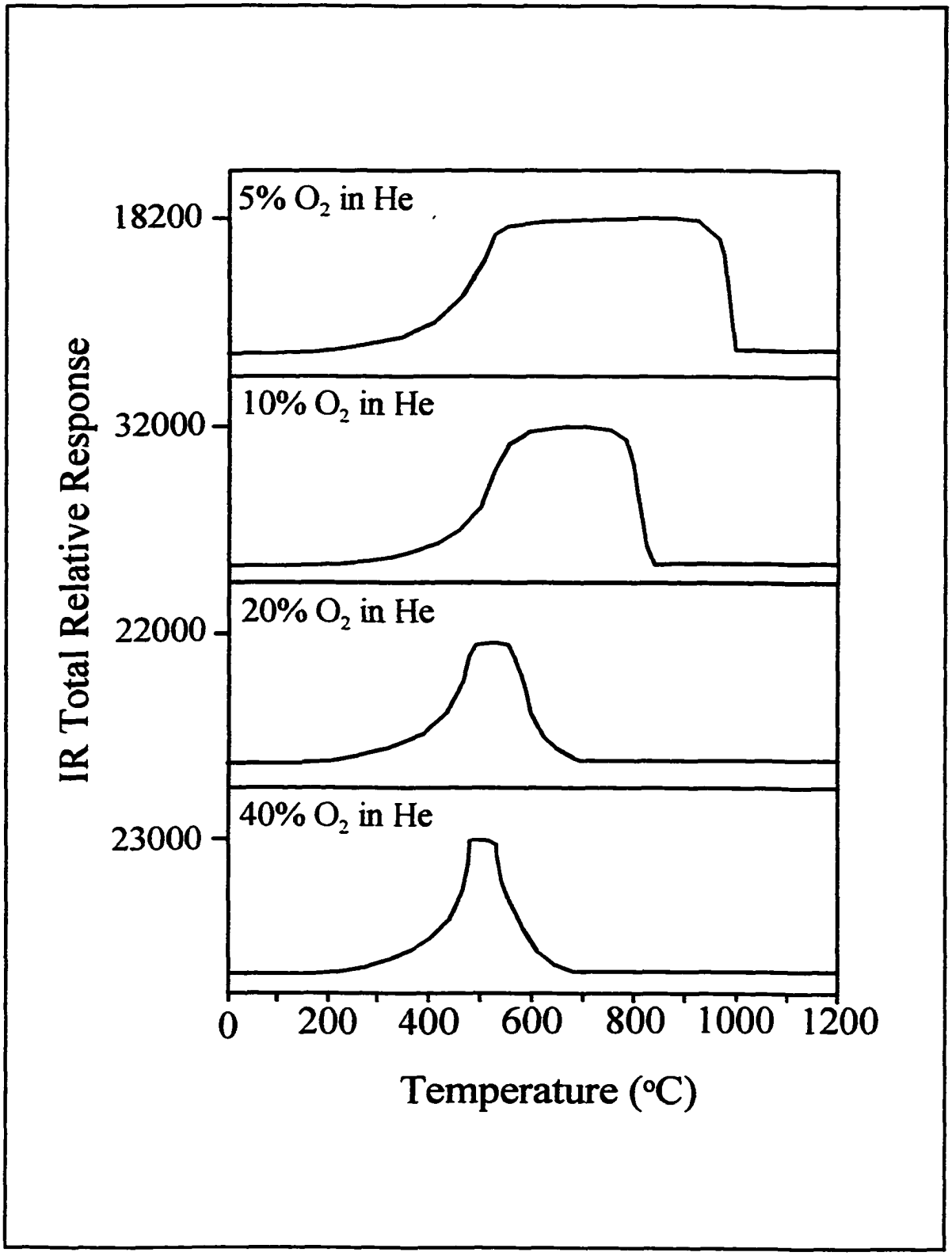


Figure 5.7 Total relative IR response chromatograms from the oxidation of PSOC-1498 char in 5%, 10%, 20% and 40% $O_2$ in He at 25 °C/min (tubular reactor configuration).

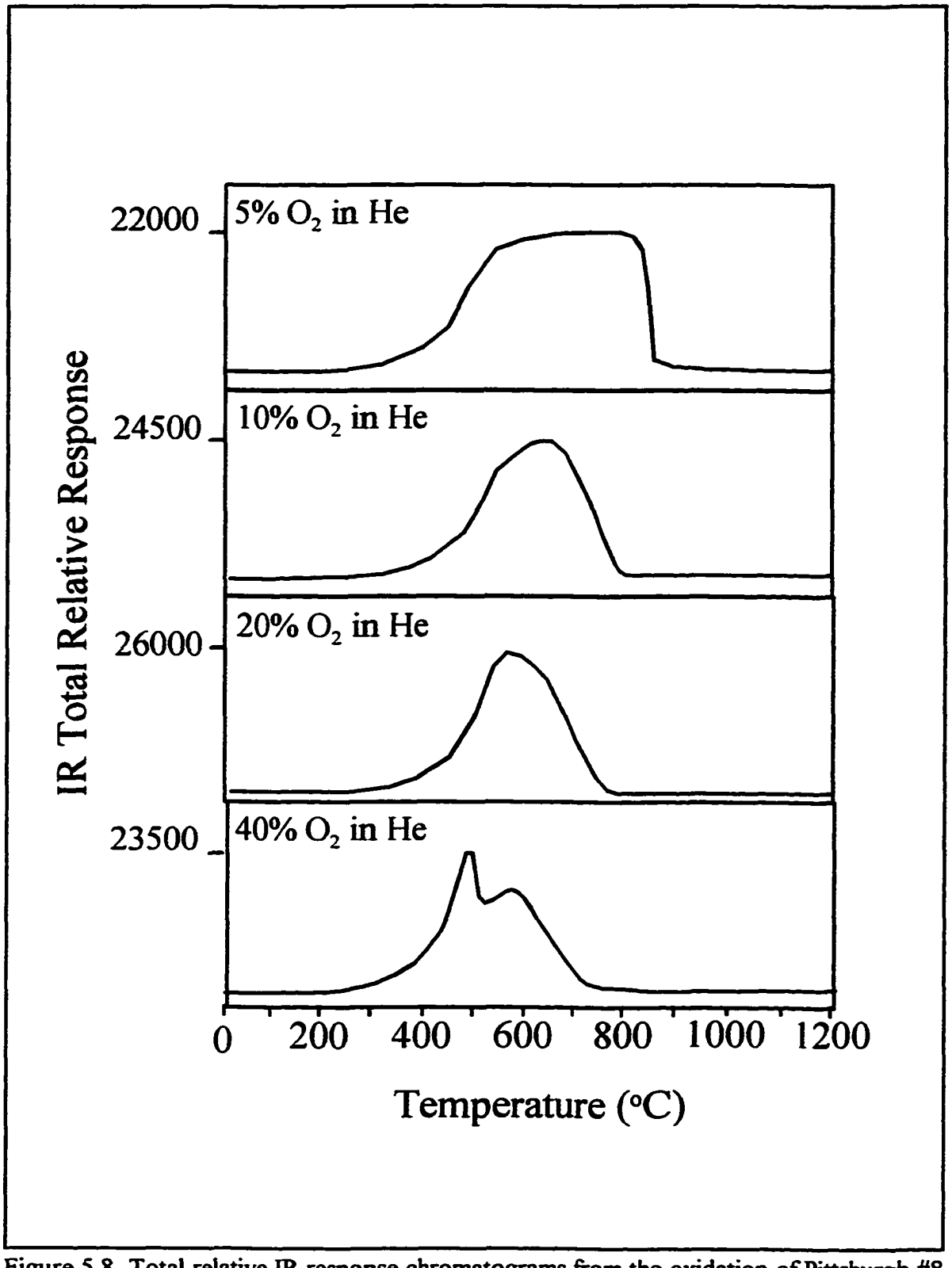


Figure 5.8 Total relative IR response chromatograms from the oxidation of Pittsburgh #8 char in 5%, 10%, 20% and 40% $O_2$ in He at 25 °C/min (tubular reactor configuration).

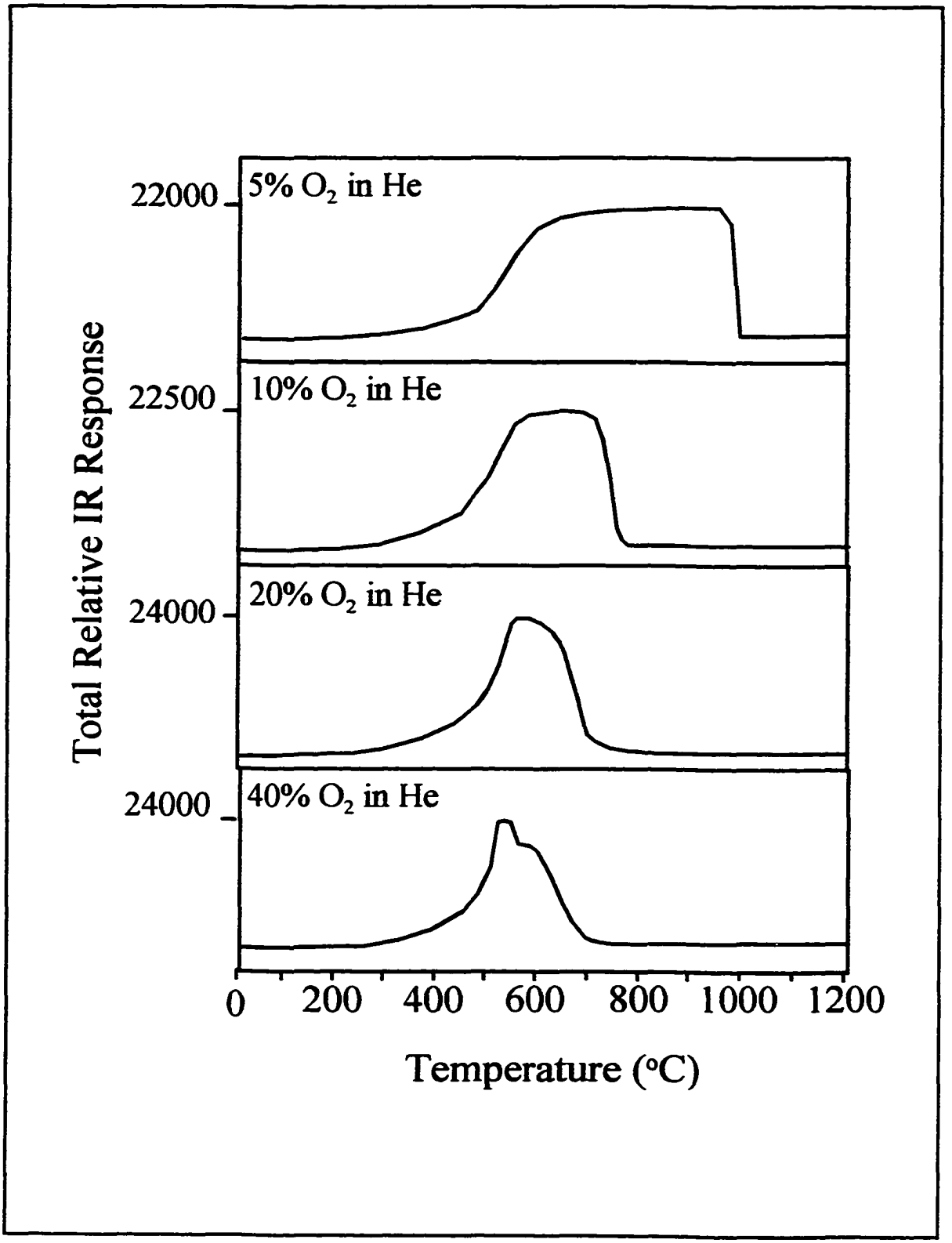


Figure 5.9 Total relative IR response chromatograms from the oxidation of PSOC-1521 char in 5%, 10%, 20% and 40% $O_2$ in He at 25 °C/min (tubular reactor configuration).

temperature for each char whereas the overall product termination temperature appears to decrease with increasing oxygen concentration.

Formation of a plateau at lower oxygen levels (5% and 10% $O_2$ in He) is another prominent effect seen for all chars. As pointed out in Chapter 4, this is caused by the saturation of the IR detector at a certain wave number. At the highest oxygen level (40% $O_2$ in He) Pittsburgh #8 and PSOC-1521 chars exhibit an abrupt increase (spurt) at the beginning of the char oxidation process. This phenomenon was also observed in the model char oxidation processes. As explained previously, this spurt effect is caused by the ignition of materials on the char surface. At the highest oxygen levels, an ignition can take place resulting in the evolution of products appearing in the form of a spurt in the overall product evolution profile. It is noteworthy that the sudden evolution of products from the char surface should, in turn, help create a diffusion barrier against the oxygen, preventing it from reaching the char surface for further oxidation reactions. This could explain the dip on the right shoulder of the Pittsburgh #8 product evolution profiles. Once the evolved gases are dispersed and the diffusion barrier is vanished, the oxygen would proceed to the char surface once again and a new scenario of product evolution would start (Figures 5.8). These effects may be most pronounced in the Pittsburgh #8 char, possibly due to its higher porous nature (Table 5.1). The spurt effect is not observed in the PSOC-1498 char oxidation at 40% $O_2$ in He, probably due to the fact that it has the lowest porosity amongst all three chars (Table 5.1). Another evidence supporting this argument is that, even at the lowest oxygen level (5% $O_2$ in He), the PSOC-1498 char overall product release takes place over a larger temperature range compared to the other two.

Another interesting observation is that at lower oxygen levels the right hand shoulders of all three overall product release profiles drop faster as the oxygen level is increased. This effect is consistently observed in all three coal char oxidation processes. This could be explained by the fact that at lower oxygen concentrations, oxygen transport to the char surface be limited by the evolution of gaseous products from the char. In addition, secondary gas phase reactions in the pores of the char can also deplete oxygen and significantly reduce the oxygen concentration at the char surface for any heterogeneous oxidation reactions. As a result the surface oxidation would take place at a very slow pace due to insufficient oxygen concentration. As the process approaches the end, the reduction in char quantity compensates for the lower oxygen concentration at the char surface. In other words, the char reaches a quantity that the evolved gaseous products and/or secondary homogeneous gas phase reactions would neither cause an oxygen diffusion barrier nor deplete oxygen completely. At this point, the char would heterogeneously react with oxygen at a high rate resulting in the appearance of a sharp drop in the right hand shoulder of these profiles.

### 5.4.3 Evaluation of the Selected IR and MS Response Chromatograms

For mechanistic studies selected response chromatograms (i.e. specific evolution profiles) of $O_2$, $CO_2$, CO, HCN, $H_2O$, NO and $N_2O$ were obtained from the oxidation of the three coal chars in various oxygen levels (5%, 10%, 20% and 40% $O_2$) in He (Figures 5.10-5.12). Similar to all other chars, due to the presence of carbon as the primary element, and the presence of activated carbon sites, $CO_2$ and CO formation starts prior to any other

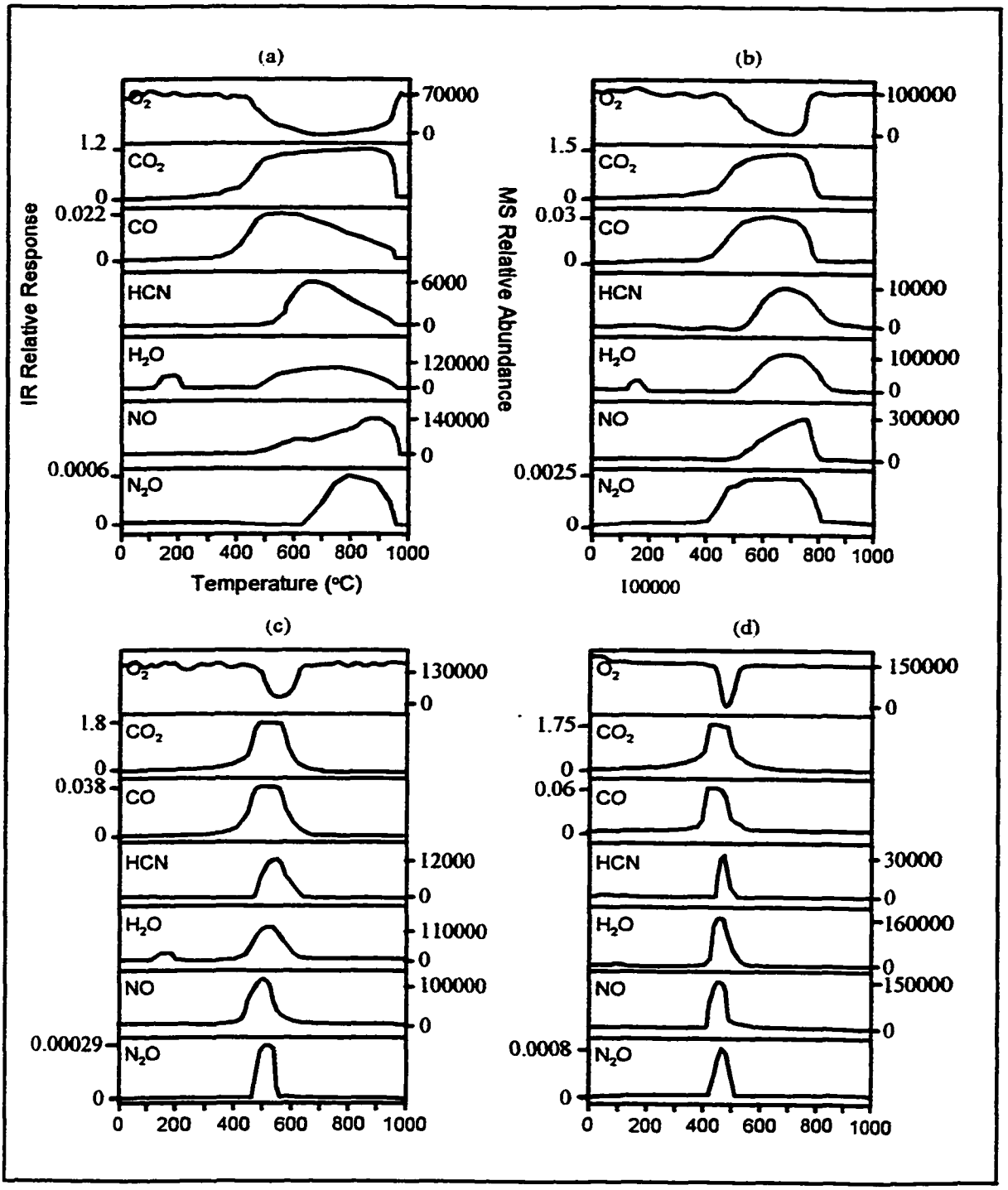


Figure 5.10 Temperature-resolved evolution profiles of $O_2$, $CO_2$, CO, HCN, $H_2O$, NO and $N_2O$ from the oxidation of PSOC-1498 char in (a) 5%, (b) 10%, (c) 20% and (d) 40% $O_2$ in He at 25 °C/min (tubular reactor configuration). Note that figures (a), (b), (c) and (d) all posses similar axes but only (a) has been labeled. All left hand vertical axes ($O_2$, HCN, $H_2O$ and NO) represent relative IR response whereas all right hand axes ($CO_2$, CO and $N_2O$) show relative MS response.

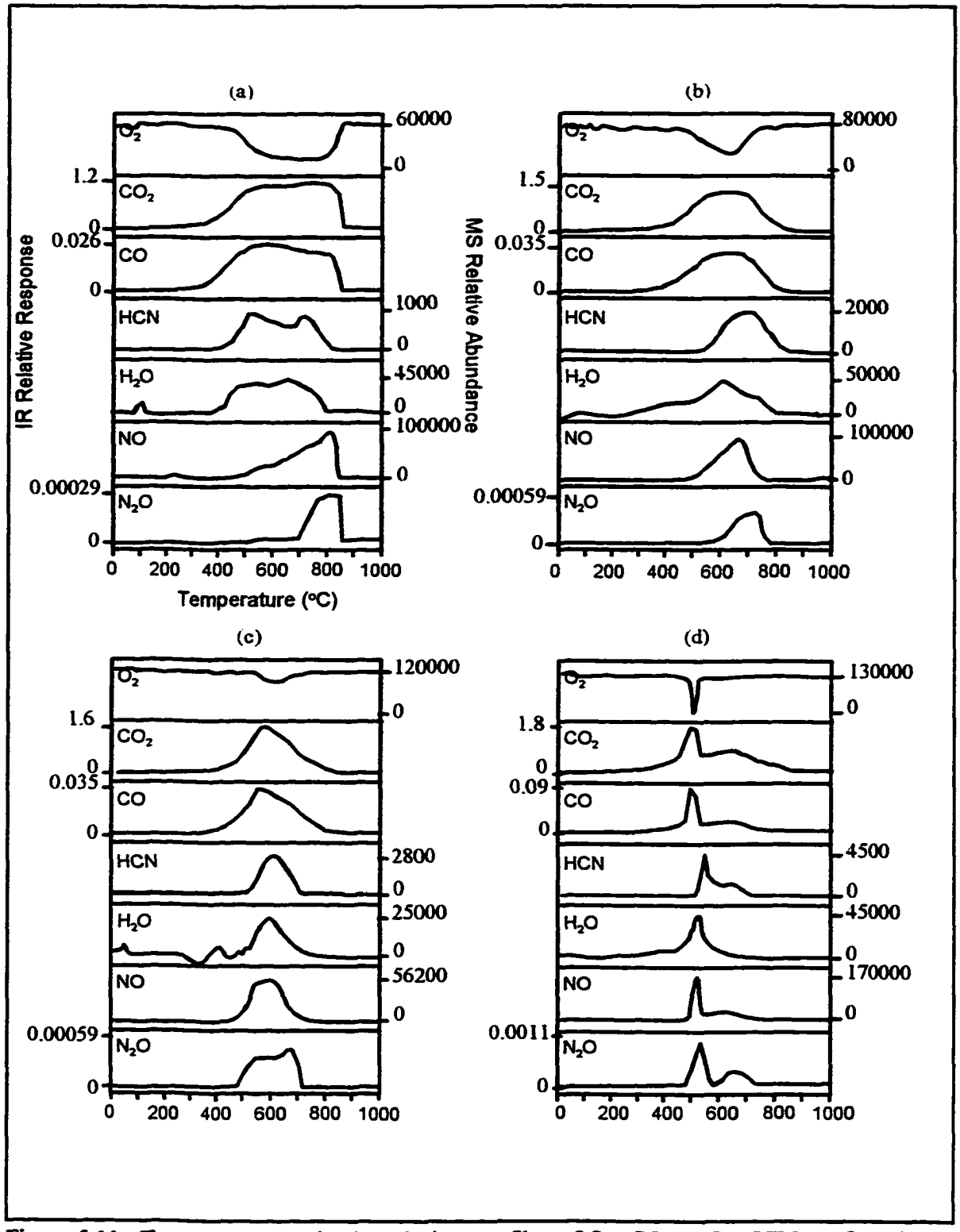


Figure 5.11 Temperature-resolved evolution profiles of $O_2$, $CO_2$, CO, HCN, $H_2O$, NO and $N_2O$ from the oxidation of Pittsburgh #8 char in (a) 5%, (b) 10%, (c) 20% and (d) 40% $O_2$ in He at 25 °C/min (tubular reactor configuration). For axes definitions refer to Figure 5.10.

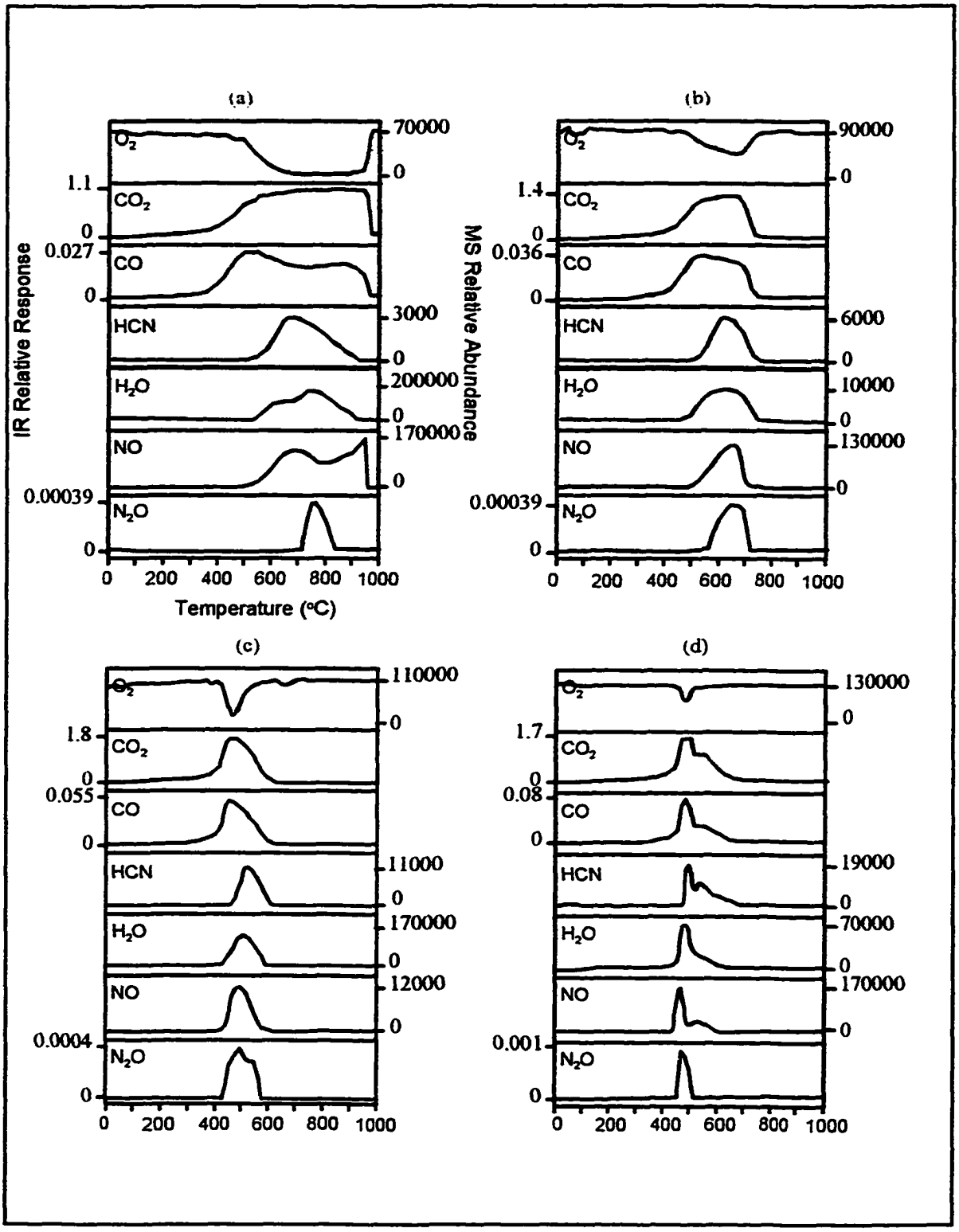


Figure 5.12 Temperature-resolved evolution profiles of $O_2$, $CO_2$, CO, HCN, $H_2O$, NO and $N_2O$ from the oxidation of PSOCl-1521 char in (a) 5%, (b) 10%, (c) 20% and (d) 40% $O_2$ in He at 25 °C/min (tubular reactor configuration). For axes definitions refer to Figure 5.10.

compound and lasts until the end of the process for all three chars. $H_2O$ formation starts up next, followed by that of nitrogen containing products HCN, NO and $N_2O$. The HCN profiles illustrate maxima right after those of $H_2O$. NO follows the HCN profile and, depending upon the char and the oxygen level, maximizes in most cases after, and in a few cases prior to the HCN maxima. The $N_2O$ profile, however, maximizes right after the first NO maxima in all three char oxidation processes.

An important observation is that the $H_2O$ profiles maximize directly prior to those of HCN in all three chars and at various oxygen levels, suggesting that $H_2O$ is somehow involved in the formation of HCN. The same observation was also made in the model char mechanistic oxidation processes and its potential implications were discussed in Chapter 4. The relative MS abundances of HCN show decreasing trend of HCN with decreasing oxygen levels and, thus increasing temperature. For $H_2O$, however, a well-defined trend as a function of oxygen level cannot be deduced. At the lowest oxygen concentration (5% $O_2$ in He) for Pittsburgh #8 and PSOC-1521 chars the $H_2O$ profile shows a bimodal behavior. It should be noted that as explained previously these two chars are less porous than the PSOC-1498 char. In Pittsburgh #8 char this behavior in $H_2O$ is also noticeable at 10% $O_2$ in He. It is very possible that after the formation of the first hump (or first $H_2O$ release), $H_2O$ undergoes a reaction pathway that would result in the formation of HCN. The HCN profile in these cases show a maximum right after the first $H_2O$ hump. As the process continues the HCN production slows down. There are two explanations for this phenomenon: (1) the production of HCN decreases and gradually ends at a certain point of time during the overall char oxidation or (2) a new reaction pathway, i.e., secondary gas phase reactions involving HCN,

emerges which consumes HCN at a higher rate than its production and produces $H_2O$ and CO as shown in Chapter 4.

Prior to any further evaluation it is noteworthy that as pointed out at the beginning of this chapter, the Pittsburgh #8 char is a high temperature char compared to the other two. Therefore, many properties of this char can be expected to be different from both PSOC-1498 and PSOC-1521 chars. A possible example of such different behavior can be seen in the bimodal behavior of the HCN from the oxidation of Pittsburgh #8 char at 5% $O_2$ in He. The "dip" between the two humps in this profile corresponds to the second hump in the $H_2O$ profile. It is possible that a noticeable portion of the produced HCN is somehow involved in a reaction pathway to form $H_2O$. As the formation of $H_2O$ slows down (second hump), HCN picks up again. Another explanation could be that there are two different nitrogen functionalities involved in the formation of the two HCN humps. For example one of these could represent the pyrrolic and/or pyridinic functionalities [35] whereas the other might involve activated nitrogen complexes of NO or $N_2O$ with carbon. [3 & 28]

Oxidation of all three coal chars show that at lower oxygen concentrations (5% and 10% $O_2$ in He), NO profiles maximize, e.g., reaches its $T_{max}$ value following that of HCN. The same trend was also observed in the model char oxidation processes. As shown in Chapter 3, NO is the product of a homogeneous oxidation of HCN. At higher oxygen levels, i.e., 20% and 40% $O_2$ in He, however, the trend appears to be exactly opposite. Apparently, the lower average reaction temperatures associated ~~with higher~~ oxygen percentages tend to preserve HCN rather than promote gas phase conversion to NO in spite of the higher oxygen levels (i.e., temperature appears to be more important than oxygen level here).

The HCN/NO ratios are of the same order of magnitude as those obtained in Chapter 3 reiterating the fact that NO formation is a result of the same reaction pathway explained in the same chapter. It is noteworthy that the HCN/NO ratio for PSOC-1498 and PSOC-1521 chars at 20% and 40% $O_2$ in He, however, is an order of magnitude higher than what obtained for spherocarb chars exposed to HCN. This is thought to be due to transport limitations imposed by the products leaving the pores of these chars, leading to more gas phase oxidation of HCN to NO during the longer residence time within the pores.

The $N_2O$ profiles follow the NO profiles very closely. At the lowest oxygen level (5% $O_2$ in He) the $T_{max}$ of the $N_2O$ profile, i.e., right between the two humps of the NO profiles. These observations strongly support the relevant argument presented in Chapter 2, mainly that NO is a precursor to the formation of $N_2O$. It should also be noted that in case of any NO bimodality, the second hump coincides with the disappearance of carbon (decrease in $CO_2$ and CO profiles) supporting the argument that the chemisorbed NO on the active carbon sites is desorbed as the carbon is oxidized.

### 5.4.4 Effect of $O_2$ Level on the Maximum Product Evolution Rate Temperatures ($T_{max}$)

Similar to the investigation performed on model chars, the temperatures at which the formation of the nitrogen end products (NO, HCN and $N_2O$) reached a maximum were studied as functions of the oxygen level (Figure 5.13). In the case of bimodality the $T_{max}$ is determined based on the behavior of the profile. If the $T_{max}$ of another product lays right in between the two maxima of a product of interest, based on a thorough comparison with

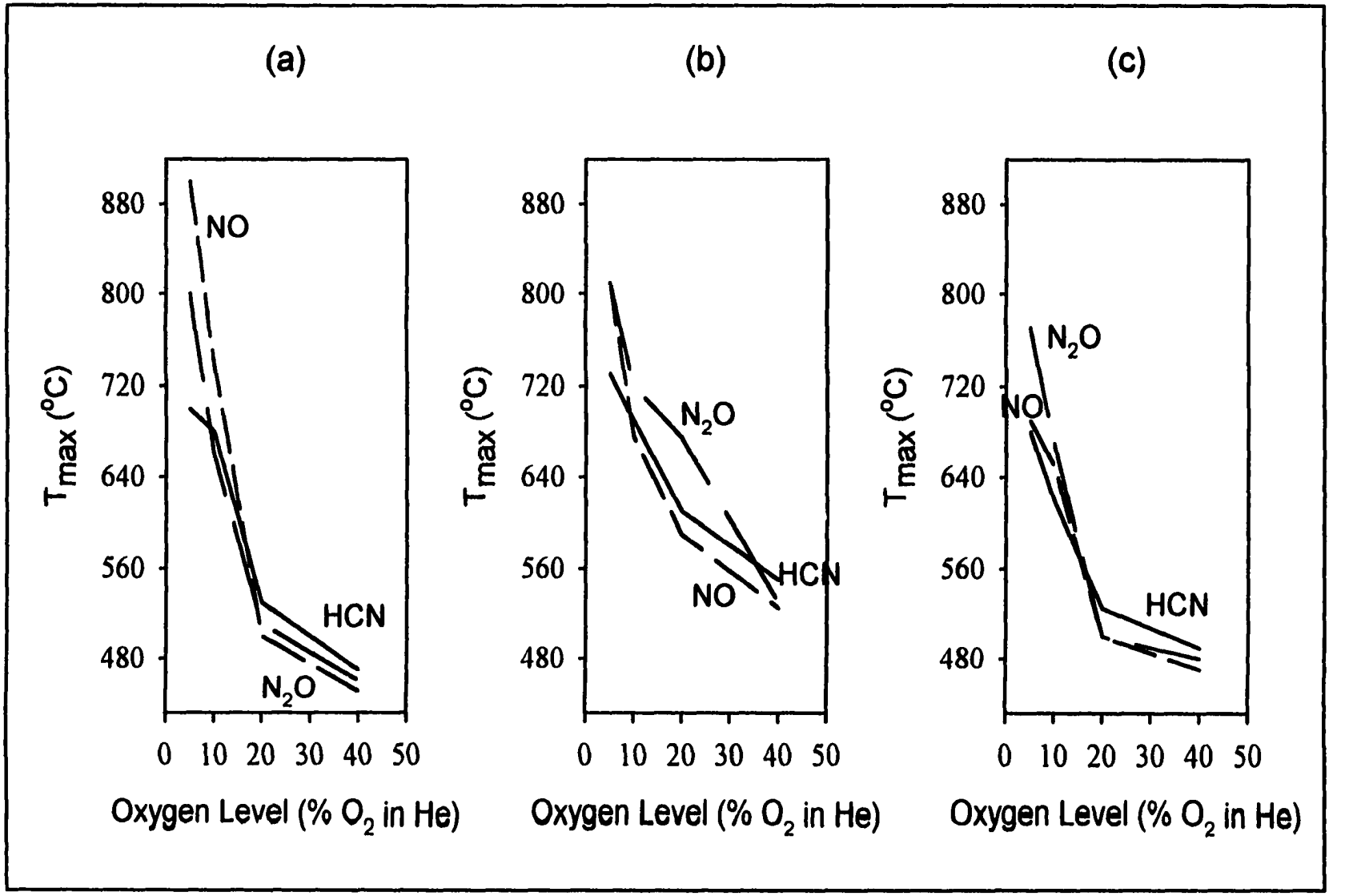


Figure 5.13 The maximum product release temperature versus oxygen level for NO, HCN and $N_2O$ during oxidation of (a) PSOC-1498 (b) Pittsburgh #8 and (c) PSOC-1521 chars at 25 °C/min (tubular reactor configuration).

similar profiles at other oxygen levels the $T_{max}$ is then estimated. In case of NO bimodality, the second maximum is mainly caused by the desorption of the chemisorbed NO molecules onto the carbon active site and does not represent the actual formation of NO. The first maximum, however, represents NO formation and, therefore, can be used to obtain the $T_{max}$ value. From these profiles it is readily evident that at lower oxygen levels the NO, HCN and $N_2O$ formation reach a maximum at much higher temperatures than at higher oxygen levels. This phenomenon is consistently observed in all char oxidation processes. This is due to the fact that at lower oxygen levels the reaction rates are much slower. Since ultimately the heating continues, this results in higher $T_{max}$ values for the formation of the various products.

The $T_{max}$ values for NO, HCN and $N_2O$ appear to vary strongly at oxygen levels below 20% whereas less variation is observed between 20% and 40% $O_2$ in He. It can be proposed again that mass transport is the dominant factor in this scenario. At higher oxygen levels, mass transport limitations by fast product release rates may become so significant that changes in oxygen concentration have less effect on the observed rates. The $T_{max}$ profiles of both NO and HCN appear to follow each other very closely in almost all cases. This is in line with the presumed formation of NO from HCN by gas phase oxidation as the major source of NO in our experiments.

# CHAPTER 6

# CONCLUSIONS

## 6.1 Secondary Reaction Studies

Exposing Carbosieve to 2% NO (in He + 20% $O_2$) causes rapid chemisorption above 150 °C (accompanied by slow CO + $CO_2$ + $N_2O$ evolution). A sharp NO evolution peak is observed during the final stages of the carbon burn-out process at ~ 600-650 °C. Related phenomena (both chemisorption and late NO release) are observed when spiking with HCN. Thus, the second maximum in the often observed bimodal NO evolution profiles may be due to secondary NO release from chemisorbed nitrogen moieties. The reaction between chemisorbed and a bypassing NO molecules could result in the formation of $N_2O$. This is confirmed by the trends of NO and $N_2O$ production, as explained earlier.

In the presence or absence of Carbosieve HCN reacts with $O_2$ homogeneously to form NO. The chemisorption of NO onto the active carbon sites is also evident when Carbosieve is present in these experiments. $N_2O$ appears to posses oxidizing effects at temperatures above 600 °C. Additionally, at temperatures in the access of 900 °C formation of HCN from reaction of $N_2O$ with Carbosieve (and some residual hydrogen content) is prominent. Reduction of $N_2O$ to $N_2$ is also a possibility at temperatures above 520 °C.

## 6.2 Model Char Studies

An unsuccessful attempt to achieve a closed nitrogen mass balance in the original thermogravimetry tube reactor configuration suggested that mixing of the gases inside the reactor as well as their percolation through the char bed was not adequate.

The attempted mass balance in the tubular reactor configuration accounted for about 80% of the total char nitrogen. The HCN and $H_2O$ formation profiles in this reactor configuration also support the fact that HCN is produced at the expense of $H_2O$. The bimodality of $H_2O$ from the oxidation of tetraphenyl porphine char and its dependence on the HCN also supports this argument. High relative MS abundances for HCN at any given oxygen concentration suggest that formation of HCN is somehow oxygen dependent. The HCN/NO ratios were calculated to be of the same order of magnitude as those obtained in Chapter 3. The relative MS profiles of HCN, NO and $N_2O$ suggest that HCN is homogeneously oxidized to form NO and $N_2O$ formation is due to a reaction between an activated NO (chemisorbed onto an active carbon site) and a passing-by NO molecule. All the reactions involved in production of HCN, NO and $N_2O$ appear to be heterogeneous except for the formation of NO from the homogeneous oxidation of HCN. In case of NO bimodality, the second hump coincides closely with disappearance of carbon (decrease in both $CO_2$ and CO profiles) supporting the argument that the chemisorbed NO on the active carbon sites is desorbed as the carbon is oxidized. NO formation increases with increasing oxygen concentration, whereas HCN illustrates an opposite trend.

The $T_{max}$ profiles indicate that at higher oxygen levels (20% and 40% $O_2$ in He) chemical kinetics control the overall processes, whereas at lower oxygen levels (5% and 10%

$O_2$ in He) oxidation process rates are controlled by transport mechanisms.

## 6.3 Coal Char Studies

The TG data indicate that, under the experimental conditions used, the early stages of the coal char oxidation processes are under chemical control. During the middle portion of the gasification reaction, falling oxygen levels within the reactor bed strongly affect measured reaction rates. The observed effects are in good agreement with the first order relationship between oxygen levels and char oxidation rates often proposed in the literature. Towards the end of the carbon gasification process, oxygen levels within the char bed as well as the corresponding reaction rates tend to recover to the initial levels.

The experiments described here afford a direct measurement of average oxygen levels in the fixed bed during the QTR experiments and suggest a novel way of estimating average oxygen levels in TG bed experiments.

Formation of a plateau in the total IR response chromatograms (summed product release profiles) obtained during quartz tube reactor experiments at lower oxygen levels is primarily due to oxygen transport resistance as this corresponds closely with the strong reduction in oxygen concentration seen in the selected ion profiles at m/z 34 $(^{18}O^{16}O)^{+}$. Abrupt increase (spurt!) at the beginning of the char oxidation processes for PSOC-1521 and Pittsburgh #8 appears to be caused by runaway exothermic and/or ignition processes at the char surface at high oxygen levels.

At lower oxygen concentrations char oxidation process is completed at much higher temperatures than at lower oxygen levels. Consequently, the process ends very abruptly as

stoichiometric conditions and, thus, high chemically controlled rates are restored during final burnout.

From the selected response chromatograms it is evident that $H_2O$ production appears prior to HCN suggesting that $H_2O$ (in the form of hot steam) plays a direct role in the formation of HCN. A bimodal behavior in the $H_2O$ profiles of Pittsburgh #8 and PSOC-1521 chars oxidation at 5% $O_2$ in He and the occurrence of the HCN maximum right between the two humps in the $H_2O$ profile suggest that $H_2O$ takes part in a reaction pathway that results in the formation of HCN.

The HCN/NO ratios are of the same order of magnitude as those obtained in Chapter 3 (0.4) and observed nitrogen rich model chars (Chapter 4). The HCN/NO ratio of PSOC-1498 and PSOC-1521 chars at 5% and 10% $O_2$ in He, however, is an order of magnitude smaller than what obtained in Chapter 3. This is thought to be due to transport limitations imposed by the products leaving the pores of these chars, leading to more gas phase oxidation of HCN to NO during the longer residence time within the pores.

The most important conclusion that can be drawn from these observations is that the three coal chars studies generally exhibited the same overall reaction behavior, product state and evolution profiles as the model chars described in Chapters 3 and 4. One of the few exceptions is the bimodal behavior seen in the oxidation of Pittsburgh #8 char (high temperature char) at 5% $O_2$ in He the "dip" between the two humps in this profile corresponds to the second hump in the $H_2O$ profile suggesting that a noticeable portion of the $H_2O$ is produced by high temperature gas phase oxidation of HCN. As the formation of $H_2O$ slows down (second hump), HCN levels pick up again.

## REFERENCES


1. Houser, T. J.; McCarville, M. E.; Houser, B. D. *Combustion Science and Technology* **1982**, *27*, 183.

2. Houser, T. J.; McCarville, M. E.; Zhuo-Ying, G. *Fuel* **1988**, *67*, 642.

3. De Soete, G. G. *Combustion and the Environment, The International Flame Research Foundation* **1990**, Ilmuiden, Holland K/25/y/5.

4. Cabrita, I.; Costa, M. R.; Esparteiro, H.; Gulyurtlu, I. *Proceedings of the 1991 International Conference on Fluidized Bed Combustion, The American Society of Mechanical Engineers* **1991**, *2*, 985.

5. Åmand, L. E.; Andersson, S. *Proceedings of the 1989 International Conference on Fluidized Bed Combustion, The American Society of Mechanical Engineers* **1989**, *1*, 49.

6. Lázaro, M. J.; Ibarra, J. V.; Moliner, R.; González de Andrés, A.; Thomas, K. M. *Fuel* **1996**, *75(8)*, 1014.

7. Harding, A. W.; Brown, S. D.; Thomas, K. M. *Combustion and Flame* **1996**, *107*, 336.

8. Yue, G. X.; Pereira, F. J.; Sarofim, A. F.; Beer, J. M. *Combustion Science and Technology* **1992**, *83(4-6)*, 245.

9. Crelling, J. C.; Thomas, K. M.; Marsh, H. *Fuel* **1993**, *72(3)*, 349.

10. Brown, S. D.; Thomas, K. M. *Fuel* **1993**, *72(3)*, 359.

11. Illán-Gómez, M. J.; Salinas-Martinez de Lecea, C.; Linares-Solano, A.; Phillips, J.; Radovic, L. R. *211th American Chemical Society National Meeting* **1996**, *41(1)*, 174.

12. Teng, H.; Suuberg, E. M.; Calo, J. M. *Energy and Fuels* **1992**, *6*, 398.

13. Visona, S. P.; Stannore, B. R. *Combustion and Flame* **1996**, *106*, 207.

14. Shimizu, T.; Sazawa, Y.; Adschiri, T. *Fuel* **1992**, *71*, 361.

15. Goel, S.; Zhang, B.; Sarofim, A. F. *Combustion and Flame* **1996**, *104*, 213.

16. Thomas, K. M.; Grant, K.; Tate, K. *Fuel* **1993**, *72(7)*, 941.

17. Miettinen, H.; Paulsson, M.; Strömberg, D. *Energy and Fuels* **1995**, 9, 10.

18. Miettinen, H.; Miroslawa, A. *Energy and Fuels* **1996**, *10*, 421.

19. Tullin, C. J.; Goel, S.; Morihara, A.; Sarofim, A. F.; Beér, J. M. *Energy and Fuels* **1993**, *7*, 796.

20. Pels, J. R.; Wójtowicz, M. A.; Kapteijn, F.; Moulijn, J. A. *Energy and Fuels* **1995**, *9*, 743.

21. Feng, B.; Liu, H.; Yuan, J.; Lin, Z.; Liu, D. *Energy and Fuels* **1996**, *10*, 203.

22. Lu, Y. *Energy and Fuels* **1996**, *10*, 357.

23. Illán-Gómez, M. J.; Linares-Solano, A.; Radovic, L. R.; Salinas-Martínez de Lecea, C. *Energy and Fuels* **1996**, *10*, 158.

24. Miettinen, H. *Energy and Fuels* **1996**, *10*, 197.

25. Wojtowicz, M. A.; Pels, J. R.; Moulijn, J. A. *Fuel Processing Technology* **1993**, *34(1)*, 1.

26. Tullin, C. J.; Sarofim A. F.; Beer, J. M. *Proceedings of the 1993 International Conference on Fluidized Bed Combustion* **1993**, 599.

27. Gavin, D. G.; Dorrington, M. A. *Fuel* **1993**, *72(3)*, 381.

28. Kramlich, J. C.; Cole, J. A.; McCarthy, J. M.; Lanier, S. *Combustion and Flame* **1989**, *77*, 375.

29. De Soete, G. G. *Twenty-Third Symposium (International) on Combustion* **1990**, 1257.

30. Åmand, L. E.; Leckner, B. *Combustion and Flame* **1991**, *84*, 181.

31. Wang, W. X.; Thomas, K. M.; Cai, H. Y.; Dugwell, D. R.; Kandiyoti, R. *Energy and Fuels* **1996**, *10*, 409.

32. Chambrion, P.; Orikasa, H.; Kyotani, T.; Tomita, A. *211th American Chemical Society National Meeting*, **1996**, *41(1)*, 170.

33. Naruse, I.; Yamamoto, Y.; Imanari, M.; Yuan, J.; Ohtake, K. *Twenty-Fourth Symposium (International) on Combustion* **1992**, 1415.

34. Gulyurtlu, I.; Esparteiro, H.; Cabrita, I. *Fuel* **1994**, *73(7)*, 1098.

35. Wójtowicz, M. A.; Pels, J. R.; Moulijn, J. A. *Fuel* **1995**, *74(4)*, 507.

36. Moritomi, H.; Suzuki, Y.; Kido, N.; Ogisu, Y. *Proceedings of the 1991 International Conference on Fluidized Bed Combustion, The American Society of Mechanical Engineers* **1991**, *2*, 1005.

37. Tullin, C. J.; Sarofim, A. F.; Béer, J. M. *Proceedings of the 1993 International Conference on Fluidized Bed Combustion, The American Society of Mechanical Engineers* **1993**, *1*, 599.

38. Tullin, C. J.; Sarofim, A. F.; Béer, J. M.; Teare, J. D. *Combustion Science and Technology* **1995**, *106*, 153.

39. Winter, F.; Wartha, C.; Löffler, G.; Hofbauer, H. *26th Symposium (International) on Combustion* **1996**, 3325.

40. Kilpinen, P.; Hupa, M. *Combustion and Flame* **1991**, *85*, 94.

41. Krammer, G. F.; Sarofim, A. F. *Combustion and Flame* **1994**, *97*, 118.

42. Glarborg, P.; Kristensen, P. G.; Jensen, S. H.; Dam-Johansen, K. *Combustion and Flame* **1994** *98*, 241.

43. Glarborg, P.; Miller, J. A. *Combustion and Flame* **1994**, *99*, 475.

44. Hayhurst, A. N.; Lawrence, A. D. *Combustion and Flame* **1996**, *105*, 341.

45. Pels, J. R.; Wójtowicz, M. A.; Moulijn, J. A. *Fuel* **1993**, *72*, 373.

46. Oude Lohuis, J. A.; Tromp, P. J. J.; Moulijn, J. A. *Fuel* **1992**, *71*, 9.

47. Aho, J. M.; Rantanen, J. T.; Linna, V. L. *Fuel* **1990**, *69*, 957.

48. Hulgaard, T.; Glarborg, P.; Dam-Johansen, K. *Proceedings of the 1991 International*

*Conference on Fluidized Bed Combustion, The American Society of Mechanical Engineers* **1991** *2*, 991.

49. Khan, T.; Lee, Y. Y.; Brown, R. A. *Proceedings of the 1991 International Conference on Fluidized Bed Combustion, The American Society of Mechanical Engineers* **1993**, *1*, 441.

50. Suuberg, E. M.; Teng, H.; Aarna, I. *211th American Chemical Society National Meeting* **1996**, *41(1)*, 160.

51. Wang, W.; Brown, S. D.; Hindmarsh, C. J.; Thomas, K. M. *Fuel* **1994**, *73(9)*, 1381.

52. Khan, R. M.; Everitt, C. E.; Lui, A. P. *Combustion and Flame* **1990**, *80*, 83.

53. Kunii, D.; Furusawa, T.; Wu, K. T. *Fluidization* J. Grace and J. M. Matsen Eds., Plenum, **1980**, 175.

54. Beer, J. M.; Sarofim, A. F.; Sharma, P. K.; Chaung, T. Z.; Sandhu, S. S. *Fluidization* J. Grace and J. M. Matsen Eds., Plenum, **1980**, 185.

55. Chan, L. K.; Sarofim, A. F.; Beer, J. M. *Combustion and Flame* **1983**, *52*, 37.

56. Levy, J. M.; Chan, L. K.; Sarofim, A. F.; Beer, J. M. *Eigtheenth Symposium (International) on Combustion, The Combustion Institute* **1981**, Pittsburgh, 111.

57. Yamashita, H.; Tomita, A.; Yamada, H.; Kyotani, T.; Radovic, L. R. *Energy and Fuels* **1993**, *7*, 85.

58. Song, Y. H.; Beér, J. M.; Sarofim, A. F. *Combustion Science and Technology* **1982**, *28*, 177.

59. Wendt, J. O. L.; Schulze, O. E. *AICHE Journal* **1976**, *22(1)*, 102.

60. Harding, A. W.; Brown, S. D.; Thomas, K. M. *211th American Chemical Society National Meeting* **1996**, *41(1)*, 165.

61. Wang, W.; Thomas, K. M. *Fuel* **1992**, *71(3)*, 871.

62. Thomas, K. M.; Grant, K.; Tate, K. *Fuel* **1993**, *72(7)*, 941.

63. Wang, W.; Thomas, K. M. *Fuel* **1993**, *72*, 293.

64. Holbrook, K. M.; Buchanan, R. M.; Meuzelaar, H. L. C. *Proceedings of The 38th*

*ASMS Conference on Mass Spectrometry and Allied Topics* **1990**, 900.

65. Dworzanski, J.; Chapman, J.; Meuzelaar, H. L. C.; Lander, H. R. *ACS Reprints, Division of Petroleum Chemistry* **1992**, *37(2)*, 424.

66. McClennen, W. H.; Buchanan, R. M.; Arnold, N. S.; Dworzanski, J.; Meuzelaar, H. L. C. *Analytical Chemistry* **1993**, *65*, 2819.

67. Meuzelaar, H. L. C. *Advances in Coal Spectroscopy* **1992**, 1st Ed., Plenum Press, 49.

68. Klemen, S. R.; Gorbaty, M. L.; Kwiatek, P. J. *Abstracts of Papers of America Chemical Society* **1993**, 205.

69. Turner, N. H.; Schreifels, J. A. *Analytical Chemistry* **1993**, *64(12)*, 302.

70. Fletcher, T. H.; Bai, S.; Pugmire, R. J.; Solum, M. S.; Wood, S.; Grant, D. M. *Energy and Fuels* **1993**, *7(6)*, 734.

71. Solum, M. S.; Pugmire, R. J.; Grant, D. M. *Energy and Fuels* **1989**, *3(2)*, 187.

72. Johnsson, J. E. *Fuel* **1993**, *73(9)*, 1398.

73. Hayhurst, A. N.; Lawrence, A. D. *Progresses in Energy & Combustion Sciences* **1992**, *18*, 529.

74. Wójtowicz, M. A.; Pels, J. R.; Moulijn, J. A. *Fuel* **1995**, *74(4)*, 507.

75. Várhegyi, G.; Szabó, P.; Jakab., E.; Till, F. *Energy and Fuels* **1996**, *10(6)*, 1208.

76. Várhegyi, G.; Antal, M. J.; Jakab, E.; Szabó, P. *Journal of Analytical and Applied Pyrolysis* **1996**, *42*, 73.

77. Álvarez, T.; Fuertes, A. B.; Pis, J. J.; Ehrburger, P. *Fuel* **1995**, *74*, 729.

78. Maswadeh, W. *University of Utah, Ph.D. Dissertation: Devolatilization Studies of Single Coal Particles at High Heating Rates*, **1993**, 146.

79. Suuberg, E. M.; Wójtowicz, M.; Calo, J. M. *Twenty-Second Symposium (International) on Combustion* **1988**, 79.

80. Fogler, S. H. *Elements of Chemical Reaction Engineering* **1992**, 2nd Ed., 62, Prentice-Hall.

81. Spinti, J. C. P. *University of Utah, Ph.D. Dissertation: An Experimental Study of The Fate of Char Nitrogen in Pulverized Coal Flames* **1997**, 258.

# IMAGE EVALUATION
# TEST TARGET (QA-3)

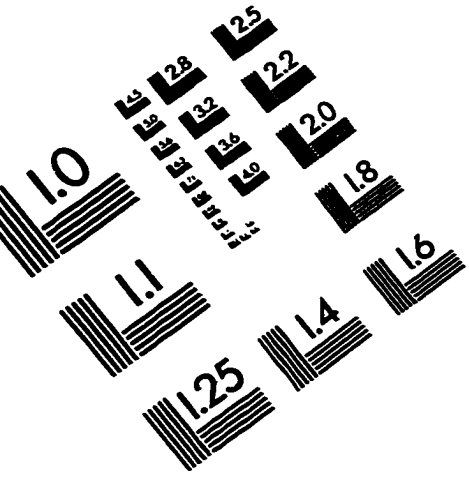


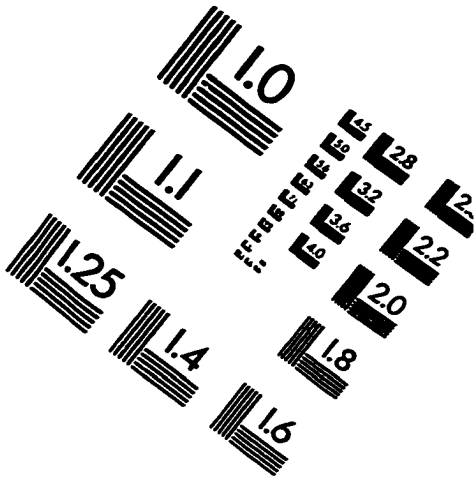


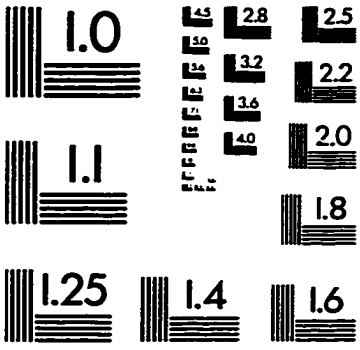


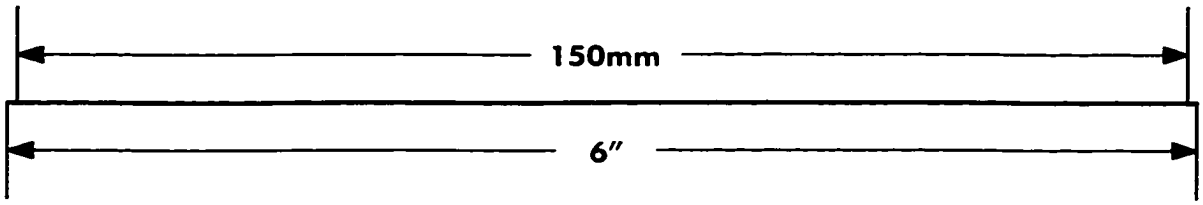


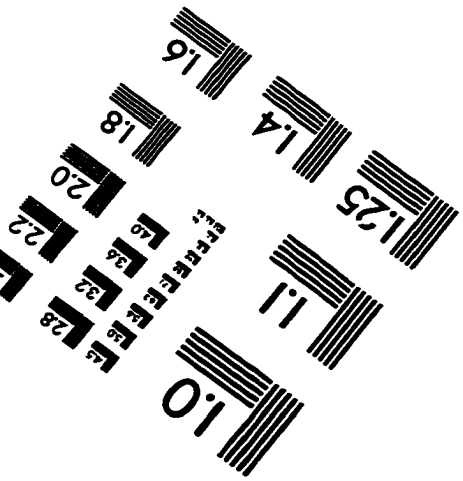


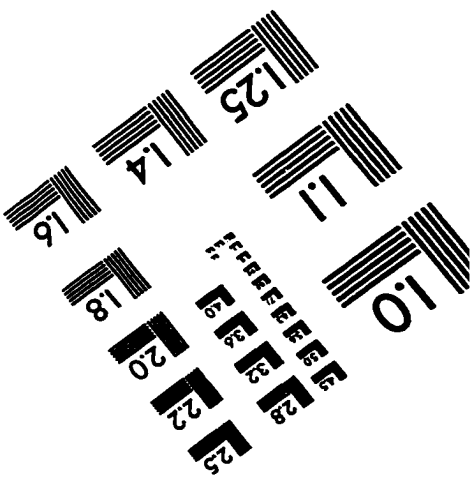


APPLIED IMAGE, Inc
1653 East Main Street
Rochester, NY 14609 USA
Phone: 716/482-0300
Fax: 716/288-5989